AN ABSTRACT OF THE THESIS OF

RICHARD WILLIAM SPINRAD for the degree of DOCTOR OF PHILOSOPHY

in OCEANOGRAPHY presented on MARCH 2, 1982

TITLE: OPTICAL CHARACTERISTICS OF THE SUSPENDED SEDIMENT IN THE HIGH ENERGY BENTHIC BOUNDARY LAYER EXPERIMENT

ABSTRACT APPROVED: Redacted for privacy
J. Ronald V. Zaneveld

Redacted for privacy
Hans J. Schrader

Redacted for privacy
LaVerne D. Kulm

Profiles of light transmission versus depth have been studied in the region of the High Energy Benthic Boundary Layer Experiment (HEBBLE) at bottom depth between 4900 m and 5000 m. A component model has been developed and consists of five components of transmission which can be combined to accurately duplicate any given transmission profile. The components are shown to be representative of three basic phenomena: the particle concentration within an even flow; the separation of a benthic nepheloid layer; and the trailing edge of a benthic cloud. In the case of even flow it is the relative magnitudes of settling and eddy diffusion which determine the shape of the transmission profile. Separation of the benthic nepheloid layer was inferred to be caused by an occasional cross-slope velocity component. The component model yields diffusion coefficients comparable to those estimated by a simple diffusion/settling model.

Using the components, various features of the HEBBLE area have been studied. Integration of the transmission profiles together with reasonable estimates of the size of the benthic turbidity cloud indicate mass fluxes on the order of a metric ton per second over a period of four or five days past a cross-sectional area of 10 km^2. In addition, Eulerian and Lagrangian transformations have been performed on the data obtained over several weeks and covering distances of hundreds of kilometers. The Eulerian transformation shows that benthic storms that were detected at one location and time appear nearly identical at a later time downstream. Similarly, Lagrangian transformation shows that separate benthic storms can be detected over a large distance. Distance and time scales obtained from these transformations show the HEBBLE area to be one characterized by bottom storms which keep their general form over periods of at least two weeks and for distances travelled of at least 400 kilometers.

An excellent correlation exists between transmission and particle volume concentration. A nearly identical correlation was obtained in the same area at a time eighteen months after the initial correlation was determined. Index of refraction determination yield indices ranging from 1.55 to 1.60, characteristic of typical marine clays.

OPTICAL CHARACTERISTICS OF THE SUSPENDED SEDIMENT IN THE HIGH ENERGY BENTHIC BOUNDARY LAYER EXPERIMENT

by

RICHARD WILLIAM SPINRAD

A THESIS
submitted to
Oregon State University

in partial fulfillment of
the requirements for the
degree of
DOCTOR OF PHILOSOPHY

Completed March 2, 1982

Commencement June 1982

APPROVED:

Redacted for privacy

Associate Professor of Oceanography in charge of major

Redacted for privacy

Professor of Oceanography in charge of major

Redacted for privacy

Professor of Oceanography in charge of major

Redacted for privacy

Dean of the School of Oceanography

Redacted for privacy

Dean of Graduate School

Date thesis is presented March 2, 1982

Typed by Sandy Orr for Richard William Spinrad

Dedication

ACKNOWLEDGEMENTS

I would like to express my strongest thanks to the members of my committee for their help, cooperation, toleration, advice, encouragement and confidence during my graduate career. Ron Zaneveld was a fount of creative thinking and his provocative suggestions changed me from Sisyphus the student to Perseus the scientist. I hope I can, some day, be as helpful to him. Hans Schrader and Vern Kulm helped me realign my goals and got me back on the track when some important decisions needed to be made. Ross Heath supported me and reconfirmed my belief that the oceanographic community need not be "cubby-holed" to be productive. The elusive Charley Hollister provided a plethora of pregnant porisms for my perusal and indeed showed me the light at the end of the tunnel several times. Dr. T. Lindstrom graciously and carefully helped me walk through the mire of hegemonical university rules and regulations.

Bob Bartz, Dave Menzies, Jim Kitchen and Hasong Pak all helped me make it through my graduate education. I am duly grateful to them for the time and effort they have shared with me both at sea and on land.

Nick McCave and Steve Swift both provided several stimulating ideas and discussions which played an integral part in the development of this thesis. Mary Jo

Richardson, Georges Weatherly, and Sandy Williams also provided important data for this work and I thank them.

Without question all of my friends were the saving grace which sustained me through what, at times, seemed a torment of insanity. Above all Tom, Jane Anne, Mick and Phyllis shone. It is a measure of friendship that the time spent with them was never quite long enough.

Finally, heaps of gratitude are due Sandy Orr. Without her nimble fingers of lightning speed this thesis would never have been presented as neatly or as promptly.

Funding for this research was supplied by the Office of Naval Research under the HEBBLE program through contract N00014-80-0004 under project NR 083-102.

TABLE OF CONTENTS

PAGE

LIST OF FIGURES

LIST OF FIGURES (cont'd)

LIST OF FIGURES (cont'd)

LIST OF FIGURES (cont'd)

LIST OF TABLES

OPTICAL CHARACTERISTICS OF THE SUSPENDED SEDIMENT IN THE HIGH ENERGY BENTHIC BOUNDARY LAYER EXPERIMENT

I. INTRODUCTION

Optical characteristics of deep sea suspended particulate matter shall be used in conjunction with models of sediment transport to determine various features of the flow of near-bottom water masses in the region of the High Energy Benthic Boundary Layer Experiment (HEBBLE). HEBBLE is a multi-disciplinary, multi-institutional program developed in order to "... increase dramatically our understanding of the flow dynamics and geological effects of strong flows in the deep-ocean benthic boundary layer." (Hollister et al., 1980). The zone of study lies about 400 miles east of Woods Hole, Massachusetts and 250 miles south of Nova Scotia, covering the shelf, slope and abyssal plain within the area bounded by 39° to 43°N and 59° to 66°W (Figure 1). The data contained within this thesis were collected primarily during Cruise Number 74, from 7 September 1979 to 4 October 1979, aboard the R/V KNORR from Woods Hole Oceanographic Institute. A large amount of data was collected over the whole HEBBLE region (nearly 50 CTD[1] casts were made on this one cruise)

---

[1] The CTD is a Conductivity-Temperature-Depth measuring instrument designed by Neil Brown Instrument Systems. A light transmissometer designed at Oregon State University and a General Oceanics - Niskin bottle rosette sampler were used in conjunction with the CTD on each cast.

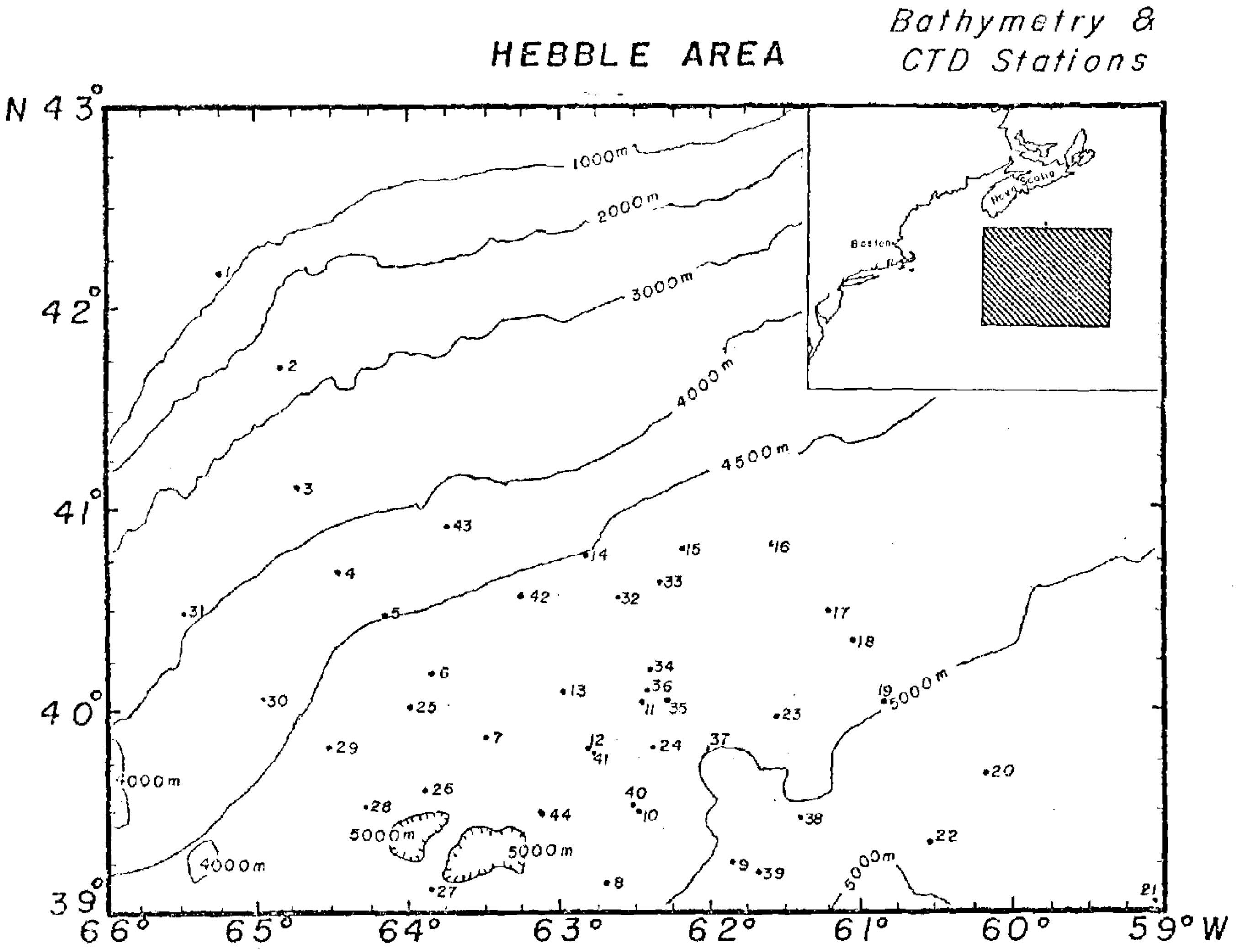

Figure 1. Map of the HEBBLE area showing bathymetry and CTD Station numbers

and several zones of interest were surveyed. It was found, however, that the region of highest activity lay at the deepest part of the continental rise, near the landward edge of the Sohm Abyssal Plain. It was in this zone that bottom photographs, current meters, transmissometers and sediment traps indicated the highest levels of near bottom turbulence (Hollister et al., 1980; personal communication Hollister, Biscaye, Weatherly). For this reason the work described herein will concentrate on the data obtained from the stations that were located in bottom depths between 4900 m and 5000 m. This depth range also corresponds to the zone where the fixed-location instruments (e.g., Bottom Ocean Monitor, Chandelier, and TRIFFID[2]) were placed during this time. The CTD stations within this depth zone were numbers 8, 10, 11, 12, 19, 23, 24, 27, 35, 36, 37, 40, 41 and 44 (corresponding Ship Station numbers are 8, 10, 11, 12, 21, 25, 27, 30, 38, 39, 40, 43, 44 and 50, respectively). Station number 35 (Ship Station 38) was aborted due to equipment failure in mid-cast so there is insufficient data to include that station in the analysis.

Profiles of transmission provide excellent records of suspended particulate concentration. In turn, profiles of particle concentration supply valuable

---

[2] The Bottom Ocean Monitor contained an OSU transmissometer, a nephelometer, and an Aanderaa current meter. Chandelier was a vertical array of current meters to be described later. TRIFFID contained bottom cameras, transmissometer and sediment trap.

information regarding transport processes because, in much the same way as salinity or temperature, turbidity may be used as a water mass tracer (Pak, 1970). By measuring light transmission at a number of times and locations the processes involved in sediment transport within the HEBBLE area may be detected and analyzed. The usefulness of this type of measurement lies in the need to better understand the effects of bottom currents on the geology of the world's oceans.

The use of precise optical instruments in the sea is fairly new. Kalle (1939) first developed the concept of using the Tyndall effect as an indicator of the size of suspended particles. He also proposed the hypothesis that light scattering and particle cross-sectional area were directly proportional. Using the theory of Mie (1908), Van de Hulst (1959), Jerlov (1953), and Burt (1956) accurately calculated the dependence of light scattering on the size and index of refraction of spherical suspended particles. Measurements of light scattering were improved with the use of photographic techniques and the development of *in situ* nephelometers such as the ones of Jerlov (1957), and Lamont-Doherty Geological Observatory (Thorndike and Ewing, 1967). The L-DGO nephelometer has been used for many years in the world's oceans (Eittreim et al., 1972; Eittreim and Ewing, 1972; Biscaye and Eittreim, 1974). With the advent of light-emitting diodes and electronic microprocessors nephelometers of higher resolution were developed and used by Oregon State University (Beardsley et al., 1970) and the Visibility Lab at Scripps Institute of Oceanography (Smith et al., 1974). Presently, measurements of extremely fine resolution of suspended particulate matter can be made with highly collimated beam transmissometers (Tyler et al., 1974; Bartz et al., 1978). As a tracer of water masses measurements of light transmission have been made in conjunction with salinity and temperature (Drake, 1971; Pak and Zaneveld, 1977; Zaneveld et al., 1979), current velocity (Harlett and Kulm, 1973), irradiance (Spinrad and Zaneveld, 1979), and particle size distributions (Kitchen et al., 1978; Zaneveld et al., 1978). It is these types of light transmission measurements that will be used in the work described here.

The history of the study of sediment transport is reviewed extensively in the texts of Raudkivi (1967), Graf (1971) and Yalin (1972). More recent work is contained in Goldberg et al. (1977). Nearly all of the models of sediment transport have been for the determination of the processes involved in sedimentation or deposition on the continental shelves but they all utilize the same basic concept of conservation of mass of sediment. Within a given volume of sea water a change in suspended particulate matter (which is manifested as either erosion, sedimentation, or transport) can only be due to a combination of any of three processes:

i) advection; (including settling of the particles themselves); ii) turbulent (or eddy) diffusion; and iii) creation or dissolution within the sample volume. By varying the intensities of each of these three processes the particulate content of the volume of sea water may be varied. Using such a technique some modelers have been able to explain the existence of maxima in the vertical distribution of particles in the sea (Jerlov, 1959) and the existence of transparent (i.e., particle-free) zones in the water column (Bassin et al., 1972; Ichiye et al., 1972; Bassin, 1974).

By using a beam transmissometer as an *in situ* continuous detector of suspended particulate matter, reasonable estimates can be made of the particle volume concentration within the suspended load of the water column. In this way the sediment transport can be detected and one can make reasonable observations about the features of the flow in the region where light transmission measurements are made. This region does not include the bedload in this work.

Specifically, the major question to be answered is: what is the nature of benthic sediment transport in the HEBBLE area as determined from optical measurements? The temporal and spatial scales of formation of benthic turbiity "storms" will be analyzed as well as the stability over time and space of these phenomena. The form of transport (i.e., continuous or pulsed) will also be discussed as well as the physical systems responsible for the structure of particle concentration as detected. Several recurrent small-scale (10^2 m) and large-scale (10^2 km) optical features will be presented and their roles in the overall scheme of sediment transport will be discussed.

II. THE OPTICS

A. General

The use of optical measurements as an indicator of particle concentrations is a well accepted practice (Gibbs, 1974a,b,c; Jerlov and Steemann-Nielsen, 1974; Pak and Zaneveld, 1977; Kullenberg, 1974; Carder et al., 1974; Pak, 1974). The "optics problem" may best be expressed as:

$$c = c_w + a_p + b_p + a_y \qquad \text{(Jerlov, 1976)} \qquad (1)$$

where c = beam attenuation coefficient defined as the internal attenuance of an infinitesimally thin layer of medium normal to the beam divided by the thickness of the layer (m^{-1})

a = the absorption coefficient defined as the internal absorptance of an infinitesimally thin layer of the medium normal to the beam, divided by the thickness of the layer (m^{-1})

b = the scattering coefficient defined as the internal scatterance of an infinitesimally thin layer of the medium normal to the beam, divided by the thickness of the layer (m^{-1})

also $c = a + b$.

The subscripts w, p and y refer to water, particles and yellow matter (humic acids and dissolved organic substances which fluoresce in the blue) respectively. There is negligible scattering by yellow matter alone. In addition Kalle (1966) has shown that because of the wavelength dependence of absorption by yellow matter, a_y may be considered negligible for red light (660 nm). For this reason transmission measurements made at 660 nm will yield values of the beam attenuation coefficient of:

$$c = c_w + a_p + b_p = c_w + c_p \qquad (2)$$

The absolute value of c_w at 660 nm is not known but estimates range from roughly 0.35 to 0.50 m^{-1} (Jerlov, 1976) (the explanation for this lies in the extreme difficulty in obtaining an optically clean system to measure the attenuation of pure sea water). The beam transmissometer used in this experiment has been calibrated to yield a value of c_w of 0.40 m^{-1}. The relationship between the beam attentuation coefficient and transmission, T, is a simple one:

$$T = e^{-cr} \qquad (3)$$

where T = the fraction of incident light transmitted

r = pathlength = 1 meter in this case.

B. Correlation of Transmission and Volume Concentration

With a single measurement of light transmission at 660 nm one can obtain the beam attenuation coefficient of the suspended particles. The correlation of the beam attenuation coefficient with particle concentration is well documented (Peterson, 1978). Particle volume concentrations were measured by Coulter Counter at the same locations as transmission measurements were made for the work described herein. A strong correlation was found ($r = 0.96$; see Figure 2) and is given by

$$P = -265.1 + 569.5c \qquad (4)$$

where P is in parts per billion volume concentration and c is in m^{-1} 40 PPB $\leq P \leq$ 600 PPB.

Also shown in the figure are the 95% confidence limits of the ordinate (volume concentration) about the mean beam attenuation coefficient (0.91 m^{-1}). In addition, the limit defined by two standard deviations from the predicted concentration has also been plotted. These ranges approximately define the 95% confidence limits of the regression given by the relationship in Equation (4).

This relationship yields a value of $c = 0.47$ m^{-1} or $T = 63\%$ for clean water. While this value does not agree exactly with the previously specified calibration value it is within the range of expected attenuation coefficients for clean water and thus is quite acceptable. In this way the transmission measurement provides data for determining the particulate volume concentration. A similar correlation was calculated by McCave (personal

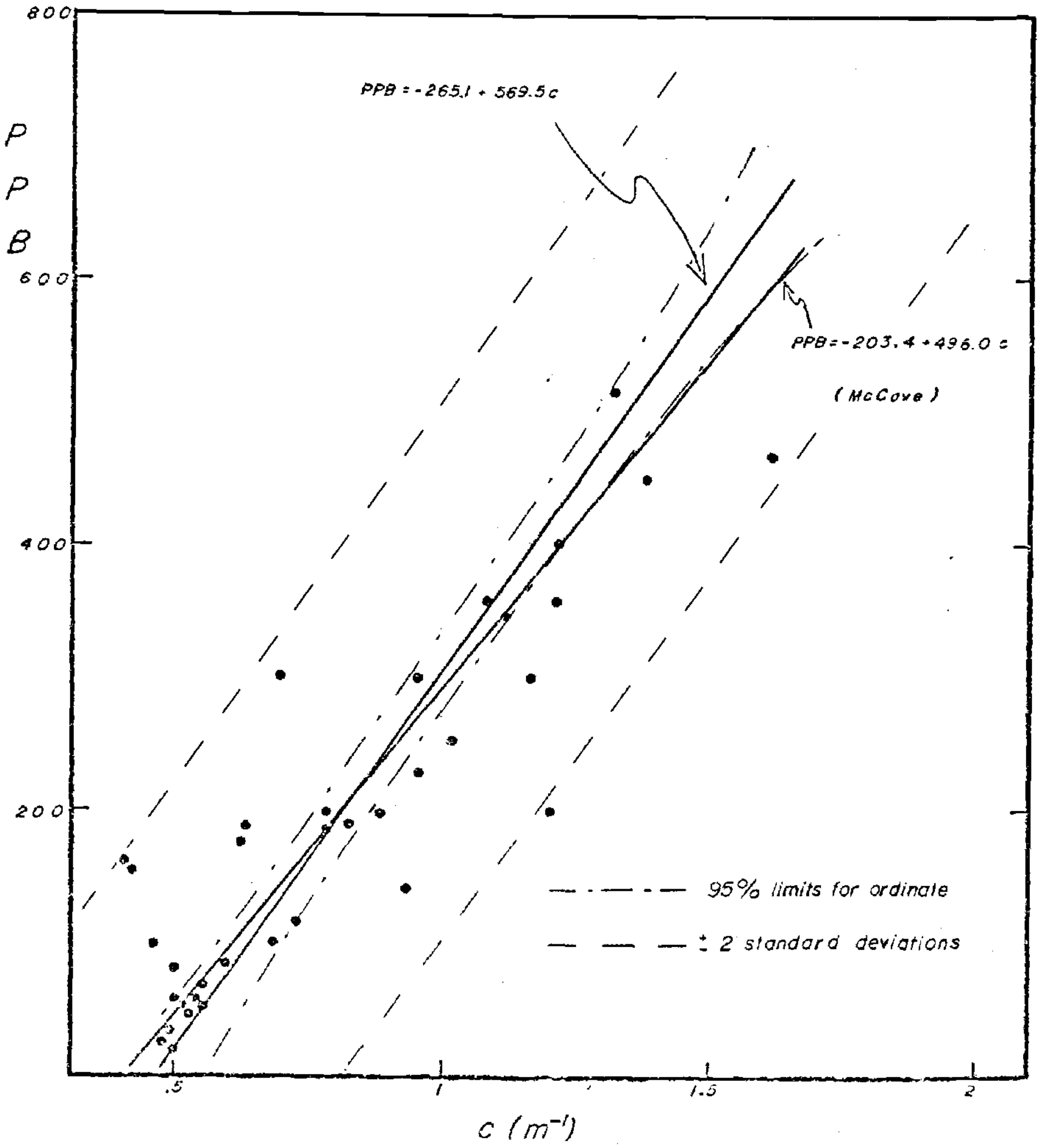

Figure 2. Particle volume concentration (PPB = parts per billion) from Coulter Counter vs. beam attenuation coefficient from transmissometer.

communication) for data collected in the same area but a year and a half later. The correlation he obtained was

$$P = -203.4 + 496.0c$$

$$r = 0.93$$

The agreement between this correlation and the one used in this work is quite good as shown by the extent of the overlap in Figure 2.

The fact that the correlation between volume concentration and beam attenuation coefficient is so good implies an important feature of the particle size distribution in this area. A given volume concentration may be obtained from an infinite number of possible size distributions. As a simple example consider a volume concentration of 100 PPB. Such a concentration could be obtained with one large (10^8 μm^3 or roughly 600 μm diameter) spherical particle per liter or ten spherical particles of diameter 300 μm per liter or one million particles of diameter 6 μm per liter or an infinite number of combinations of particle size distributions. The beam attenuation coefficient, however is dependent on the total cross-sectional <u>area</u> of the particles and consequently any changes in the particle size distribution that would otherwise go undetected in measurements of volume concentration <u>would</u> be seen by the transmissometer. The opposite situation is also valid: the particle size distribution could change without a change in the overall cross-sectional area. However in that case the volume concentration would change. Simply, the volume concentration is proportional to the integral, $\int D^3 f(D)dD$, and the total cross-sectional area is proportional to the integral, $\int D^2 f(D)dD$, (where $f(D)$ is the distribution or concentration of particles having diameters between D and D + dD) so a change in the particle size distribution will affect the volume concentration and the beam attenuation coefficient unequally. Yet the previous discussion of the excellent correlation between volume concentration and beam attenuation coefficient indicates a linear relationship between the two. Since changes in the particle size distribution over the range of volume concentrations observed would result in deviations from the curve shown in Figure 2, the conclusion is that variations in the particle size distribution in the zone under consideration are minimal. This conclusion is verified by the measurements made with a particle size analyzer.

C. Particle Size Analysis

Concurrent with the measurements of transmission, water samples were obtained and *in vitro* measurements of particle size distributions were made using a Coulter Counter particle size analyzer. These measurements were made by M. J. Richardson at Woods Hole Oceanographic Institute. Data for Stations 12, 24 and 36 have been made available to this author and are shown in Table I and Figure 3. The slopes indicated are the slopes of the differential size distribution given by:

$$\begin{array}{l}\text{Number of Particles}\\ \text{with Diameters between}\\ \text{D and D+dD per Unit}\\ \text{Volume}\end{array} \sim D^{-\gamma} \qquad \text{(Bader, 1970)} \qquad (5)$$

where γ = differential slope.

Size distributions are generally presented as cumulative or differential. Cumulative size distributions indicate the concentration of particles larger than a given diameter whereas differential particle distributions are defined as above. The differential particle distribution is therefore the first order derivative of the cumulative distribution. Since Coulter Counter data are presented in terms of the concentration of particles having diameters within a given range, the differential size distribution is used here.

The most obvious feature of Table I and Figure 3 is the homogeneity of the particle size distribution in the HEBBLE area. Within the bottom kilometer of the water column the slope of the distribution never varied by more than 0.3 from a value of 3.1. These data represent measurements taken over the course of nearly two weeks in time and roughly 80 kilometers separation in distance. In fact, at the bottom of the water column the mean slope for these three stations is 3.1 with a standard

TABLE I

CTD STATION	HEIGHT ABOVE BOTTOM (m)	DIFFERENTIAL SLOPE
12	4	3.1
	4	3.0
	57	3.1
	134	3.0
	240	3.4
	673	3.2
24	4	3.1
	4	3.0
	55	3.0
	182	3.3
	290	3.1
	434	3.1
	572	3.0
	727	3.0
36	4	3.3
	4	3.2
	127	3.3
	157	3.2
	196	3.2
	277	3.2
	360	3.0
	510	2.9

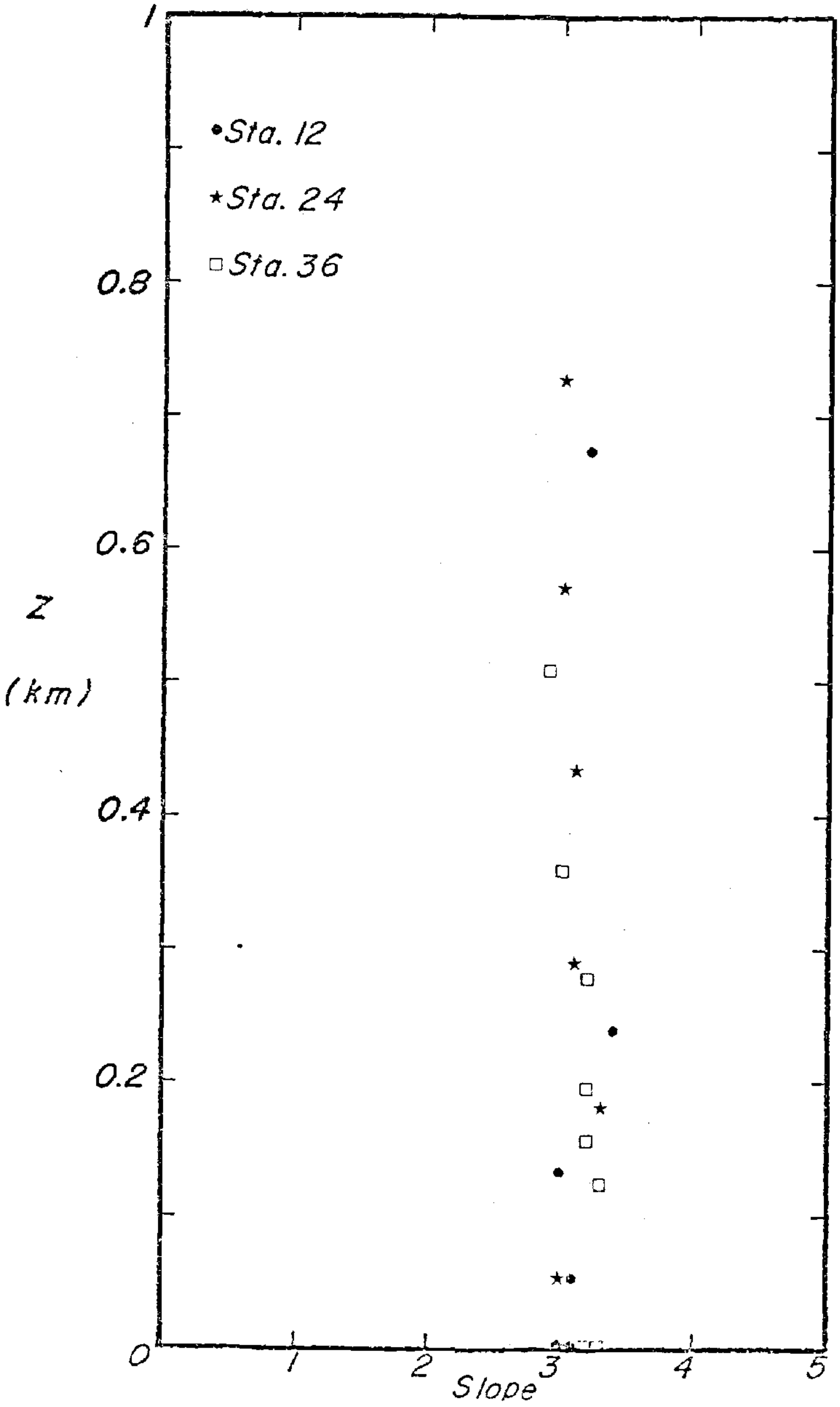

Figure 3. Differential slope of the hyperbolic particle size distribution from Coulter Counter data

deviation of only 0.1. Additional Coulter Counter data indicate that this homogeneity is the general rule for HEBBLE suspended particle distributions (personal communication, M. J. Richardson). For all samples taken at heights of less than 1000 m off the bottom the mean slope increased only a small amount and standard deviations were roughly the same as those obtained for the bottom samples.

D. Particulate Index of Refraction

In addition to supplying information about the particle concentration the transmissometer data may also be used to study the particles themselves. Specifically, an analysis may be made of the particulate index of refraction.

For a single particle of diameter D, with a single-valued index of refraction, m_p, there exists a quantity called the effective area coefficient, or the efficiency factor, Q, given by

$$Q = \frac{c_p}{\pi \frac{D^2}{4}} \tag{6}$$

where c_p = particulate beam attentuation coefficient.

Similarly, for N particles of diameter D, per unit volume, Equation (6) becomes

$$Q = \frac{c_p}{N \Pi \frac{D^2}{4}} \qquad (7)$$

and is therefore dimensionless.

Q is found to behave somewhat as a Bessel function with increasing particle size and/or refractive index and it approaches an asymptote of 2.0 (Figure 4). Van de Hulst (1957) used classical light scattering theory to define the curve shown in Figure 4 as

$$Q = 2 - \frac{4}{aD} \sin aD + \frac{4}{a^2 D^2} (1 - \cos aD) \qquad (8)$$

where

$a = \frac{2\pi}{\lambda} \mid m_p - m_w \mid$

λ = wavelength of light in a vacuum

m_w = refractive index of the water $\cong$ 1.33

and the particles are assumed to be non-absorbing spheres with refractive index near that of water.

Consequently, for a particle size distribution Equation (6) may be written as

$$c_p = \sum_{i=1}^{n} N_i Q_i \frac{\pi D_i^{\,2}}{4} \qquad (9)$$

N_i is the number of particles of diameter D_i per unit volume. As discussed earlier the HEBBLE samples have particle size distributions that are given approximately by

$$N_i = N\, D_i^{-3}$$

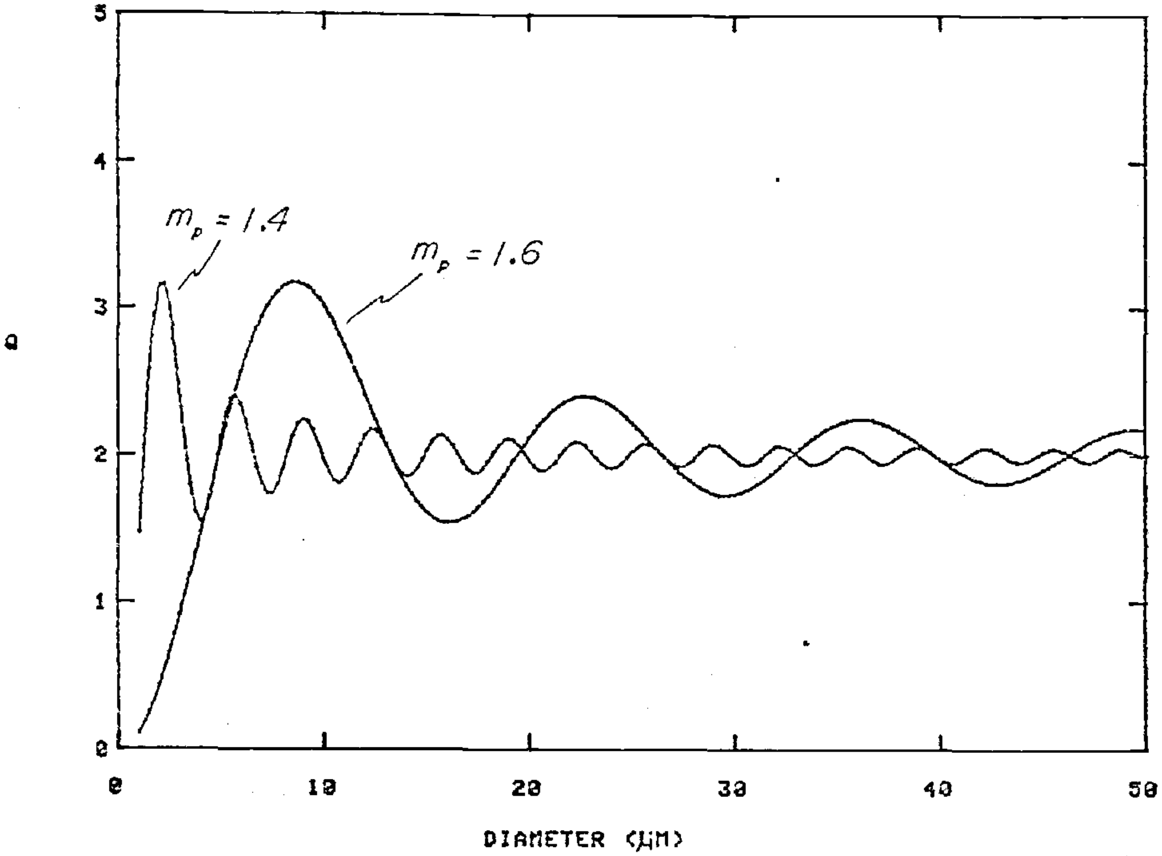

Figure 4. The curve of the effective area coefficient, Q, for two particulate indices of refraction.

However, while this equation is accurate enough to define the shape of the particle size distribution, it is much too coarse an estimate to be used in solving Equation (9). A much better solution is obtained by numerical analysis using the data as obtained from the Coulter Counter.

It would be presumptuous to try to evaluate the particulate index of refraction to a single value for the material in the HEBBLE region. In fact most particles are not characterized by a single index of refraction but rather by a distribution of values over a range of indices (Zaneveld et al., 1974; Roach, 1975). Zaneveld et al. (1974) have shown that oceanic particles display a bimodal distribution of indices of refraction with one peak near 1.05 (relative to water) and another peak at 1.15. These two peaks are thought to represent the organic and inorganic components, respectively.

By inserting Equation (8) into Equation (9) one obtains

$$c_p = \frac{\Pi}{4} \Sigma N_i (2 D_i^2 - \frac{4}{a} D_i \sin aD_i + \frac{4}{a^2} (1 - \cos aD_i)) \quad (10)$$

A numerical solution for the value of "a" in the equation above was obtained for indices of refraction varying from 1.02 to 1.30 relative to water (1.36 to 1.73 absolute). For each of the three stations observed (CTD 12, 24 and 36) the best approximation of the particulate beam attenuation coefficient was obtained when high values of the index of refraction were used. Having little or no defined variation with altitude above bottom the index of refraction was found to have an approximate range of 1.15 to 1.25 for Station 12, 1.13 to 1.26 for Station 24, and 1.13 to 1.20 for Station 36. The variations detected were a consequence of allowing an error in c_p of 0.03 m^{-1}. This error arises from the transcription of transmission values from the profiles obtained. This error also allows for the variation in the estimate of the beam attenuation coefficient of the pure water (as discussed earlier).

Since any method similar to the one used here is really a rough estimate of refractive index it is important not to try to obtain a unique value for each sample observed. Rather, the technique used here was employed solely to get an idea of what sort of values may serve to characterize the optical properties of the particles seen in the HEBBLE area. The suspended particles observed in HEBBLE are of high relative index (1.15 to 1.25 relative to water). This result is consistent with the adoption of a value of 1.15 to 1.20 for the refractive index of inorganic materials as denoted by Jerlov (1976). It would seem reasonable that the material at 5000 m depth in the ocean would be resuspended inorganic material. The high refractive indices observed here are also comparable in value to the indices of most oceanic clays (e.g., approximately 1.17 to 1.20 for most aluminosilicates). Consequently, if a single value is sought for the index of refraction of particles in the HEBBLE region any values between 1.55 and 1.60 are equally viable.

III. THE MODEL

A. Basic Concepts and Applications

From the data obtained with a beam transmissometer and using the correlation outlined previously the transmission profiles may be used to provide values of the volume concentration profile. While no two transmission profiles that were obtained were identical it has become apparent that there are only a few general types of profiles seen in the HEBBLE area. All of the profiles may be broken down into characteristic components. Each of these components will be shown to be representative of a physical system responsible for yielding such a particle profile. Thus, by considering all of the transmissometer profiles as compilations of the same components the interactions of these physical systems in the HEBBLE area may be better understood. It would also be possible to consider each profile individually by "smoothing" the data and reducing each transmission value to a particle concentration. Such a method might be inherently more precise for each unique transmission profile but it would be of little use in the consideration of the overall picture of how the physical systems of sediment transport are working amongst themselves within the HEBBLE area.

The components are shown in Figures 5 through 10. Respectively, these profiles are defined as follows:

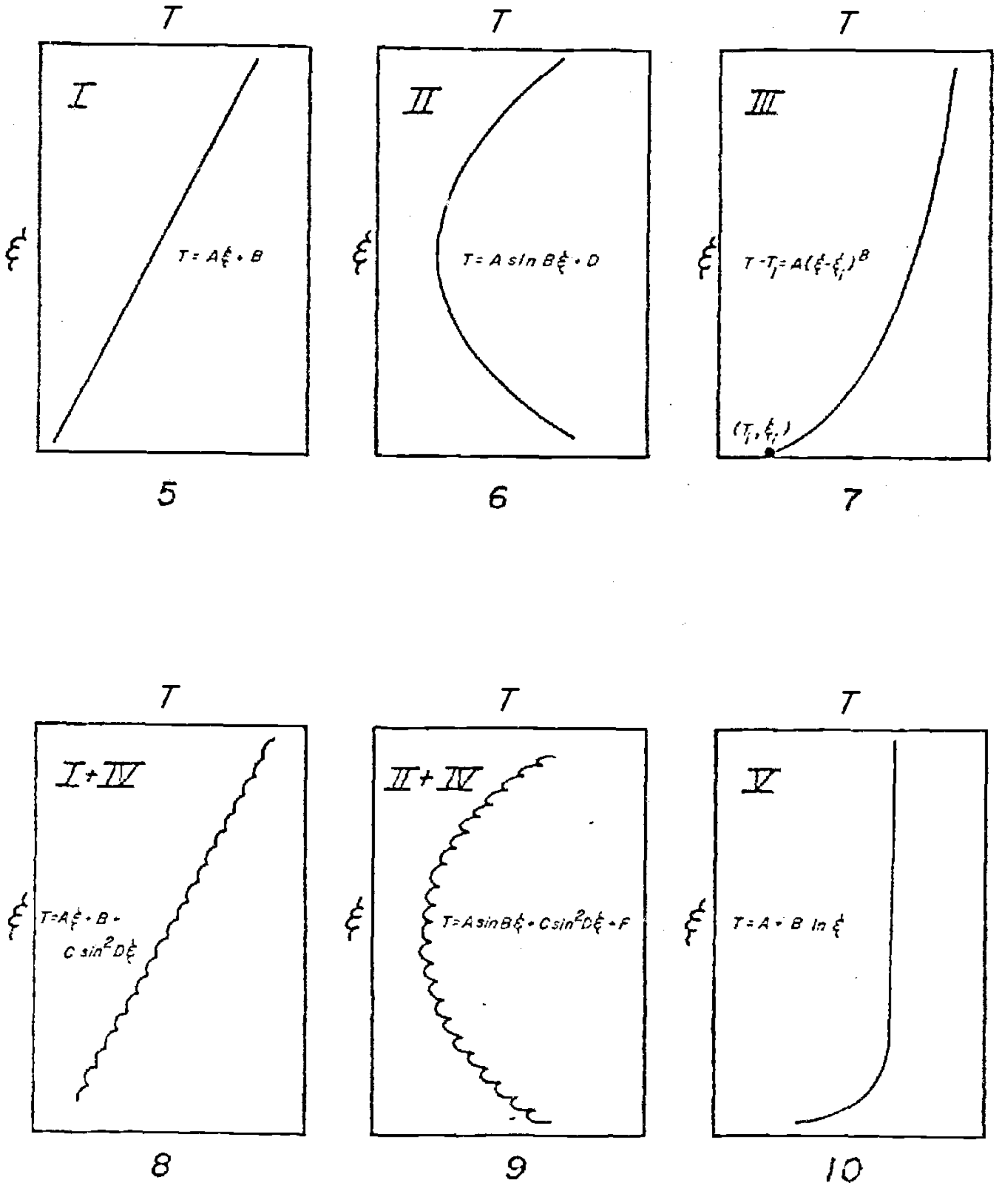

Figures 5-10. Components for the model of transmission profiles .

$$T = A\xi + B \tag{11a}$$

$$T = A \sin B\xi + D \tag{11b}$$

$$T - T_i = A\,(\xi - \xi_i)^B \quad \text{"i" indicates starting value} \tag{11c}$$

$$T = A \sin^2 B\xi + D \tag{11d}$$

$$T = A + B \ln \xi \tag{11e}$$

where T = transmission

ξ = a non-dimensional distance above the bottom given by $\frac{z}{h}$ (h = the height of the flow zone; z = + upward)

and A, B and D are constants determined by the shape of the specific profile under observation. In actuality any observed profile may be considered a construction of these components. The value of the beam attenuation coefficient, c, is then obtained from the above equations, since $c = -\ln T$. These components will be referred to as Components I through V, respectively (that is, Component I corresponds to Equation (11a); Component II corresponds to Equation (11b), etc.). Component IV never occurs by itself but is found in the data as a linear addition to either Component I or II.

The solutions of Equations (11a) through (11e) were derived numerically from the transmissometer profiles. The profiles were decomposed into segments, each having a form characterized by one of the components. The number of components in a profile varied from one to seven with a mean of three. The term h was determined as being the altitude at which the transmission reached a steady, clean value. This height varied from 60 m to 410 m with a mean value of 180 m. The value of h, the number of components and their type, as well as the values of the coefficients are shown in Table II. In addition, Figures 11 through 23 show the fit between the data and the numerical component model using the parameters given in the table (thin solid line = data).

Equations (11a) through (11e) express transmission, and therefore, beam attenuation coefficient, as a function of height above bottom; Equation (4) expresses particle concentration as a function of beam attenuation coefficient, and therefore, transmission. Thus, combining Equations (4) and (11a) through (11e) will yield the expressions of concentration as a function of altitude, $P(\xi)$:

$$P = -265.1 - 569.5 \ln (A\xi + B) \quad \text{for Component I} \tag{12a}$$

$$P = -265.1 - 569.5 \ln (A \sin B\xi + D) \quad \text{for Component II} \tag{12b}$$

$$P = -265.1 - 569.5 \ln (T_i + A(\xi - \xi_i)^B) \quad \text{for Component III} \tag{12c}$$

$$P = -265.1 - 569.5 \ln (A\xi + B + C \sin^2 D\xi) \quad \text{for Components I + IV} \tag{12d}$$

TABLE II

CTD STATION	h(m)	ξ	COMPONENT	A	B	D	C	F	T_i
8	115	0.74	I	0.01	0.54				
		1	I	0.27	0.35				
10	130	0.23	I	-0.02	0.30				
		0.69	I	0.25	0.24				
		1	III	0.63	0.55				0.41
11	215	0.47	I	0.02	0.56				
		0.81	I	0.24	0.46				
		1	I	-0.11	0.74				
12	150	0.63	I	0.03	0.41				
		0.77	I	0.43	0.16				
		1	V	0.65	0.52				
19	60	0.5	I	0.02	0.33				
		1	I	0.54	0.07				
23	410	0.09	I	0.11	0.28				
		0.21	I	0.50	0.25				
		0.28	I	1.71	-0.01				
		0.38	I	0.20	0.41				
		0.50	II	-1.48	3.57	1.94			
		0.65	II	1.39	2.69	-0.85			
		1	I	0.26	0.35				
24	365	0.19	I	0.05	0.40				
		0.23	I	2.75	-0.11				
		0.45	II	-0.71	4.69	1.15			
		0.60	I	0.23	0.46				
		0.71	II	-2.99	2.36	3.55			
		0.86	II	10.08	2.01	-9.45			
		1	I	0.50	0.15				
27	325	0.15	I	0.07	0.00				
		1	V	0.66	0.34				
36	85	1	I	0.05	0.58				
37	285	0.3	II+IV	-0.02	12.08	179	0.02	0.39	
		1	V	0.64	0.18				
40	315	0.24	I	0.04	0.38				
		0.49	V	0.75	0.24				
		1	I	0.14	0.49				
41	280	0.11	II	-0.12	28.56	0.34			
		0.36	III	0.14	0.22				0.34
		0.64	I	0.18	0.38				
		0.89	I	0.16	0.39				
		1	III	0.13	0.18				0.52
44	200	0.45	I+IV	0.02	0.40	62.83	0.01		
		1	I	0.44	0.21				

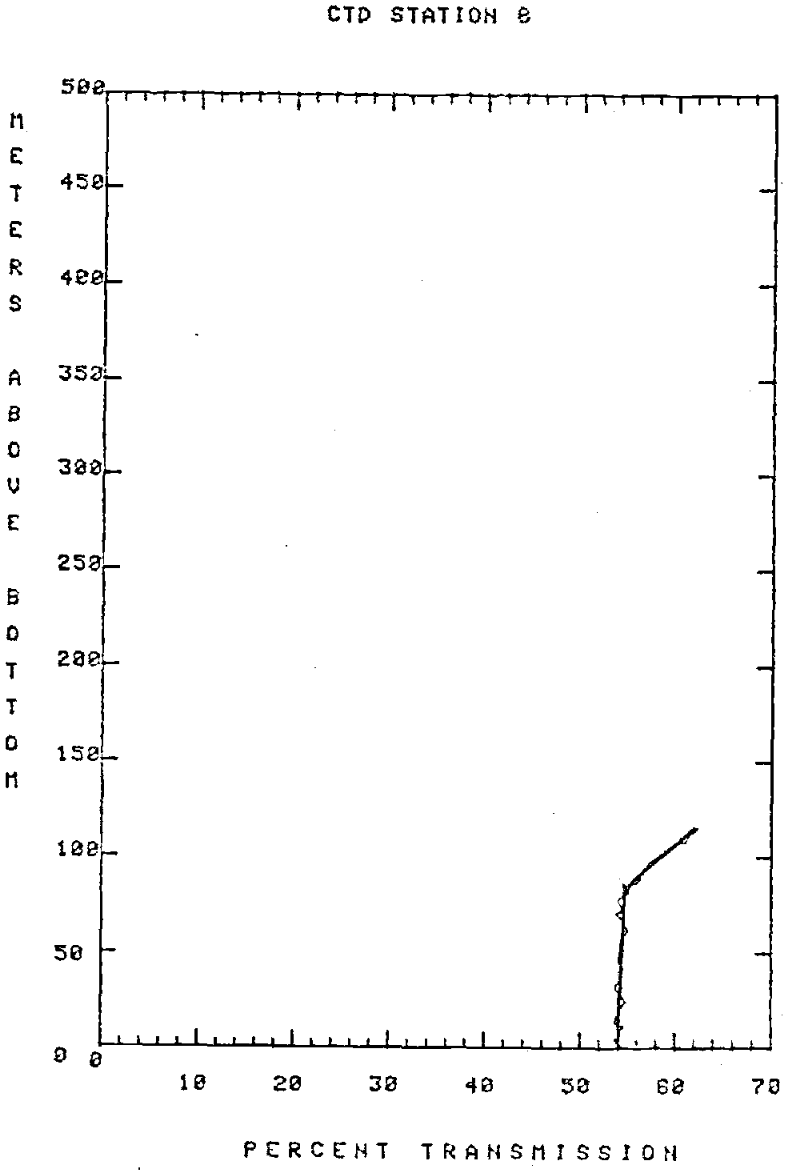

Figure 11. Comparison of actual transmission profile and component model for CTD Station 8.

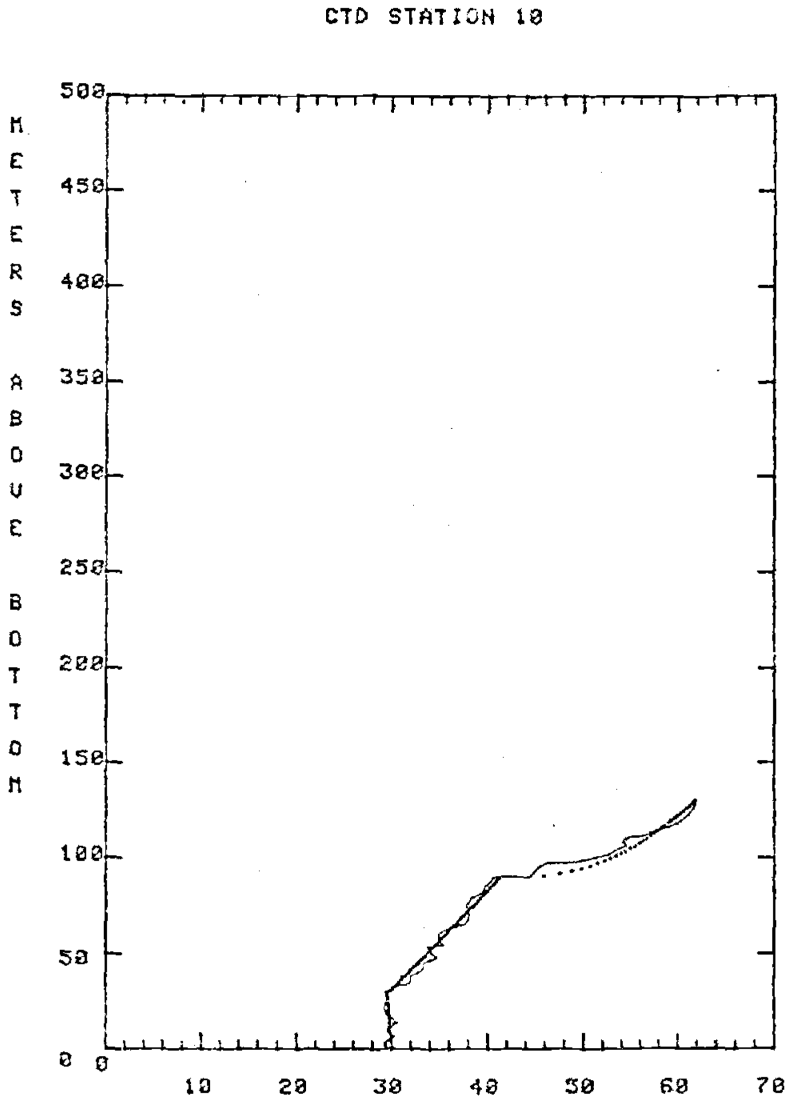

Figure 12. Comparison of actual transmission profile and component model for CTD Station 10

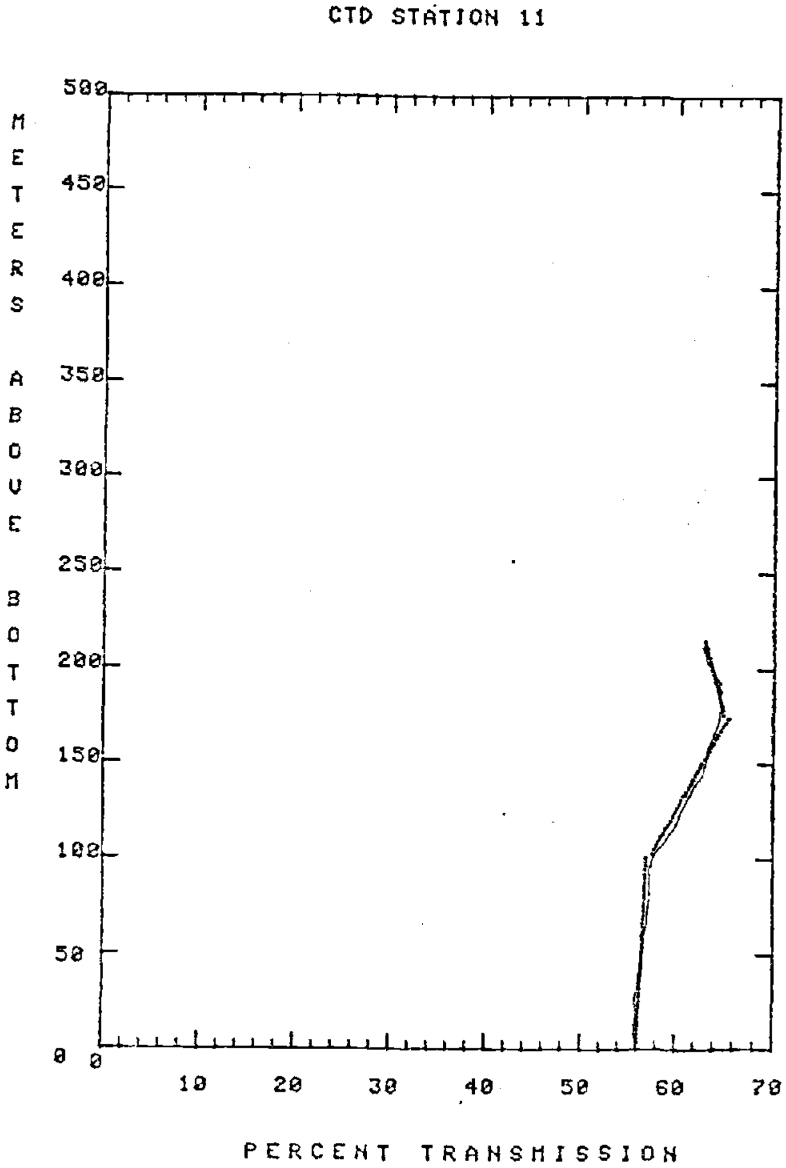

Figure 13. Comparison of actual transmission profile and component model for CTD Station 11 .

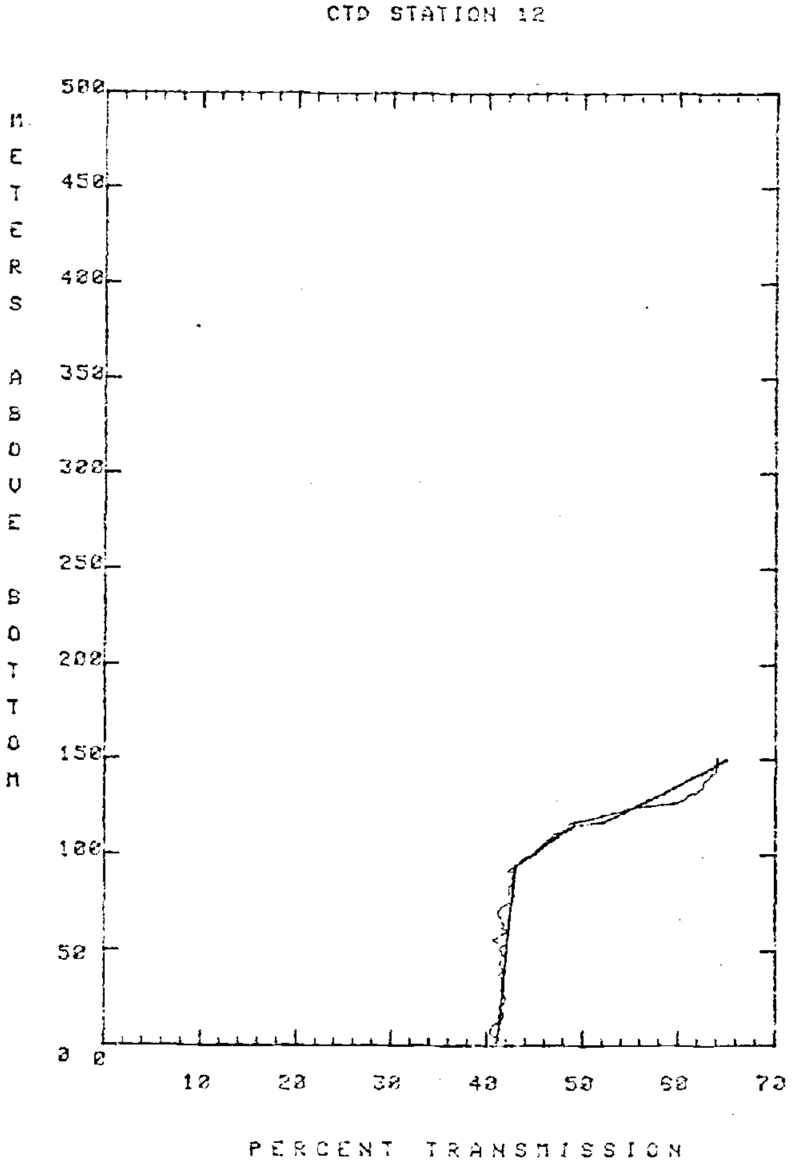

Figure 14. Comparison of actual transmission profile and component model for CTD Station 12 .

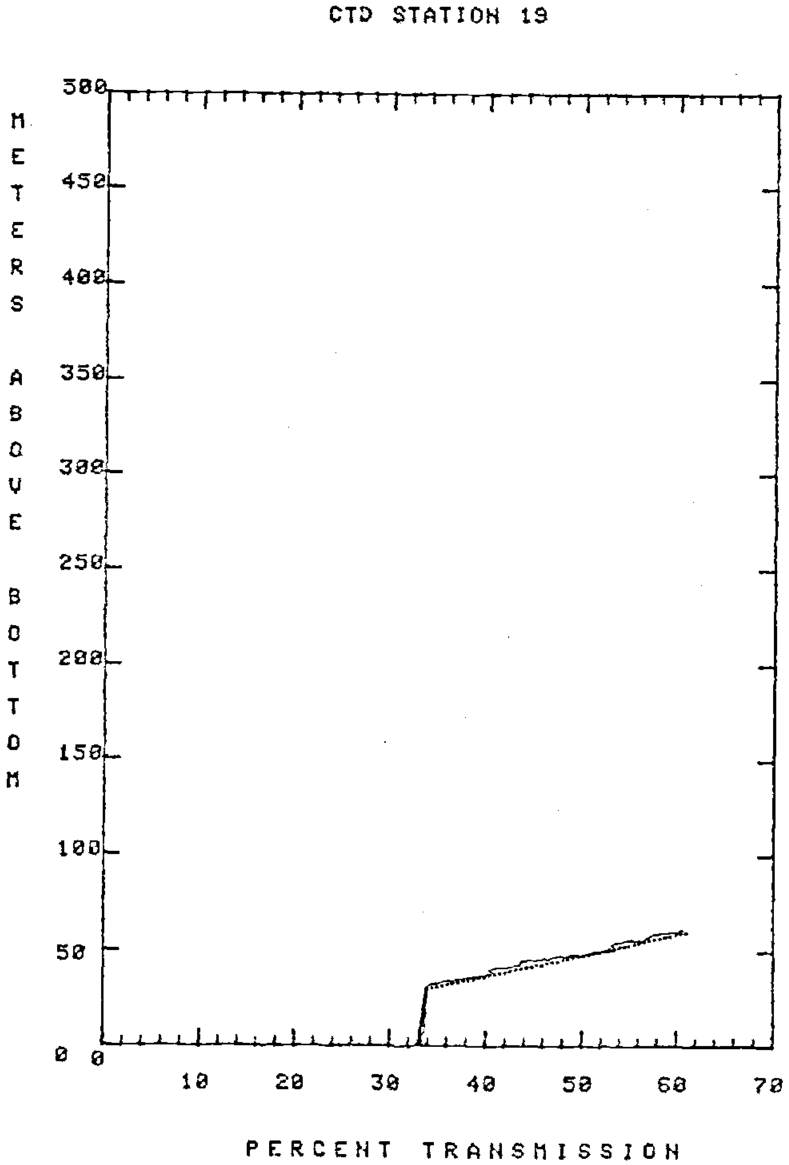

Figure 15. Comparison of actual transmission profile and component model for CTD Station 19 .

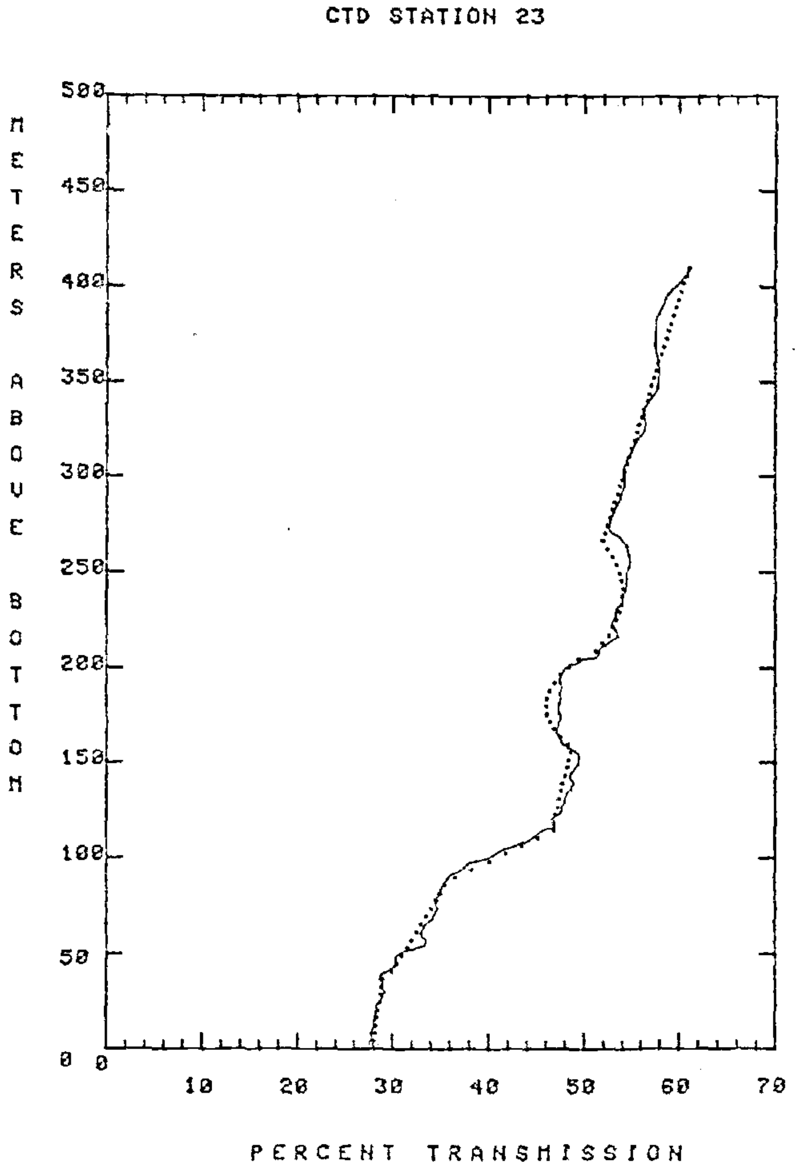

Figure 16. Comparison of actual transmission profile and component model for CTD Station 23 .

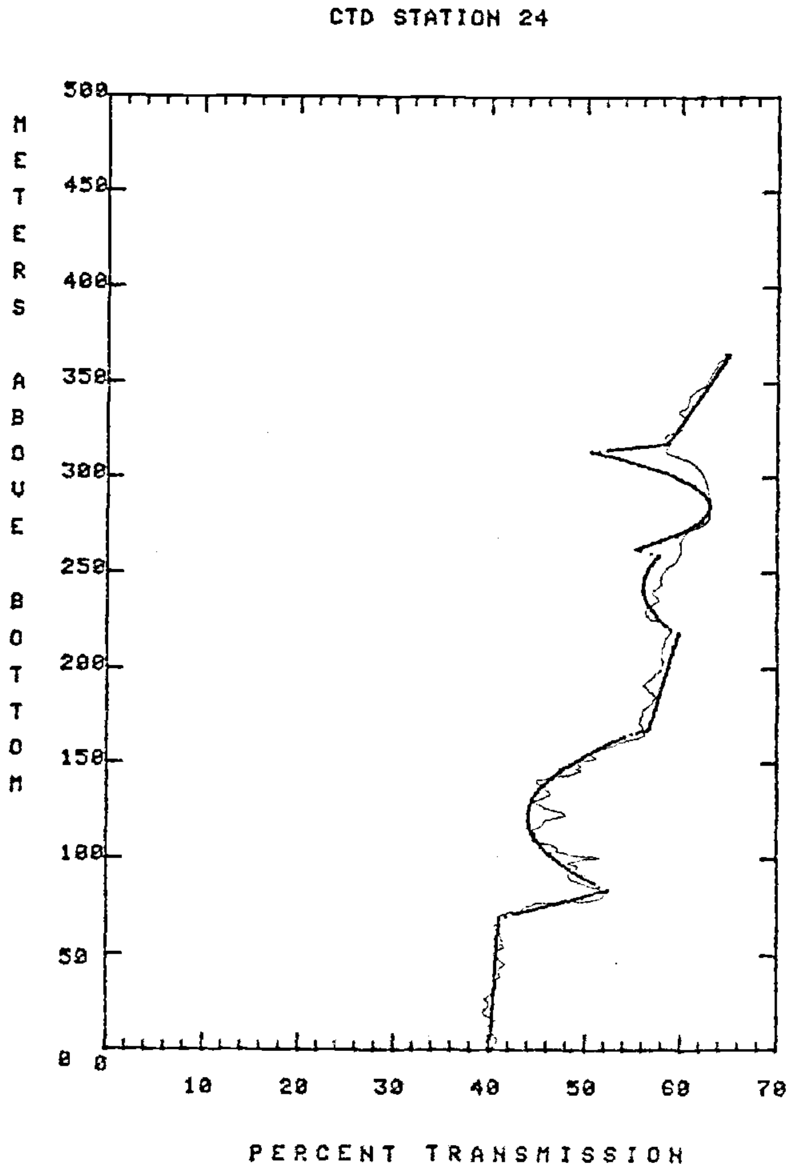

Figure 17. Comparison of actual transmission profile and component model for CTD Station 24 .

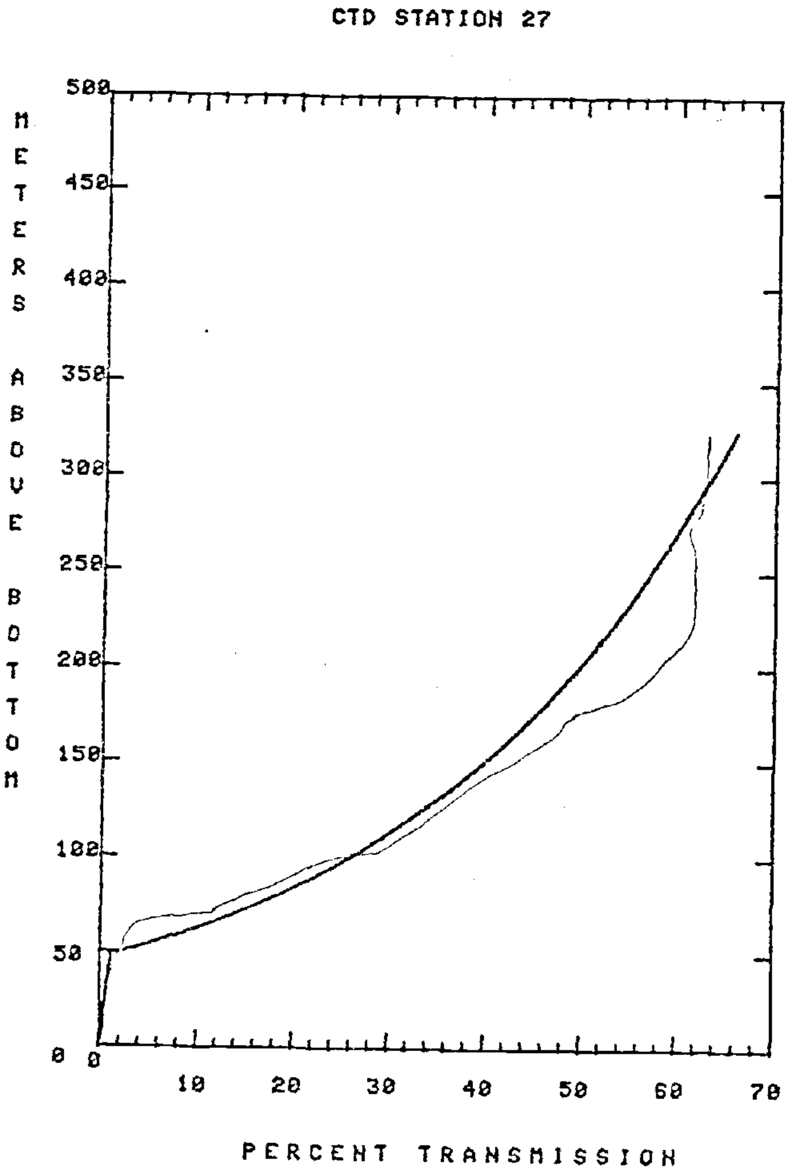

Figure 18. Comparison of actual transmission profile and component model for CTD Station 27 .

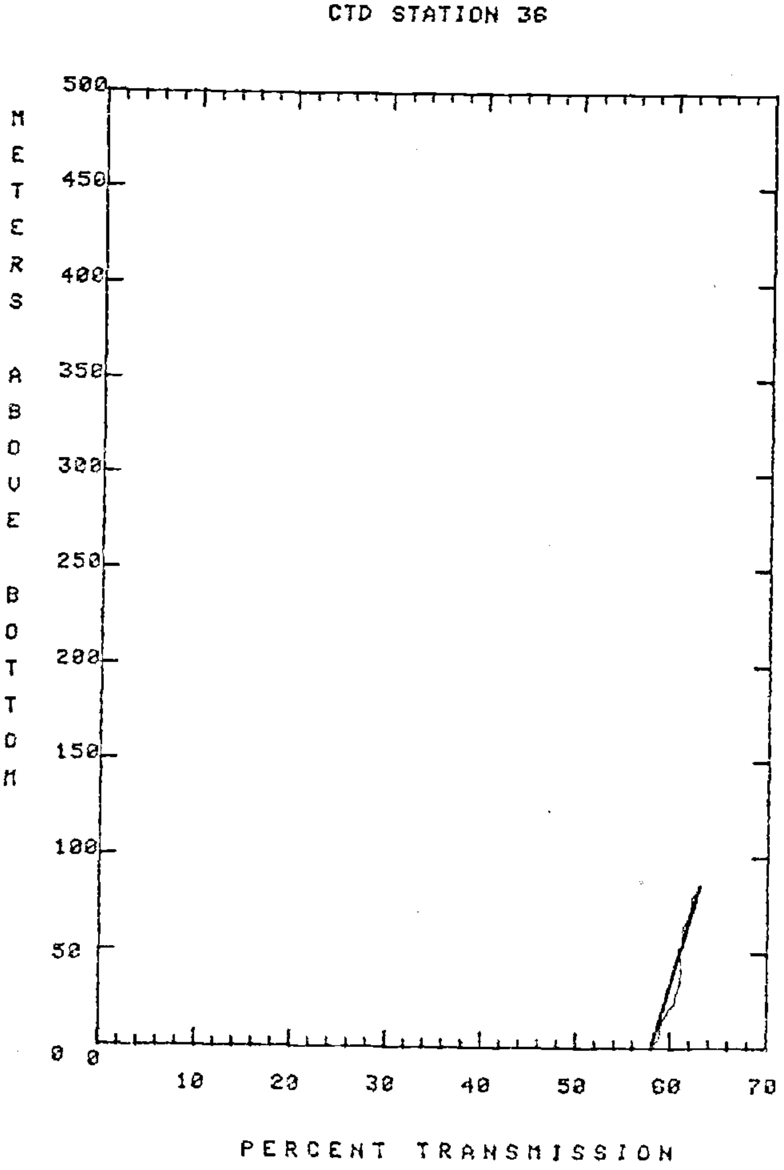

Figure 19. Comparison of actual transmission profile and component model for CTD Station 36 .

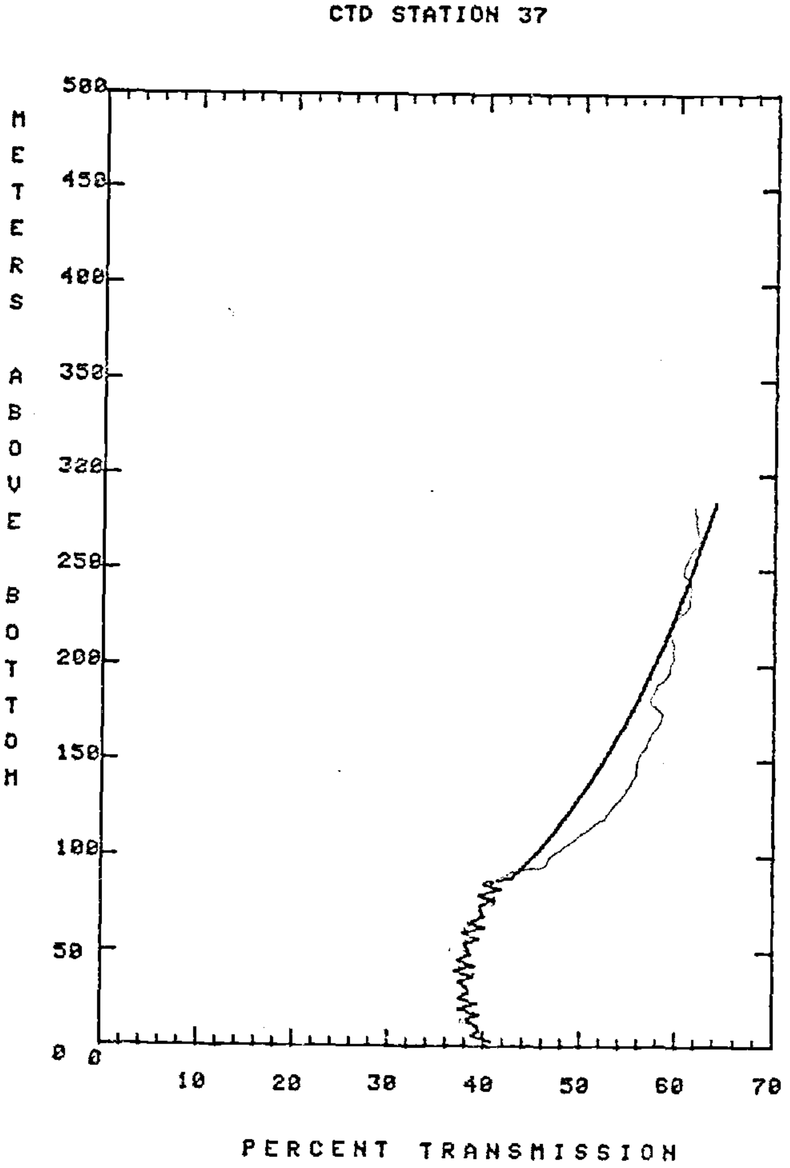

Figure 20. Comparison of actual transmission profile and component model for CTD Station 37 .

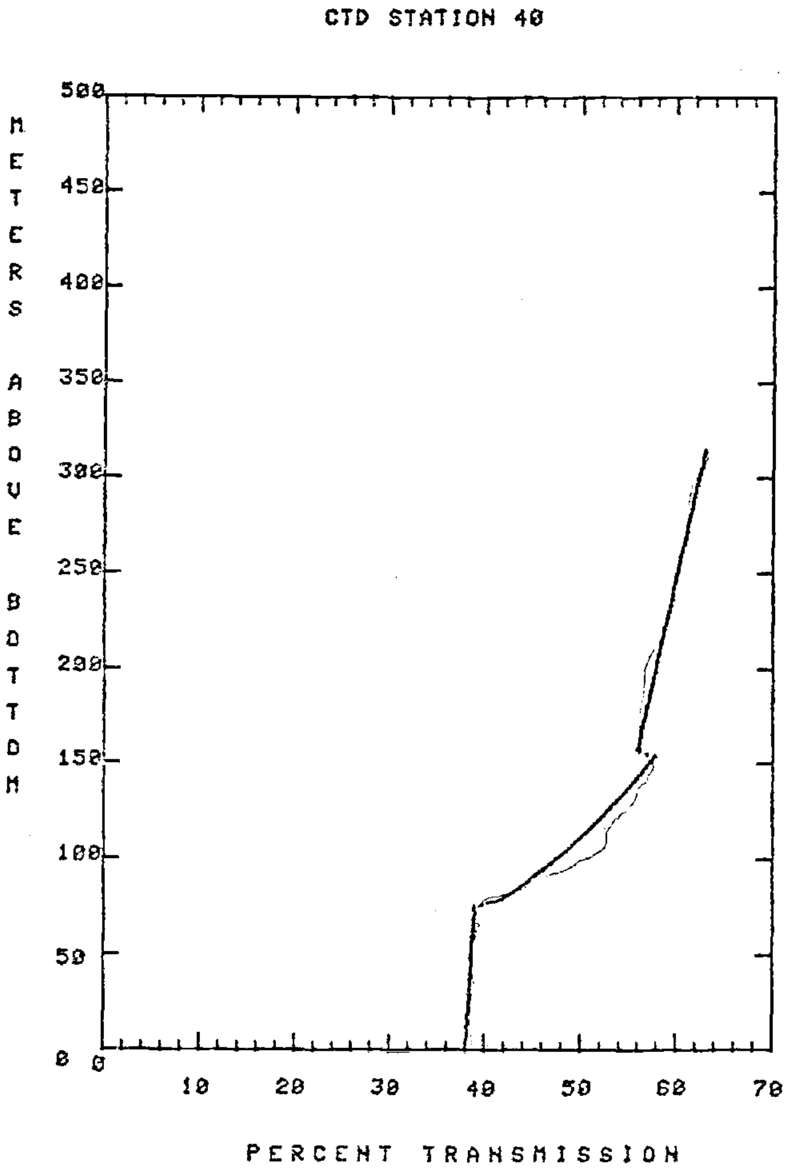

Figure 21. Comparison of actual transmission profile and component model for CTD Station 40 .

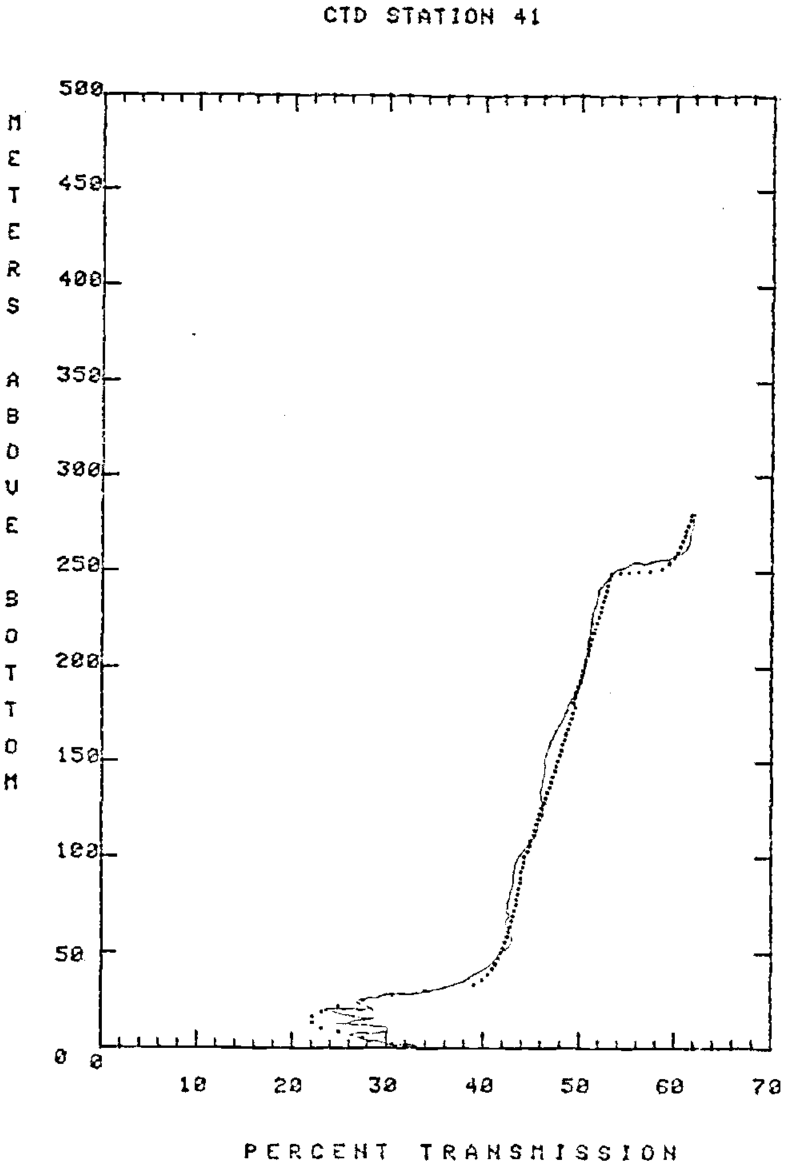

Figure 22. Comparison of actual transmission profile and component model for CTD Station 41 .

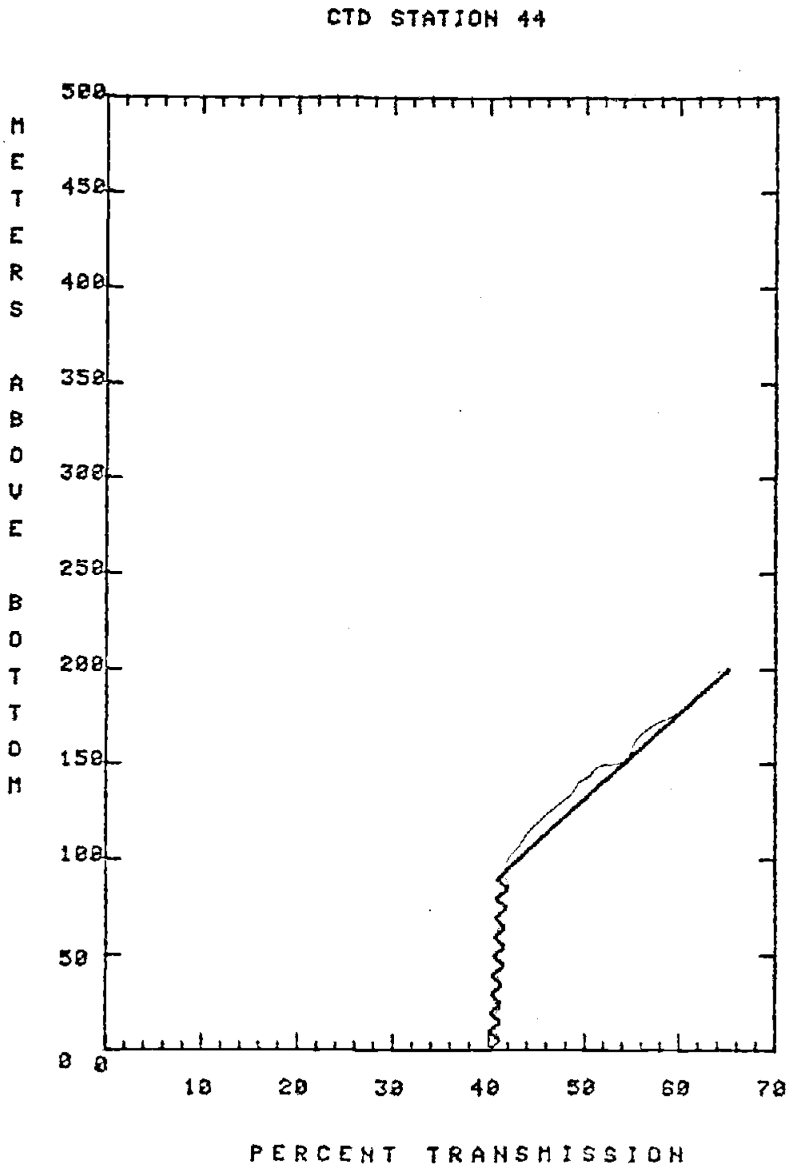

Figure 23. Comparison of actual transmission profile and component model for CTD Station 44 .

$$P = -265.1 - 569.5 \ln (A \sin B\xi + C \sin^2 D\xi + F) \tag{12e}$$

for Components II + IV

$$P = -265.1 - 569.5 \ln (A + B \ln \xi) \tag{12f}$$

for Component V

Similarly, $P' = \frac{\partial P}{\partial \xi}$ so the following relationships are obtained:

$$P' = -569.5 \left\{\frac{A}{A\xi + B}\right\} \tag{13a}$$

for Component I

$$P' = -569.5 \left\{\frac{AB \cos B\xi}{A \sin B\xi + D}\right\} \tag{13b}$$

for Component II

$$P' = -569.5 \left\{\frac{AB(\xi - \xi_i)^{B-1}}{T_i + A(\xi - \xi_i)^B}\right\} \tag{13c}$$

for Component III

$$P' = -569.5 \left\{\frac{A + 2CD \sin D\xi \cos D\xi}{A\xi + B + C \sin^2 D\xi}\right\} \tag{13d}$$

for Component I + IV

$$P' = -569.5 \left\{\frac{AB \cos B\xi + 2CD \sin D\xi \cos D\xi}{A \sin B\xi + C \sin^2 D\xi + F}\right\} \tag{13e}$$

for Component II + IV

$$P' = 569.5 \left\{\frac{B}{A\xi + B\xi \ln \xi}\right\} \tag{13f}$$

for Component V

B. Physical Explanation of the Components

i) Component I

As mentioned previously each of the five transmission components has a physical significance. In addition, the contiguity of two or more components in a given profile may be indicative of an even different physical system. The physical interpretation of these components serves as a useful tool in determining the existing transport processes.

Component I (linear) basically represents a system of particles within a uniform, steady flow. This is especially apparent in the case when T is nearly constant with altitude ($|A| \ll 1$). Such is the case in the boundary layer for several stations (e.g., Stations 8, 10, 11, 19). As the value of A increases and the transmission values increase with altitude the profile characterized by Component I is representative of a system in which particle settling has begun. If an initially well mixed polydisperse particle mixture is allowed to settle, the continuous range of particle settling velocities will produce a smooth transition from a low concentration of particles near the top to a high concentration below at a given time. The Eulerian analog for this Lagrangian view is a particle settling tube in which, at a given location over a range of time, an initially homogeneous mixture of particles slowly and smoothly gets clearer and clearer. More exactly, if a simplified eddy diffusion-settling model is considered for a steady, uniform flow the solution for particle concentration is of the form:

$P \propto \xi^{-b}$ (e.g., Shepard, 1963; Raudkivi, 1967; Smith and McLean, 1977)

where b is a coefficient that depends on particle settling velocity and magnitude of the flow. Using a series expansion for the solution above one finds that to the first order the particle concentration is characterized by a logarithmic profile:

$$\xi^{-b} \cong 1 - b \ln \xi$$

so

$$P \propto \ln \xi$$

This is in direct agreement with the profile of particle concentration that is obtained from Equation (12a) in which it is seen that for a linear transmission profile

$$P \propto \ln \xi.$$

Thus it is apparent that in general Component I represents a well-defined, even-flowing system. The slope of the transmission profile is indicative of the extent to which settling has occurred. The resemblance of profiles derived from models of steady, uniform eddy diffusion/settling and the transmission profiles shows that wherever Component I exists the system is probably dominated by a smooth, even current in which particle settling produces a logarithmic profile of particle concentration. The only exception to this physical system occurs when the transmission value is non-varying with altitude. In such a case particle settling is minimized, probably by turbulence. There is no indication in the transmission profiles that the slope is at all affected by or dependent on the degree of turbidity. Overall, Component I appears to characterize a system in which there is little vertical activity (after the initial homogenization, of course). The system may be well mixed initially and then settling and eddy diffusion become the dominant processes. This is shown quite dramatically in some of the temperature profiles that were taken concurrently with the transmission measurements. Figure 24 shows the linear transmission profile near the bottom as well as the temperature profile for Station 12. The bottom linear profile of transmission corresponds to a cold water mass near the bottom. But this bottom water mass is not being mixed as is evident by the adiabatic temperature profile from roughly 125 m above bottom down. These two profiles could only coexist in a slow-moving, non-turbulent flow in which particles could settle out and the water itself could maintain a strong adiabatic temperature profile. Such is the type of flow defined by Component I.

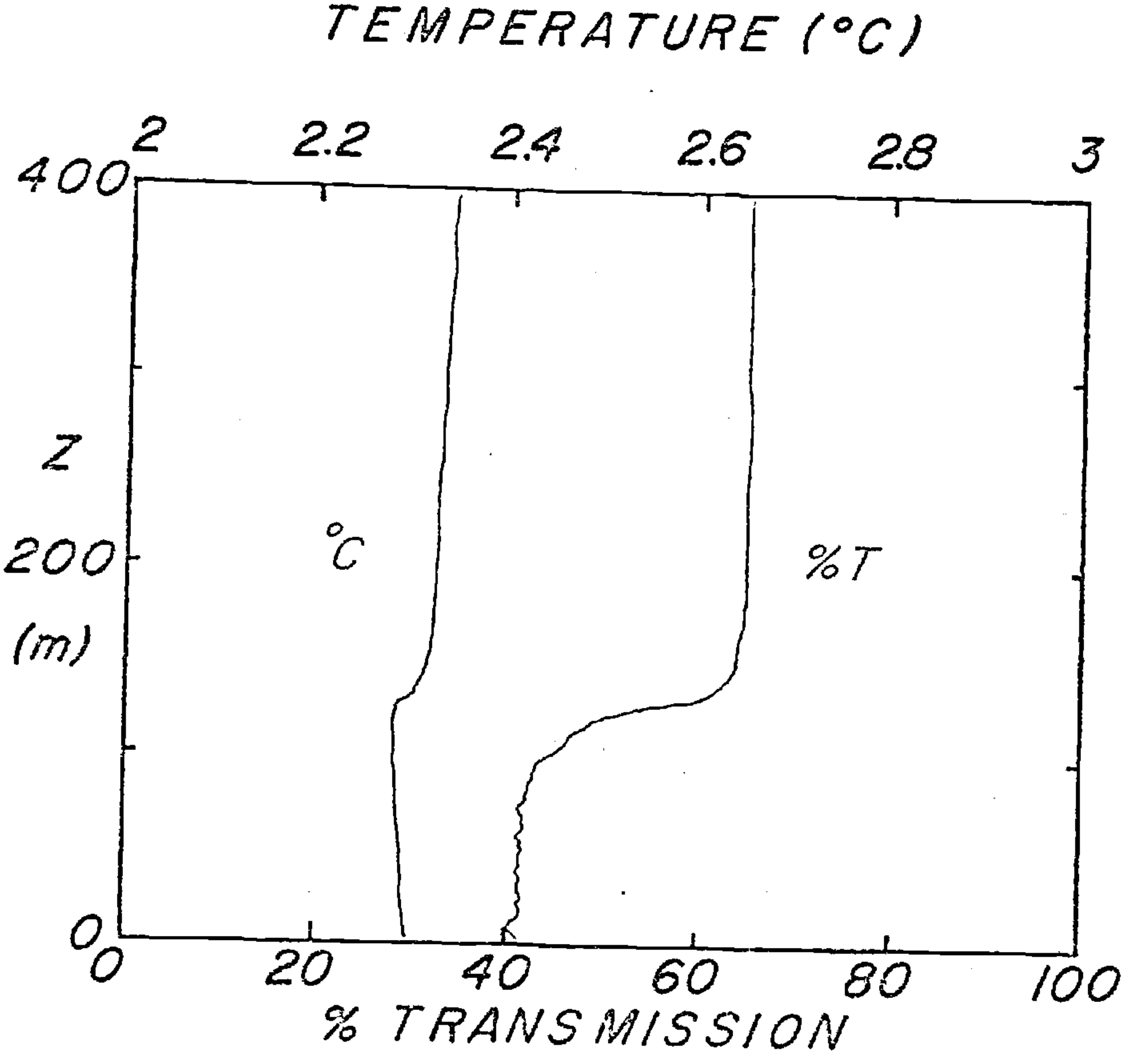

Figure 24. Temperature and transmission profiles at CTD Station 12.

ii) Component II

Component II (sinusoidal) is a transient feature which was detected above the bottom at four stations (23, 24, 37 and 41). While Figure 6 depicts Component II as a smoothly varying function of moderate amplitude and wavelength, the actual data profiles varied considerably from sharp, narrow peaks to broad, low-amplitude transmission minima. This is demonstrated by the range of values of the coefficient A and B for the stations listed previously in Table II.

Careful study of the transmission profiles and temperature profiles indicates that the water masses characterized by Component II are bottom-derived. Similar intermediate particle maxima have been detected elsewhere in the deep ocean (Armi and D'Asaro, 1980) and have been traced back to benthic boundary layers. The sinusoidal band develops as a detachment from the bottom nepheloid layer and may exist over a distance of tens of kilometers. Such a process also occurs at the shelf break where detached benthic layers flow over the slope to become intermediate nepheloid layers over the continental slope (Pak et al., 1980). The relative cleanliness of the waters above and below the intermediate band suggest that detachment from the benthic boundary layer is the most likely explanation for the appearance of Component II.

At two stations (23 and 24) the sinusoidal decrease in transmission was accompanied by a small sinusoidal increase immediately above it. This phenomenon was observed only at these two stations which also happen to be the stations with the most complex structure. The "positive sine" transmission profile (i.e., $A > 0$) was not seen to occur without the "negative sine" transmission profile directly below it. This structure may represent a complication of the simple model of a detached benthic layer. One might interpret this as a more complex situation in which the detached benthic boundary layer causes a slight turbidity decrease in the region directly above it. The exact mechanism for such a consequence is open for speculation.

At one station this process was actually detected from the onset and the profiles obtained present dramatic evidence of this growth process. Figure 25 shows a series of four transmission profiles taken consecutively at Station 23. The times for each cast are shown on the figure. Over the course of two hours an intermediate layer was detected initially at an altitude of 50 m, just at the top of the benthic nepheloid layer. As time progressed the layer detached from the benthic layer and rose to an elevation of 75 m to form a completely separate intermediate layer. The detached nepheloid layers are not necessarily stable since they are unbounded and they represent significant fluctuations from the local

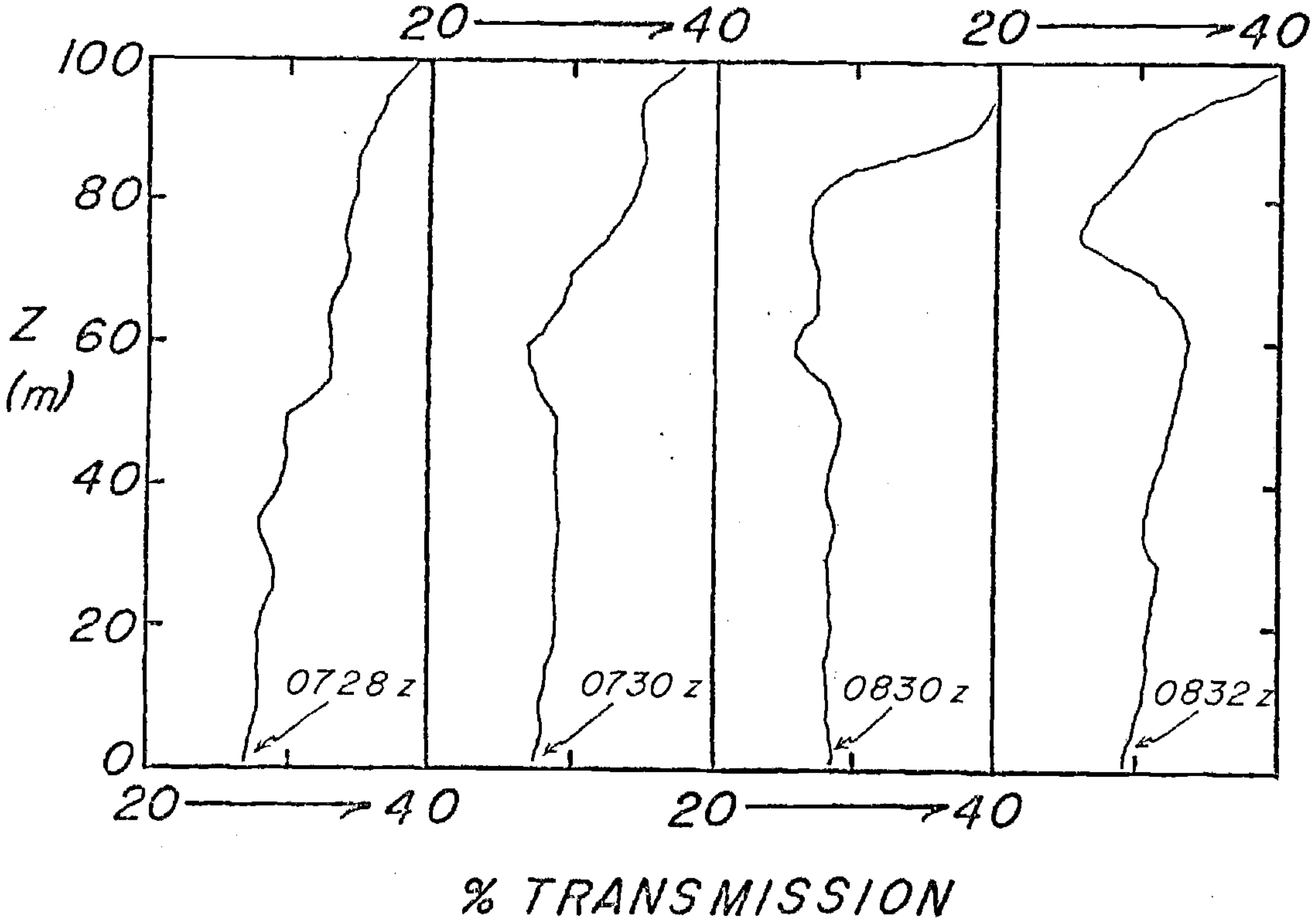

Figure 25a. Transmission profiles taken consecutively at CTD Station 23 .

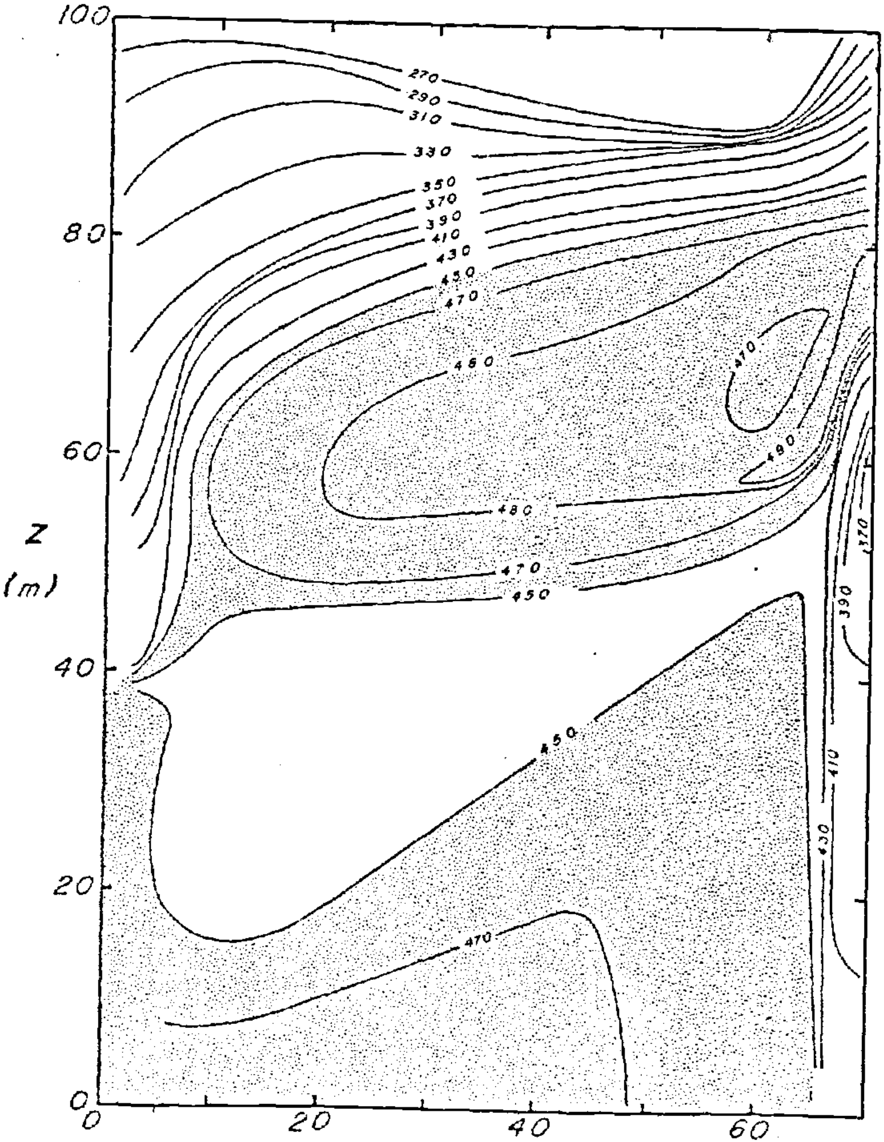

Figure 25b. Time series of particle volume concentration at CTD Station 23. Stippled portion represents particle volume concentrations greater than 450 PPB.

conditions. In fact, where Component I was seen to exist repeatedly over several casts the features of Component II within a given profile changed dramatically over periods of less than one hour. Such drastic fluctuations and variations in the intermediate nepheloid layer are shown in Figure 26 which depicts a similar "time series" of profiles for Station 24.

As discussed previously and as presented in the literature (Weatherly et al., 1980) the bottom nepheloid layer in this region is a cold, murky filament of water. This is seen in the profiles shown in Figures 27 through 29. In agreement with this fact is the observation that the appearance of Component II in the transmission profiles coincides with a drop in temperature in nearly all cases. The most dramatic example of this is shown in Figure 30 which shows the transmission and temperature profiles for Station 41. The near-bottom Component II shows a decrease in transmission of roughly 15% from the immediate value. Consequent with this is a drop in temperature of 25 m°C. Similarly, Figure 31 shows that for Station 24 the intermediate layer centered at 125 meters above bottom is accompanied by a very slightly lower temperature which shows up as a reduction in the adiabatic temperature gradient from roughly 100 m°C/km above the zone to roughly 50 m°C/km within the zone and then back up to 150 m°C/km below the zone. The cold, turbid bottom water breaks up and the detached layer (or layers) are

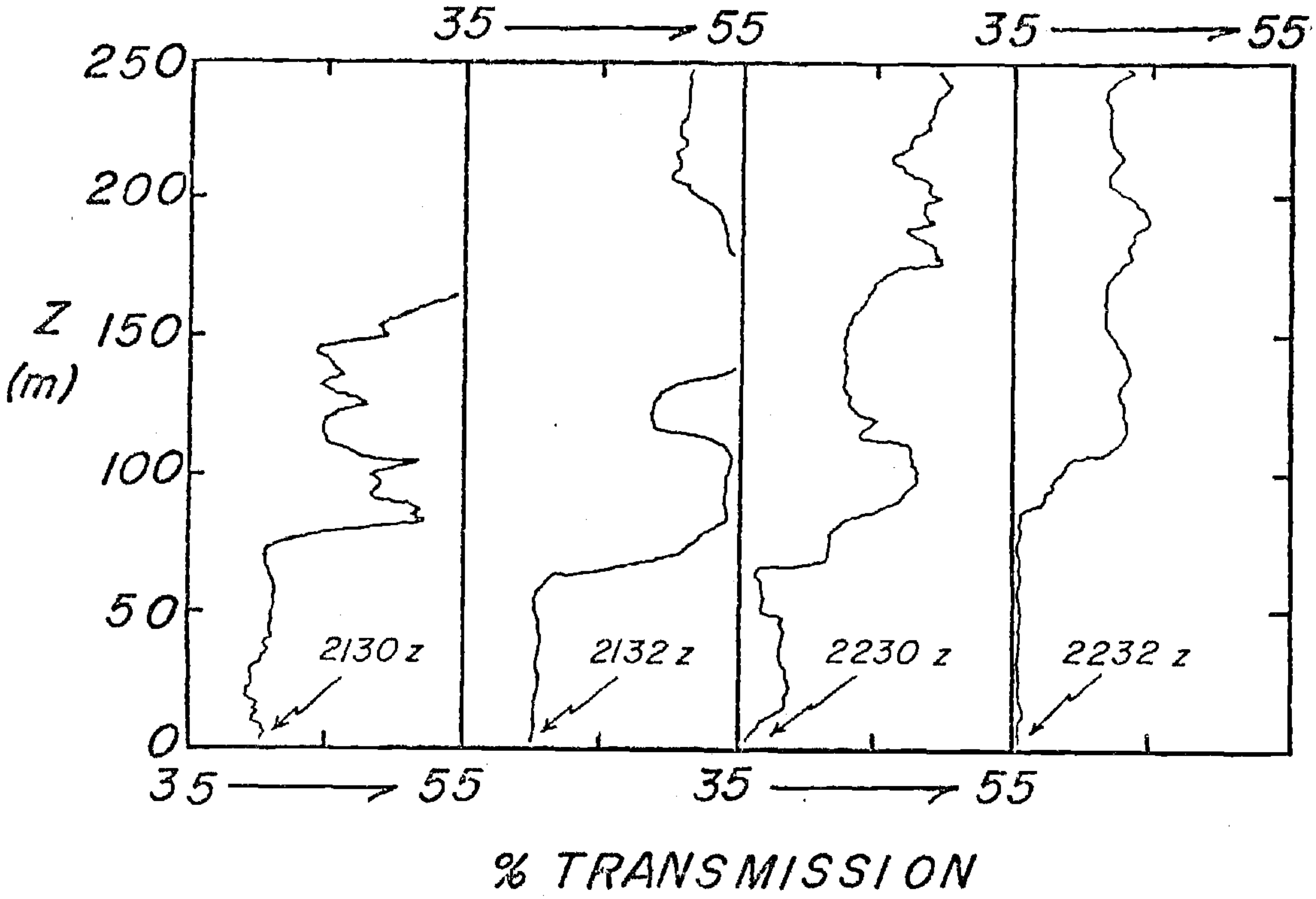

Figure 26. Transmission profiles taken consecutively at CTD Station 24.

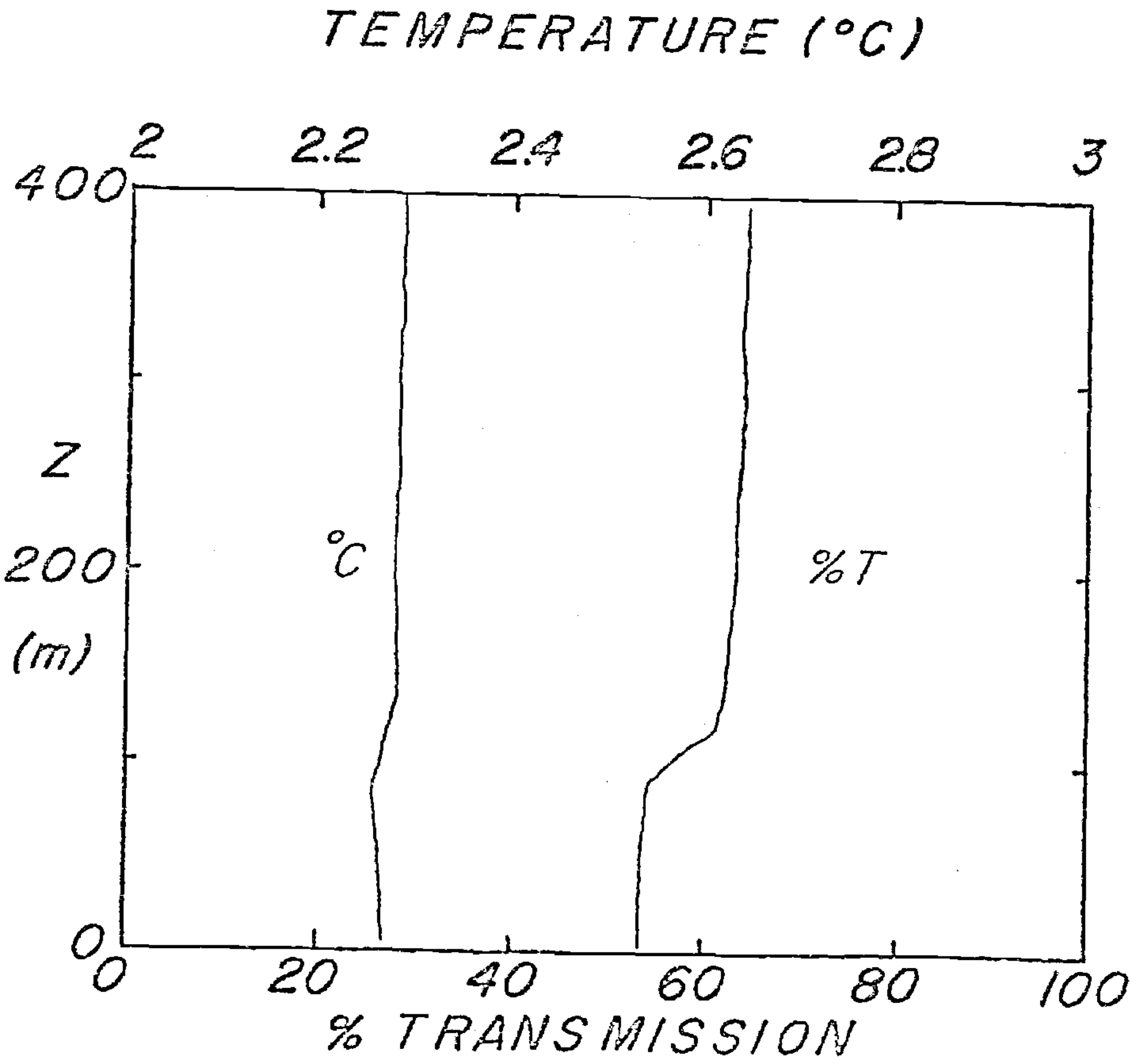

Figure 27. Transmission and temperature profiles taken at CTD Station 8

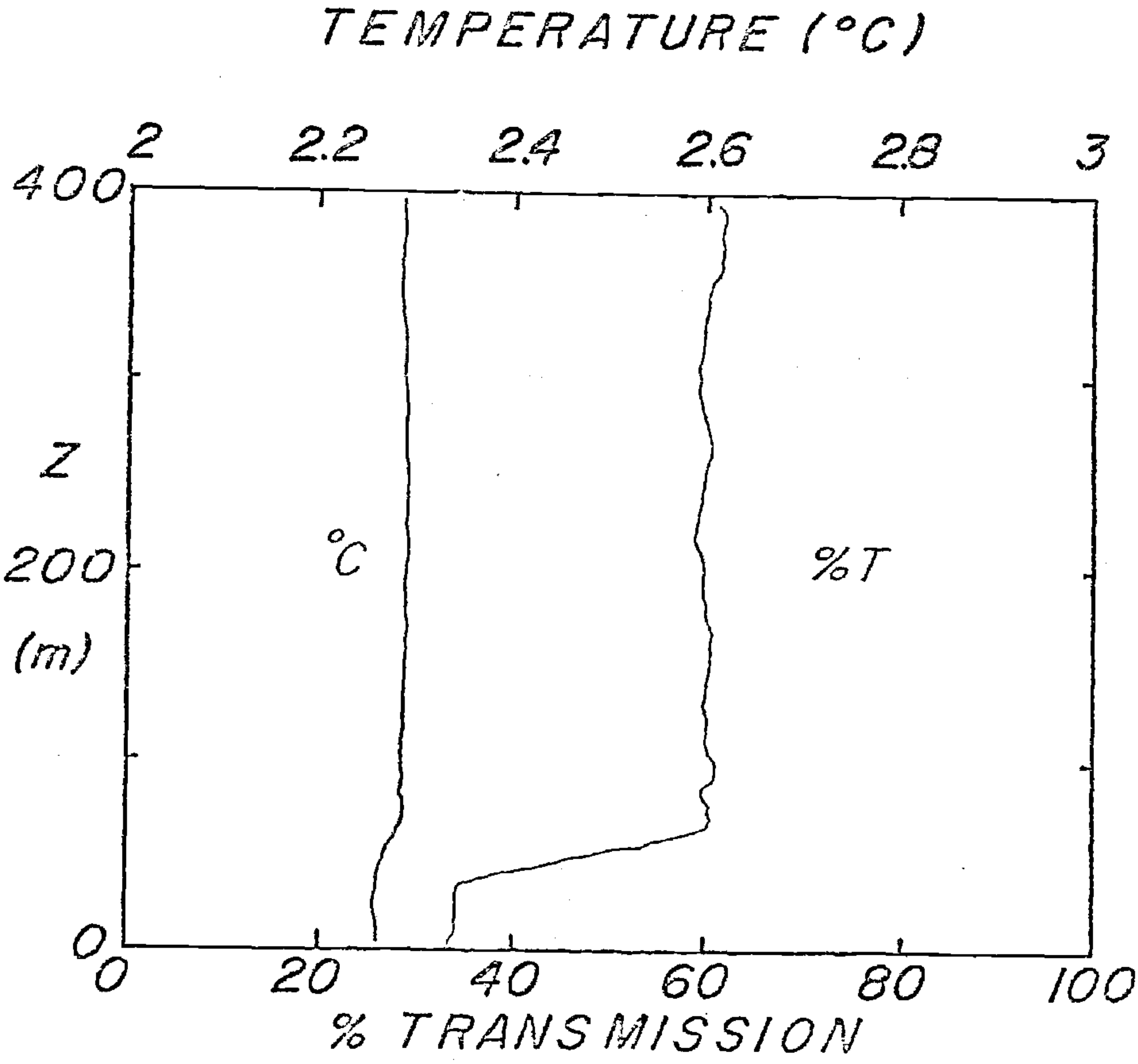

Figure 28. Transmission and temperature profiles taken at CTD Station 19.

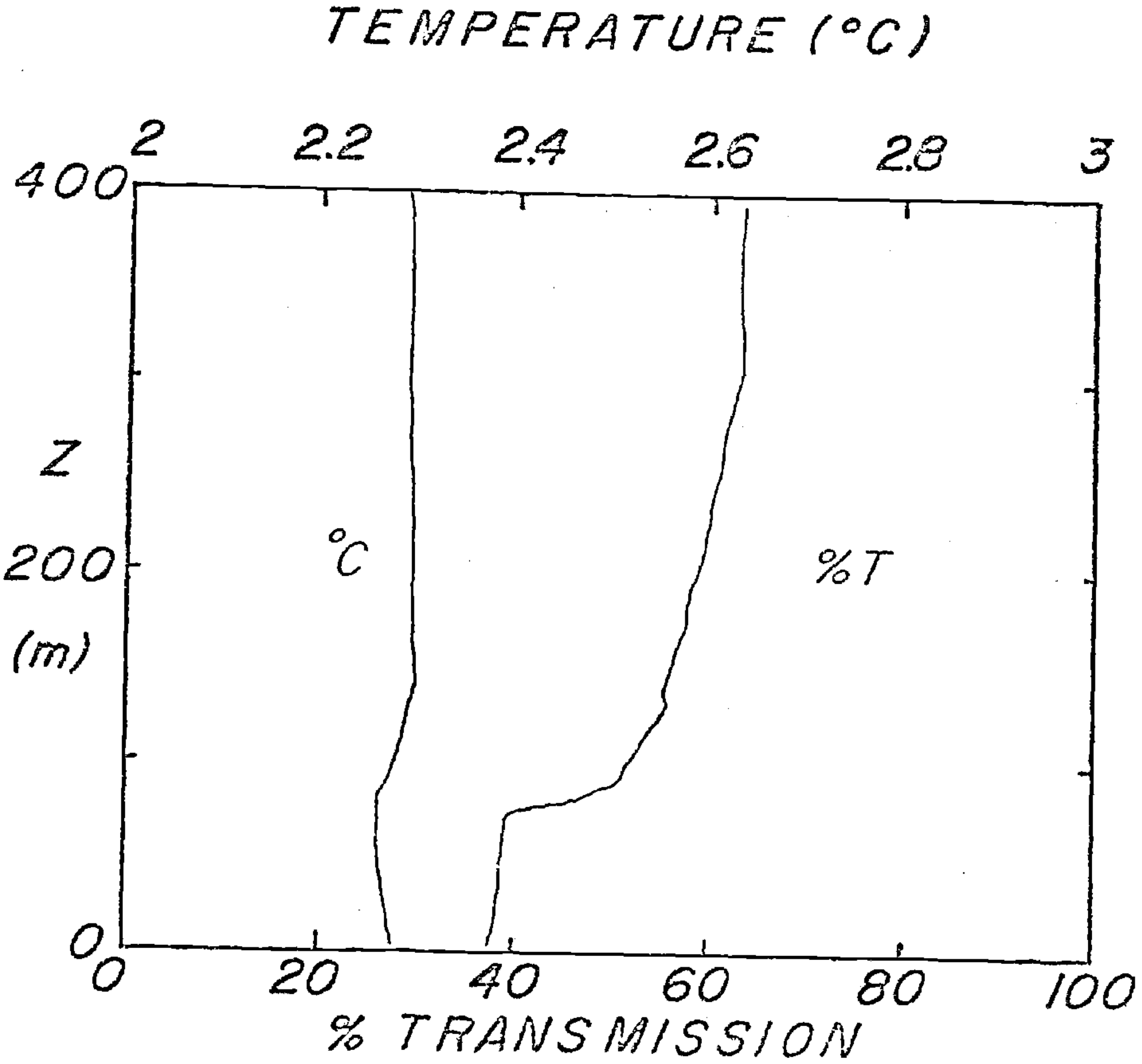

Figure 29. Transmission and temperature profiles taken at CTD Station 40.

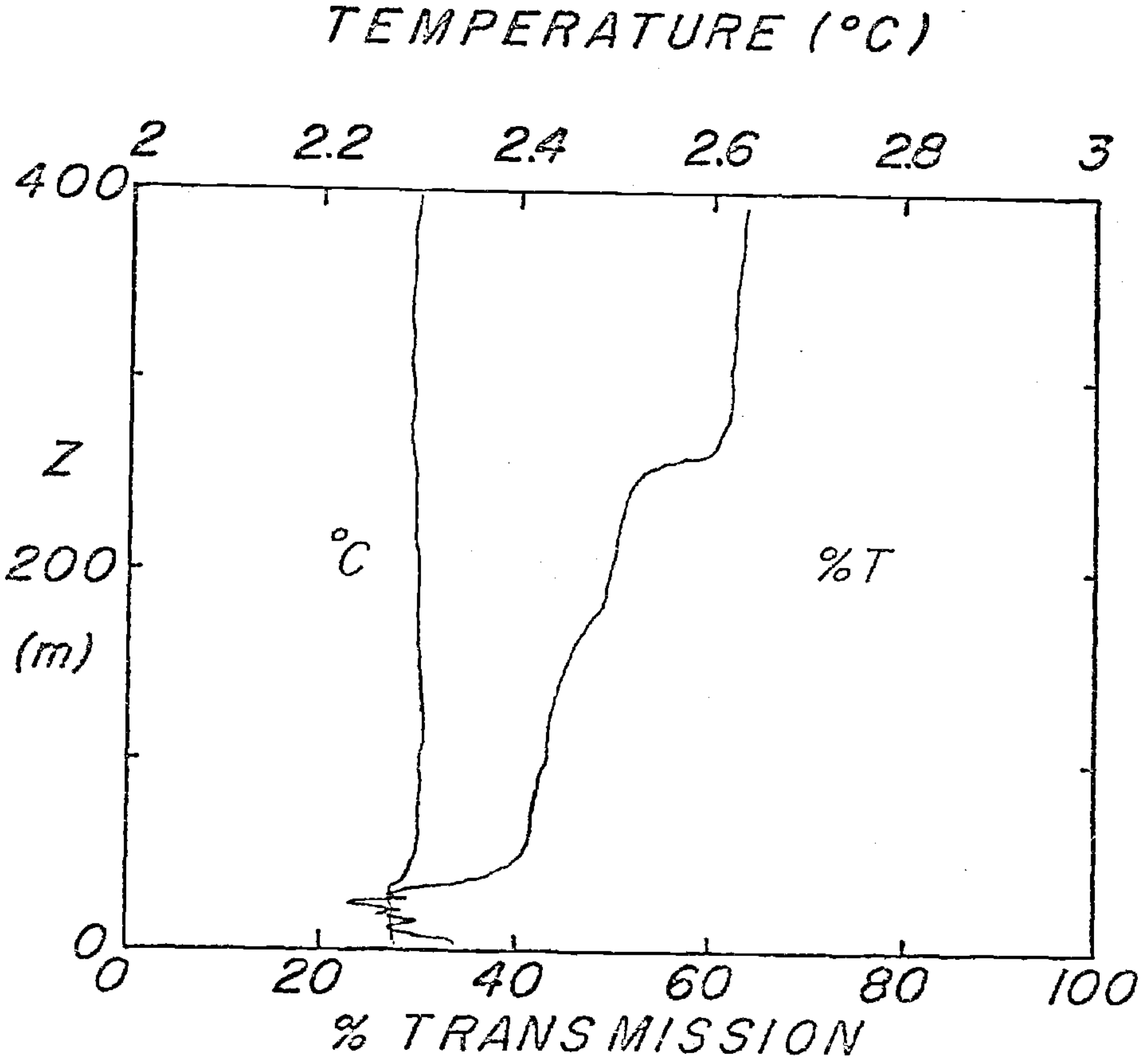

Figure 30. Transmission and temperature profiles taken at CTD Station 41.

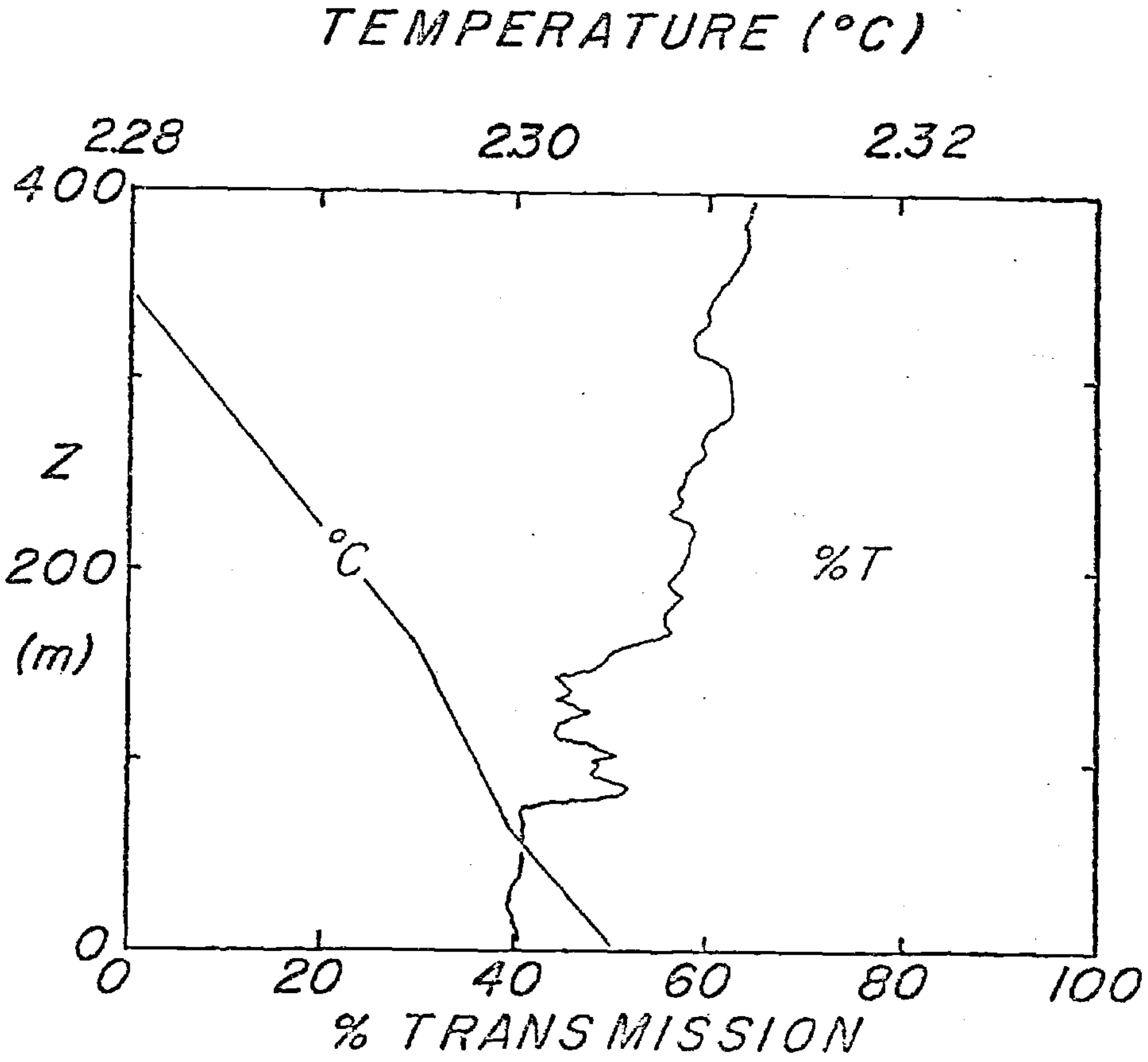

Figure 31. Transmission and temperature profiles taken at CTD Station 24.

seen in both the temperature and transmission profiles at elevations from tens to hundreds of meters above bottom. At Station 23 in which the actual separation of the intermediate layer from the bottom layer was detected optically the temperature profile also shows the time change in structure as the cool water band is seen to rise progressively from the bottom (Figure 32).

iii Components III and V

Component III (exponential) and Component V (logarithmic) are similar in appearance and are representative of the same phenomenon. The difference between the two lies only in the question of which one fits a particular transmission curve better; Component V fits curves of sharper transmission changes while Component III is characteristic of more gradual variations in transmission.

These two components are never found in the bottommost layer and in most cases they exist just above a linear (i.e., Type I) component. They represent the continuous transition from turbid to clear water. The vertical extent of these components is widely variable from thickness of 31 meters at Station 41 to a thickness of 275 meters at Station 27. The general physical process represented by these components is one of vertical mixing and entrainment of the cold, turbid benthic boundary layer. In fact these components actually represent the

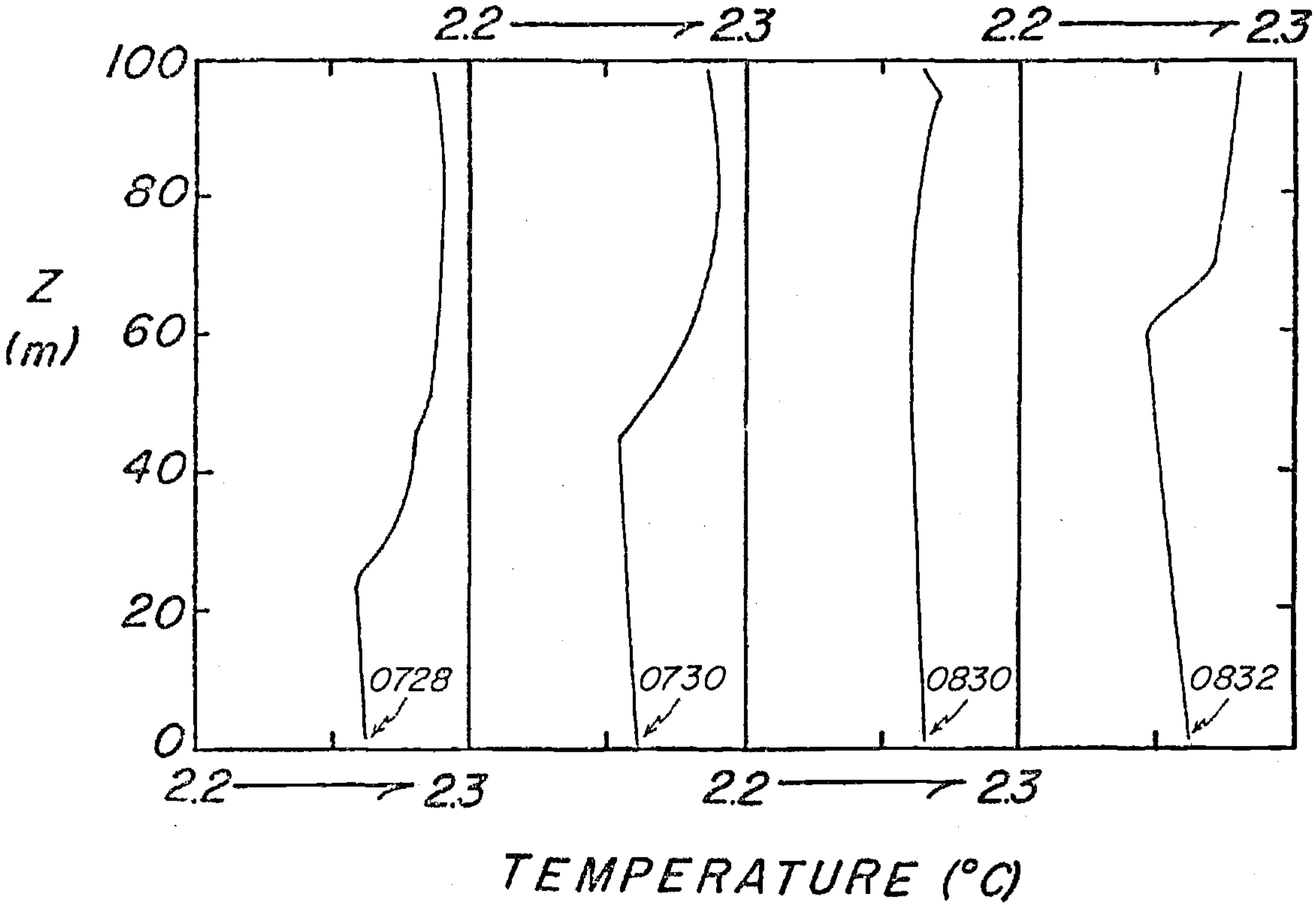

Figure 32. Temperature profiles taken consecutively at CTD Station 23.

boundary effects of the diffusion-settling model described previously for Component I.

Consider a system defined by a well contained benthic flow bound on one side by the bottom and on the other side by a zone of near-infinite shear. Figure 33 demonstrates how the theoretical particle concentration (and transmission) profile would appear in such a case. In actuality the system is one in which the upper boundary is <u>not</u> characterized by infinite shear and consequently a degree of shear-induced instability causes turbulent diffusion of particles upward into the water column. The system then takes on the qualities as outlined in the diffusion-settling model discussed previously (Shepard, 1963). With increased interaction between the lower and upper layer the particle concentration takes on the appearance of the profile shown in Figure 34. Raudkivi (1967) has shown that by varying the ratio of the relative magnitudes of settling velocity and eddy diffusion one can obtain particle concentration profiles which agree in appearance with those I have called Components III and V. Figure 35 shows the agreement between the profiles of Raudkivi (1967) and the profiles I have obtained for each of these two components. The exponents indicated on the plot are the values of the term

$$\frac{W_s}{ku_*}$$

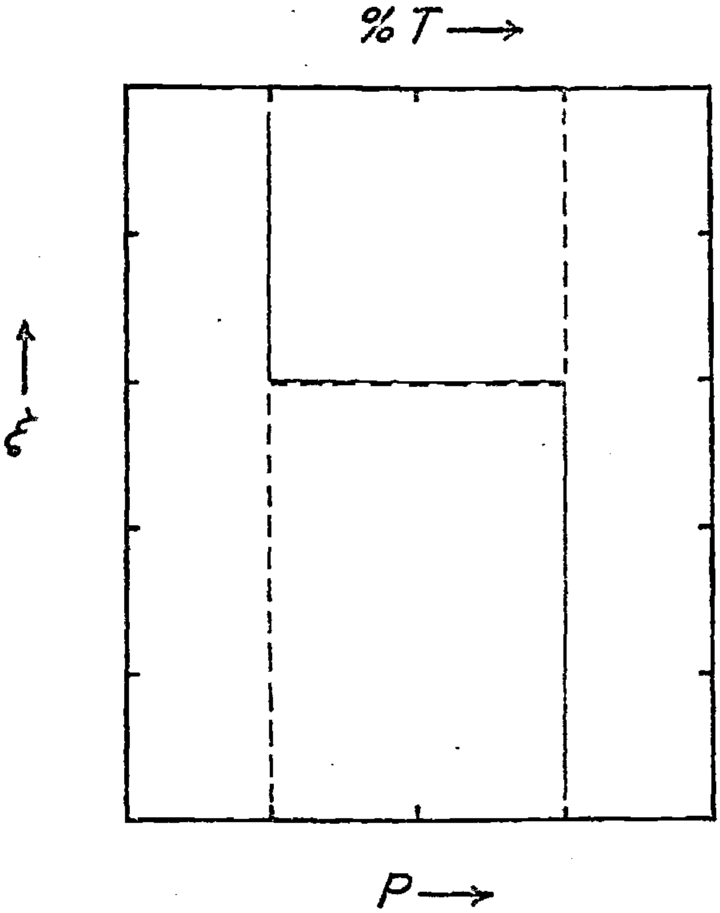

Figure 33. Theoretical particle concentration, P (solid line), and transmission (dashed line) profiles for ideal, infinite-shear flow.

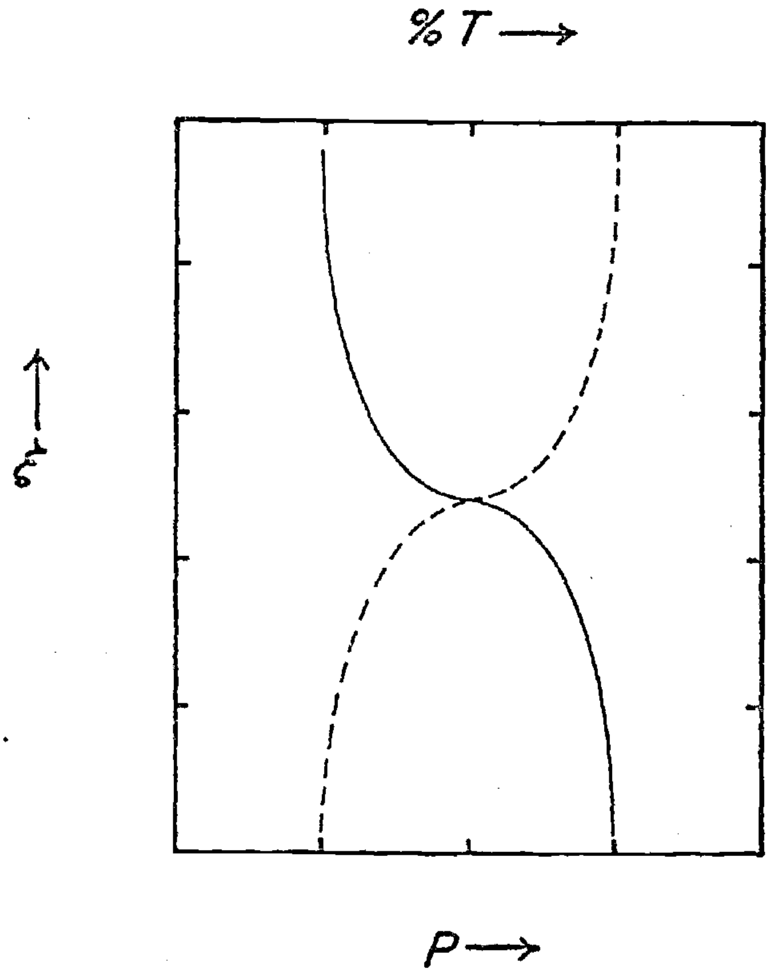

Figure 34. Actual representation of particle concentration, P (solid line), and transmission (dashed line) in system of bounded flow.

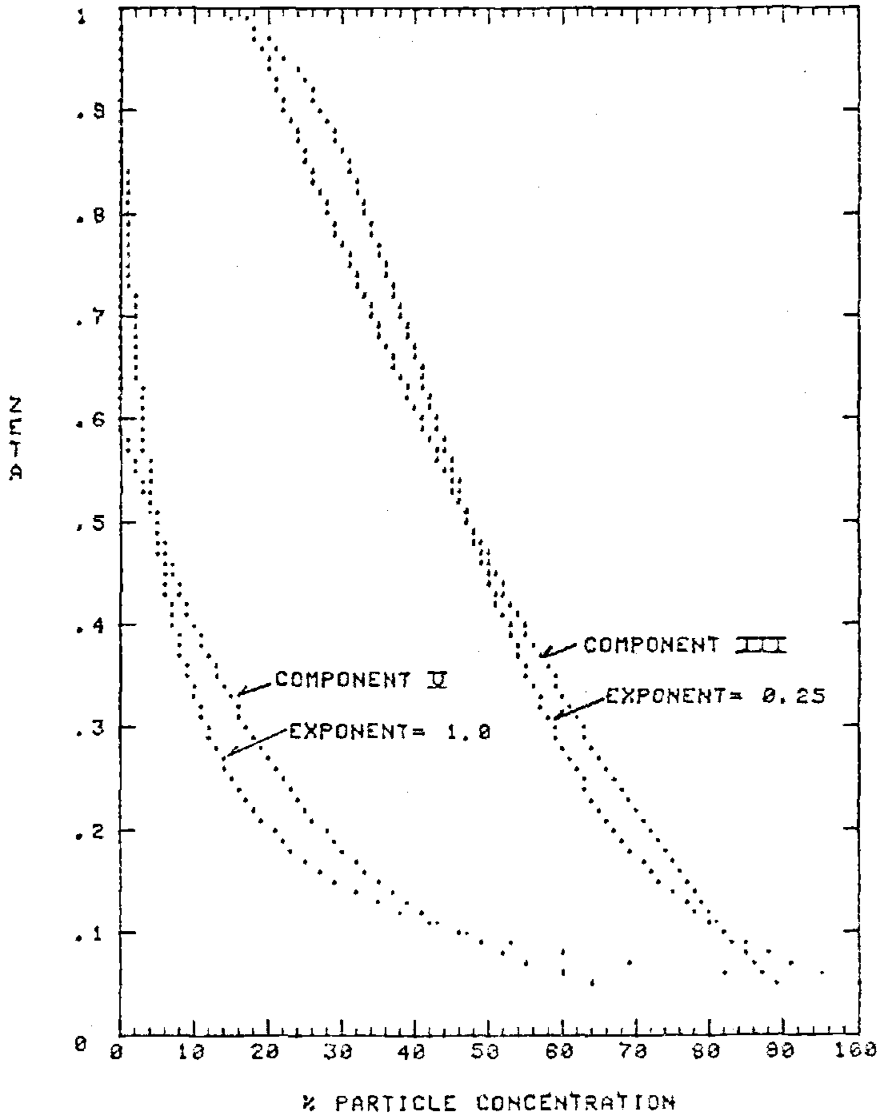

Figure 35. Comparison of profiles obtained using Raudkivi's (1967) diffusion-settling model and the component model of transmission.

where W_s = particle settling velocity

k = von Karman's constant ($\cong$ 0.40)

u_* = shear velocity defined by $u_* = \sqrt{\frac{\tau}{\rho}}$, with τ being the fluid stress and ρ the fluid density.

The figure shows that at low values of the exponent the use of Component III (with coefficients of A = 0.082 and B = 0.709) produces a particle concentration profile that is compatible to within a standard error of 3.4%. A standard error of 6.0% is found between Component V (A = 0.641; B = 0.027) and the curve for an exponent of 1.0. It is thus clear that Components III and V represent a similar type of diffusion-settling model as described by the diffusion-settling model of Raudkivi (1967). The point at which either Component III or V provides a better fit to the diffusion-settling model is not clear but it seems to occur when the value of the exponent is approximately 0.6. The source of most of the error between the components and the diffusion-settling model lies in the regions nearest the top and bottom. The diffusion-settling model tends to show a sudden drop in particle concentration near the top and an exaggerated increase in particle concentration near the bottom. These features of the model do not agree as well with the features of the profiles seen in the HEBBLE area as do the profiles obtained using Components III and V. The source of this error lies in mixing effects at the boundaries between two components.

iv) Component IV

Component IV only occurs at a very few stations and the physical explanation for it is not obvious. When the feature occurs it is characterized by uniform transmission increases and decreases on the order of 1% to 2% over a vertical distance of approximately five meters. The altitude of a particular maximum or minimum of transmission may vary over a short period of time (Figure 36). This indicates that the phenomenon is not a stagnant, sessile lamination of clean and turbid water layers. There are no concurrent anomalies in the temperature profile to indicate anything other than a uniform water mass within the zones described by Component IV. These zones are roughly 70 to 100 meters thick and they are limited to regions where the transmission is roughly between 35% and 50% (turbid, but not exceptionally so). The probability of machine error as the source of Component IV is questionable due to a number of considerations. The form of Component IV in all cases is not as uniform as would be expected from a systematic malfunction. The component only appears in several stations; these are stations which, in all other respects (temperature, pressure, turbidity, salinity), are similar to many other stations. Consequently, one must ask why the feature is

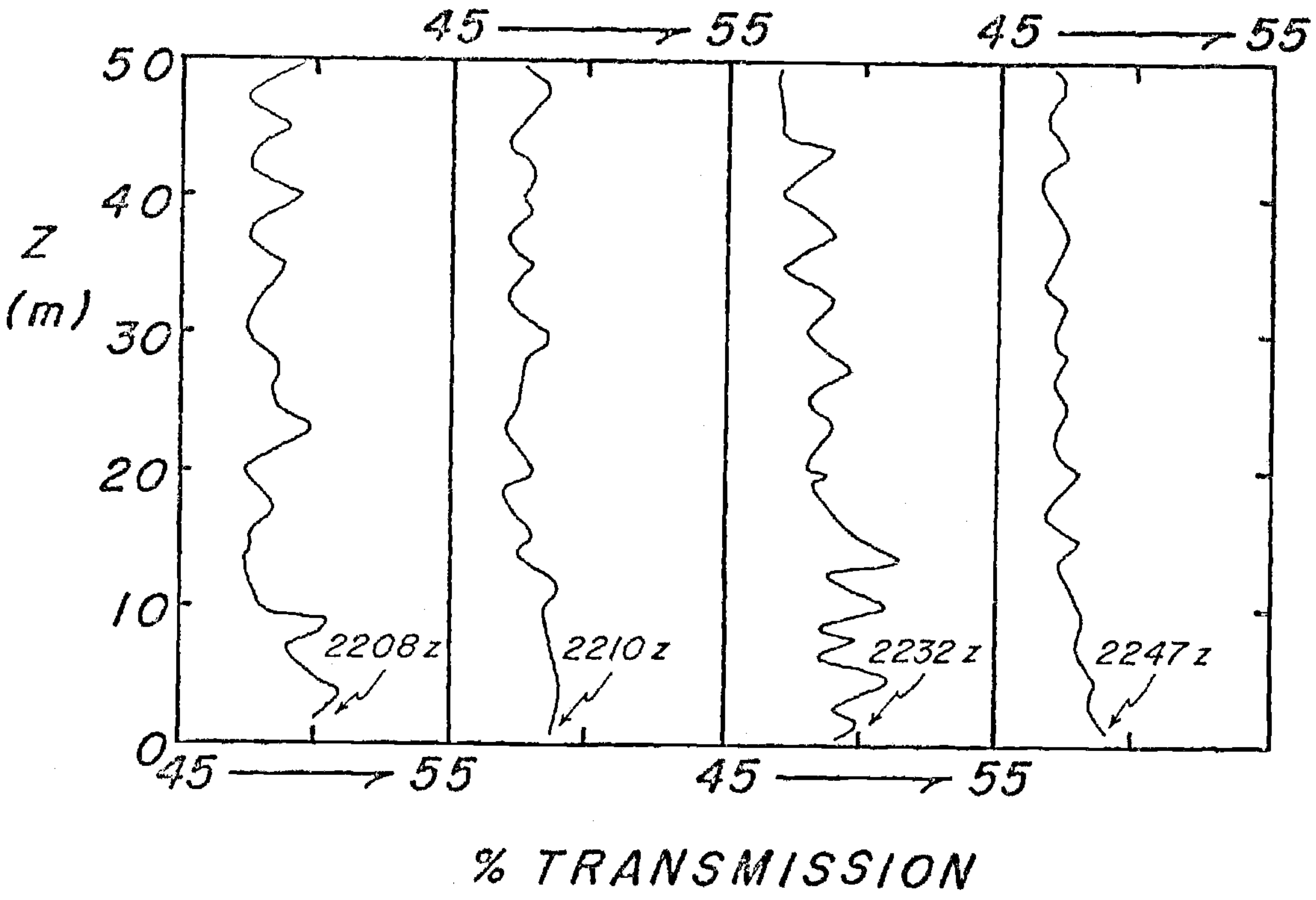

Figure 36. Consecutive transmission profiles in bottom 50 m of CTD Station 44

seen so infrequently. Finally, in one slightly shallower station (CTD Station 34; bottom depth 4880 m) Component IV was detected on the first downcast, the first upcast, and the second downcast. However, on the second upcast the turbidity was greatly decreased (from a minimum of 32% - 35% on the three earlier casts to a minimum of 53%) and Component IV was no longer present (see Figure 37). The fact that Component IV exists in conjunction with the three turbid casts and not with the fourth cleaner one indicates that the phenomenon is not a consequence of machine error. There are indications, however, that the phenomenon may be a figment of the trajectory of the instrument. The path of the instrument through the water column may, in fact be the explanation behind the appearance of these apparent particle laminae.

The original data tapes for Station 37 were re-processed and plots of pressure and transmission vs. time were composed. As the instrument is raised or lowered through the water column pressure changes detected by the instrument are not always even and smooth with time. This is a consequence of a variety of processes including shifting wire angle, ship roll and "kiting" of the instrument package. Figure 38 shows the "step-like" increase in pressure near the bottom as the transmissometer was lowered at Station 37. A coherent transmission signal is seen to fluctuate in phase with the plot of pressure changes. Pressure fluctuations are seen to be

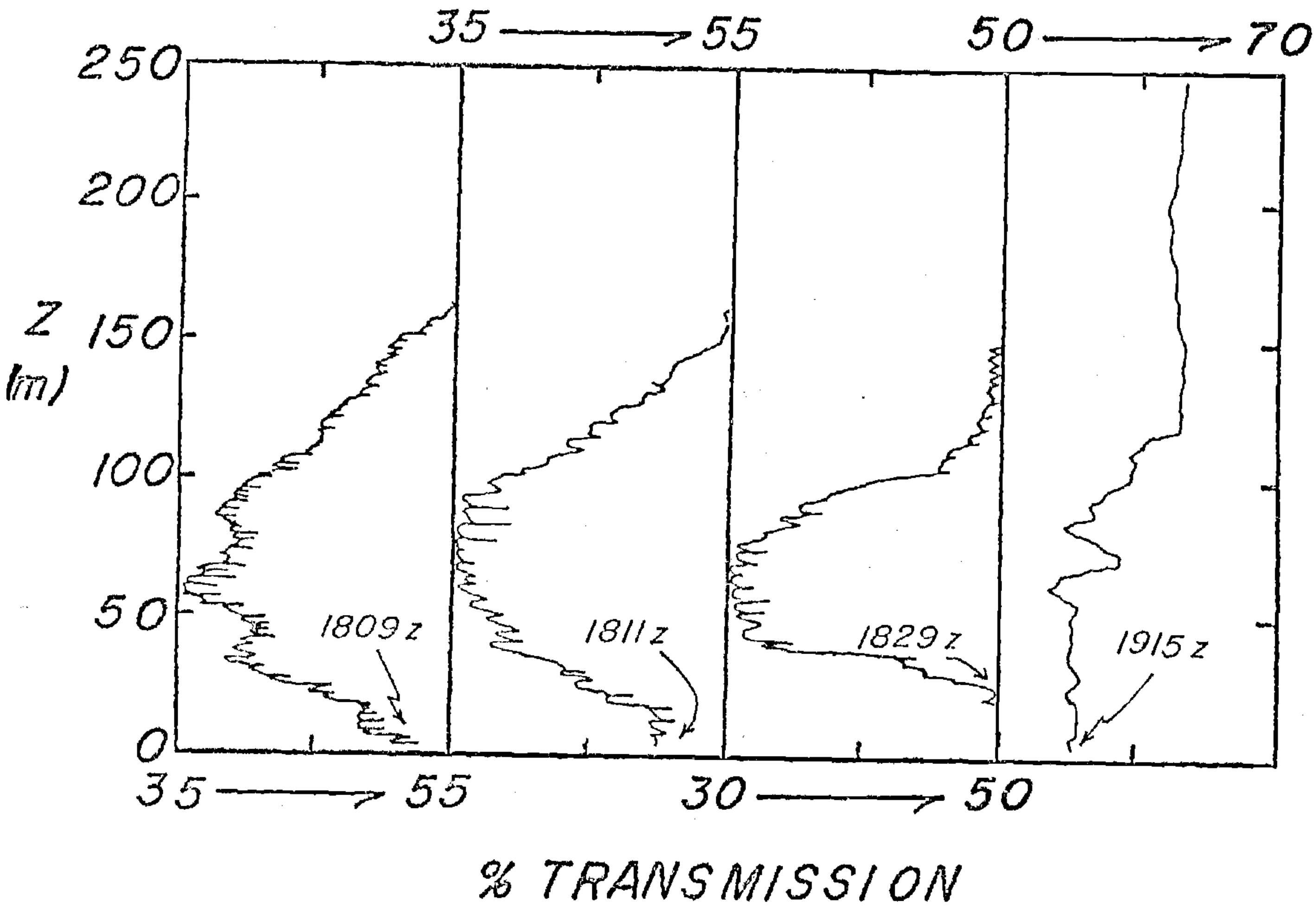

Figure 37. Consecutive transmission profiles at CTD Station 34.

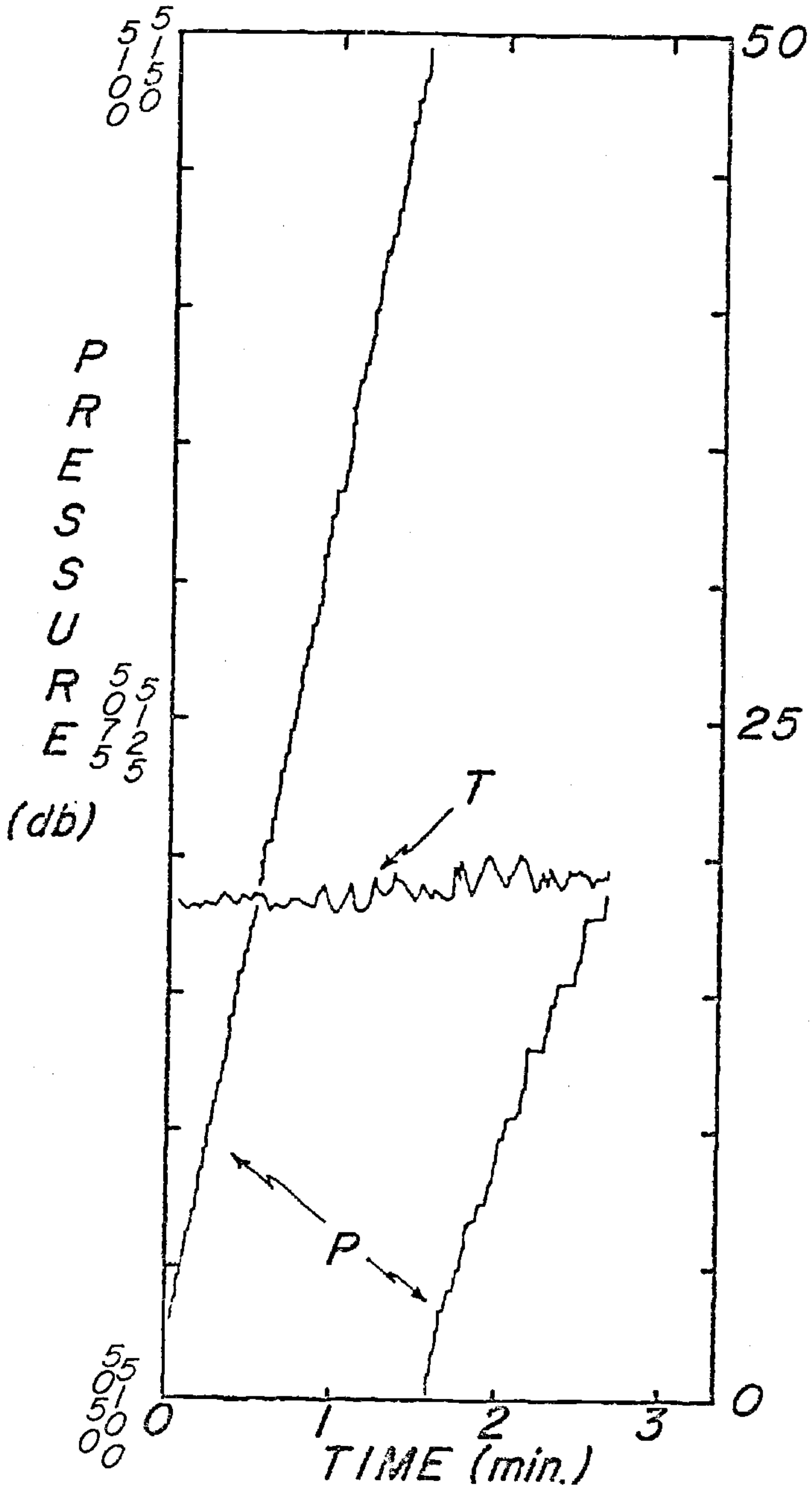

Figure 38. Time series of pressure and transmission changes near the bottom at CTD Station 37 during downcast

minimal from 5050 db (0 sec) to roughly 5080 db (55 sec). The same is true of transmission fluctuations. Below 5080 db, however, pressure and transmission exhibit coinciding steps and peaks respectively. Figure 39 shows that the duration of time spent at a specific pressure (i.e., a "step") is proportional to the magnitude of the transmission peak. For example at a pressure of 5078.5 db (time = 4 sec) the corresponding transmission profile shows an increase of 1% while the pressure remained virtually unchanged for roughly two seconds. Later (time = 61 sec) at a pressure of 5107.5 db the pressure remained unchanged for over four seconds and the transmission showed an increase of 1.5%. This same pattern is also shown in Figure 40 which shows the time profile of pressure and transmission during upcast at Station 37. Steps in pressure are not as pronounced in the upcast as in the downcast due to the fact that more tension is held on the wire to raise the instrument. Consequently, as just explained, with less prolonged pressure "stepping" the transmission peaks should be less significant and in fact this is shown by the figure. While there are exceptions to this trend, in general the more prolonged the "stepping" in pressure, the greater the magnitude of the Component IV transmission.

The concept of debris clinging to the frame of the instrument and periodically being dragged into and out of the light path must be discarded for several reasons.

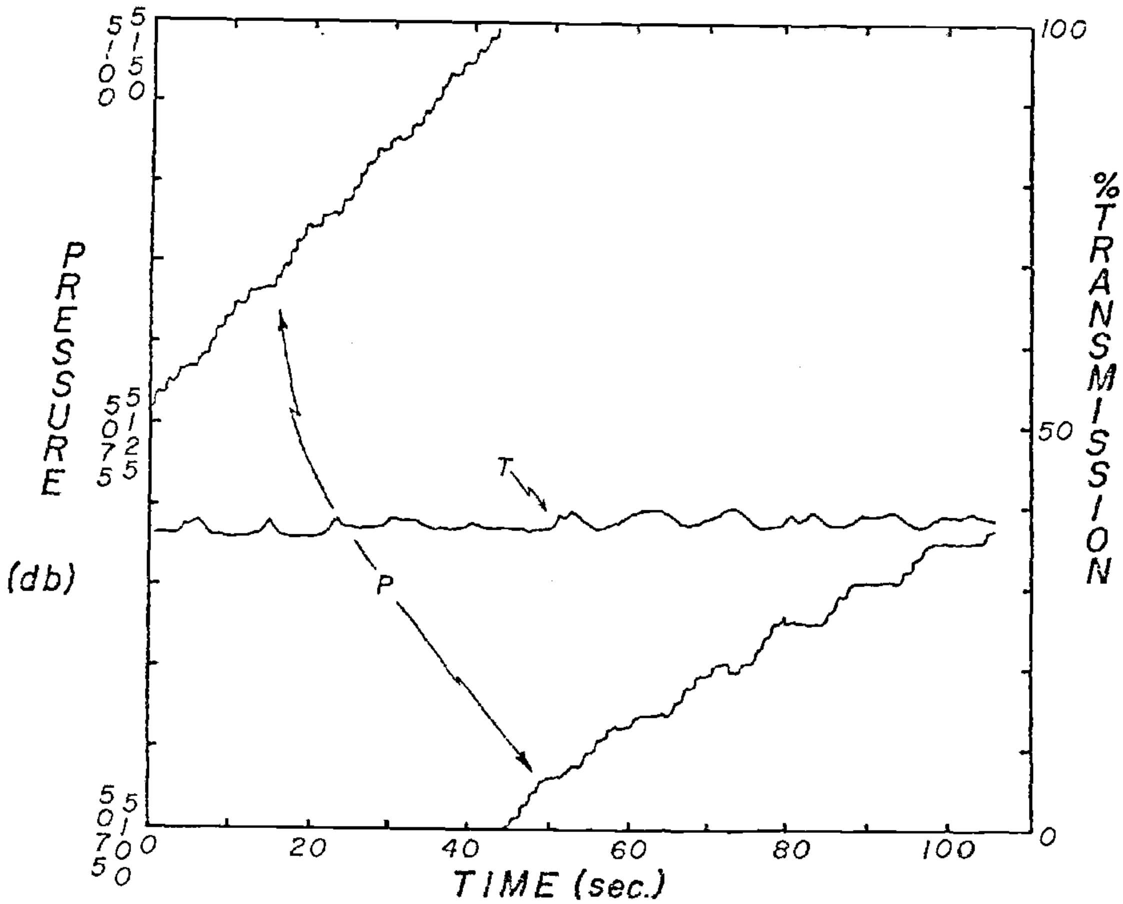

Figure 39. Time series (expanded time scale) of pressure and transmission near the bottom at CTD Station 37 during downcast

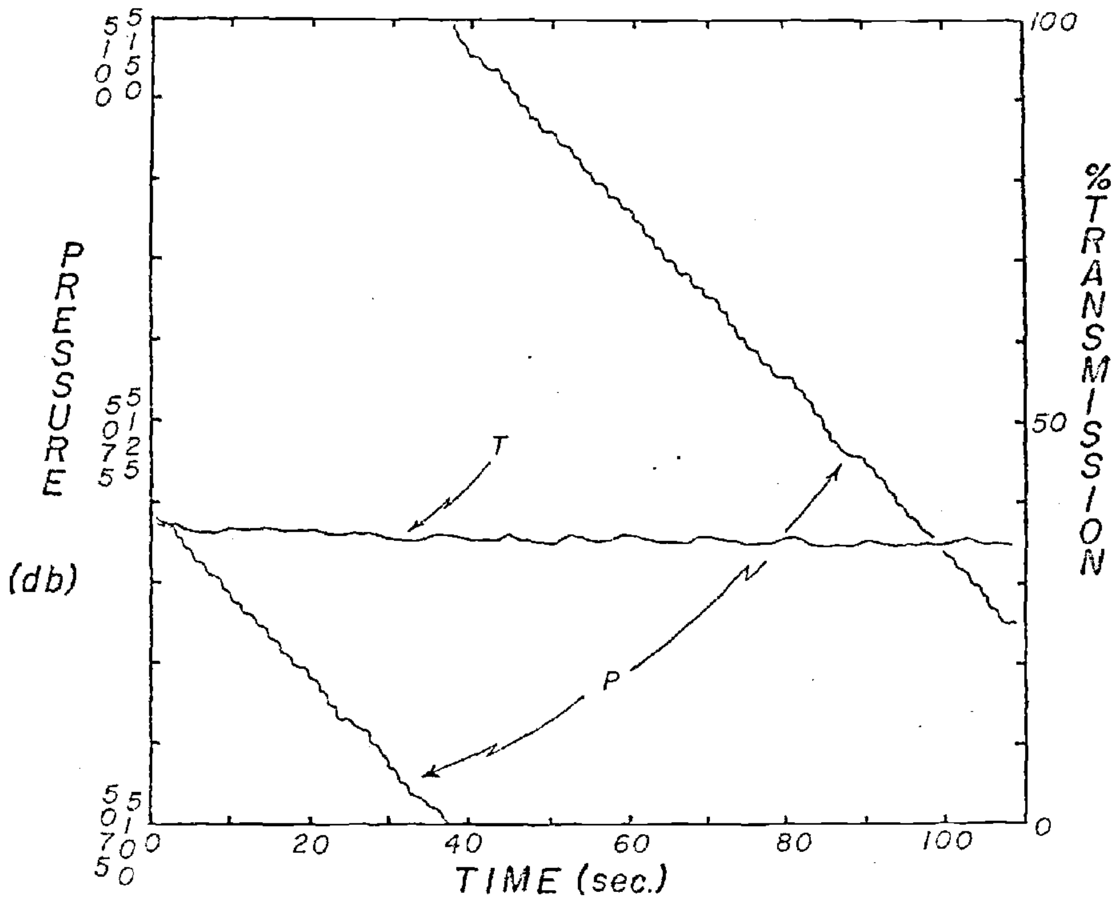

Figure 40. Time series (expanded time scale) of pressure and transmission near the bottom at CTD Station 37 during upcast.

Firstly, the altitude of appearance and disappearance of Component IV in successive upcasts and downcasts is consistent. It is highly improbable that strands of debris would continually deposit themselves and remove themselves at the same exact depth. Secondly, any debris capable of becoming snared on the instrument would most likely be large enough to induce a transmission fluctuation of significantly more than 2%. Lastly, if a strand of debris were snared on a portion of the transmissometer the correlation of pressure steps and transmission peaks would be reversed on the up- and down-casts. If debris were snagged above the instrument then transmission *minima* would be detected *at* the pressure steps on the downcast and *between* the pressure steps on the upcast due to the material settling into or being dragged through the light path in each respective case. The reverse would hold if the debris were located just below the transmissometer. However, the correlation of pressure steps and transmission maxima is the same for the upcasts and downcasts, so there cannot be debris causing these periodic transmission peaks.

A more likely explanation is that the profiles were made in or near the wide trailing edge of a benthic "cloud". This explanation requires periodic horizontal and vertical displacement of the instrument; a process explainable by "kiting" of the instrument due to ship roll combined with wire descent or ascent. From the preceding figures one can discern that the period of the fluctuations seen in both the transmission and pressure profiles is very close to eight seconds. From Airy wave theory it is found that an eight second deep water wave can develop a maximum vertical velocity of 100 cm/sec (or 60 m/min, which was the lowering rate used on the winch in these sections of the profiles) if the wave height is roughly 2.5 m. This implies that for a reasonable wave condition the instrument package will be subject to equal downward and upward velocities every eight seconds and thus will remain stationary at those times. In addition it implies that four seconds after the instrument stops it will be moving at roughly 200 cm/sec up (during upcast) or down (during downcast). The actual system is not likely to be so precise as to bring the instrument to a standstill every period but with reasonable wave conditions (in fact 2.5 m wave height were quite common during this research) the instrument is apt to periodically slow considerably as evidenced by the previous figures. This surging of the instrument may result in extensive "kiting": vertical descent coupled with small but significant horizontal deviation. If the turbid cloud through which the transmissometer is being lowered is not uniform horizontally then one would expect transmission peaks as seen. Such would be the case at the trailing edge of a benthic cloud. Figure 41 shows a simple example of how a "kiting" instrument would yield

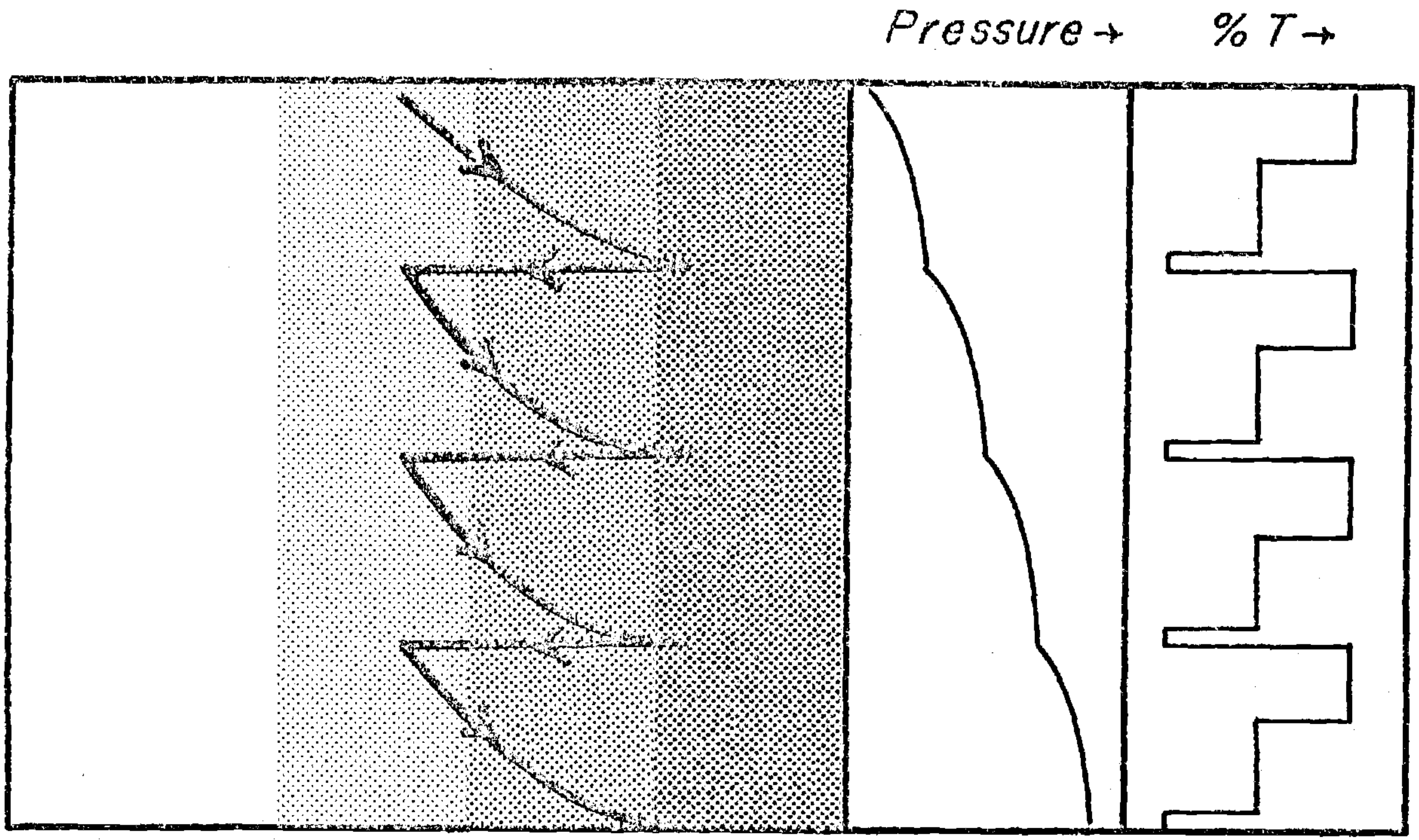

Figure 41. Simplified illustration of how horizontal kiting could induce the type of pressure and transmission changes detected .

the type of pressure and transmission profiles that are described by Component IV. This system is consistent with other data coexistent with Component IV. The sudden disappearance of the turbid zone in Station 34 (Figure 37) is consistent with the concept of a trailing edge of a benthic cloud: the first three profiles were made within the cloud, near the edge, and the fourth profile was made outside the cloud. The fact that Component IV appears at the same altitude, repeatedly, is explained by the fact that the cloud itself only exists to that altitude. Component IV also only exists in water of transmission 35% to 50%. As mentioned previously this represents water which is not excessively turbid or clear. It stands to reason that within the trailing edge of a benthic cloud the turbidity would be moderate or transitional.

The extent of "kiting" required in order for the instrument to detect a 1% to 2% change in transmission depends on the horizontal gradient of particle concentration within the cloud as well as the velocity of the cloud relative to the instrument. A change in transmission of this magnitude represents a change in volume concentration of only about 25 PPB at a transmission of 40% per meter. Horizontal particle gradients can be inferred from measurements of transmission made over time with the stationary Bottom Ocean Monitor (BOM). Unfortunately, current meter data are unavailable for the same time and location. However, it is found from the BOM data that if the velocities are slow ($\sim 10 \frac{cm}{sec}$) at the trailing edge then the profiling transmissometer would detect changes of 1% to 2% if it were to "kite" through approximately one to two meters of water horizontally (normal to the front). Considering that the average ship drift velocity during a CTD cast was on the order of 10 $\frac{cm}{sec}$ to 20 $\frac{cm}{sec}$, then an instrument being lowered from the ship could easily move horizontally a meter or two in a matter of five to ten seconds.

To positively identify this outlined process as being the driving force behind the appearance of Component IV would require extensive measurements with moored and profiling transmissometers as well as current meters and possibly even wave measuring instruments. However, careful consideration has yielded this process as being the only one that is consistent with all the data and evidence available.

C. Compatibility of the Component Model with the Equations of Mass Conservation

As shown previously for several components the component model yields particle profiles that can be made to conform well with profiles obtained from a simple diffusion-settling model. In the previous section however, the term $\frac{w_s}{ku_*}$ was specified and the component model was adjusted to fit the curves obtained. It will now be shown that for the actual profiles of transmission obtained at sea, values of $\frac{w_s}{ku_*}$, obtained independently, agree well with the values determined from other techniques. This verifies the compliance of the component model with the simplified equation of vertical mass conservation.

If we assume that the water column may be divided into a series of infinitely small volumes of dimensions dx, dy, dz, and if we assume that within each volume there is transfer of particulate matter but there cannot be spontaneous creation or destruction of material, then the conservation of suspended mass within a given volume is expressed as:

$$\begin{aligned}\frac{\partial P}{\partial t} + \frac{\partial}{\partial x}(uP) + \frac{\partial}{\partial y}(vP) + \frac{\partial}{\partial z}([w-w_s]P) \\ = \frac{\partial}{\partial x}\left(K_x \frac{\partial P}{\partial x}\right) + \frac{\partial}{\partial y}\left(K_y \frac{\partial P}{\partial y}\right) + \frac{\partial}{\partial z}\left(K_z \frac{\partial P}{\partial z}\right)\end{aligned} \tag{14}$$

(See, for example, Smith, 1977.)

where u = velocity in the + x direction (cm/sec)

v = velocity in the + y direction (cm/sec)

w = velocity in the + z (up) direction (cm/sec)

w_s = settling velocity of the particles (cm/sec)

K_x, K_y, K_z = eddy diffusion coefficients in the x, y and z direction (cm^2/sec).

In actuality, with the z-axis oriented positive upward the vertical velocity term in Equation (14) should be $w+w_s$. However, w_s is always directed downward and rather than expressing the settling velocities in the text as negative values the vertical velocity term in Equation (14) is expressed as $w-w_s$, with the settling velocities given as positive numbers.

Equation 14 expresses the conservation of suspended mass as a balance of horizontal and vertical advection with eddy diffusion. That is, a given volume observed may undergo a decrease in particle concentration at that location or an increase in particle concentration. If one assumes an initially clean system then the question becomes: what type of flow could displace the particles so that they distribute themselves as seen in any given instantaneous transmission profile? Or, what kind of sediment transport system exists which could yield particle distributions as detected? Transmissometer profiles give good representations of concentration as a function of depth but not of either x or y. For this reason it is only valid to compare the vertical component of the mass conservation equation with results obtained from the transmissometer. The vertical continuity equation is given by

$$\frac{\partial P}{\partial t} + \frac{\partial}{\partial z} \left([w-w_s]P \right) = \frac{\partial}{\partial z} \left(K_z \frac{\partial P}{\partial z} \right) \qquad (15)$$

Long-term measurements of transmission by the moored Bottom Ocean Monitor have shown that at time the HEBBLE area may be considered a highly variable (temporally) zone while at other times a steady state prevails. The repeated vertical profiles of transmission made at many stations indicate that at roughly 80% of the stations

$$\frac{\partial P}{\partial t} << \frac{\partial}{\partial z} ([w-w_s]P)$$

This statement does not define the situation as necessarily being steady state. It actually states that for a majority of stations temporal changes are much smaller than the vertical gradients of concentration. Exceptions to this were stations like Station 23 where large temporal changes were detected. Thus, for a scaling analysis or an order-of-magnitude solution, Equation (15) may generally be simplified to

$$\frac{\partial}{\partial z} ([w-w_s]P) = \frac{\partial}{\partial z} (K \frac{\partial P}{\partial z})$$

In addition, if one assumes a horizontal bottom with negligible vertical velocity then the simplified vertical sediment mass conservation equation is:

$$\frac{\partial}{\partial z} (-w_s P) = \frac{\partial}{\partial z} (K \frac{\partial P}{\partial z}) \qquad (16)$$

This expression is actually the classical equation of balanced particle settling and diffusion (see for example, Shepard, 1963, or Raudkivi, 1967). Advective effects are included in the form of the eddy diffusion coefficient, K, used in this experiment. This, in fact, is where the existing models of sediment transport vary.

Essentially, K is a function of the magnitude of the shear stress in the flow, and the location within the flow. That is, $K = K(u_*, z)$.

The most basic form of K is given by

$$K = ku_*z \tag{17}$$

where k = von Karman's constant ($\cong 0.4$).

A much safer approach to modeling is taken when no assumptions are made about the form of the eddy diffusivity, K. In this case Equation (16) is integrated over z to give

$$-w_s\ P = K\frac{\partial P}{\partial z} \tag{18}$$

or

$$\frac{w_s}{K} = -\frac{1}{P}\frac{\partial P}{\partial z} \tag{19}$$

By considering a flow of thickness, h, and using the previously defined value of ξ (= z/h) then the above equation becomes

$$\frac{w_s}{K} = -\frac{1}{h}\frac{P'}{P} \tag{20}$$

where $P' = \frac{\partial P}{\partial \xi}$.

This equation represents a very simplified form of the diffusion equation. The simplicity of this model lies in the fact that one does not need to know the concentration at a reference level, nor the height of the viscous sublayer (i.e., the roughness length); the classical solution of Equation (9) was described earlier with regard to Components I, III and V and it is given by

$$\frac{P}{P_0} = \frac{z}{z_0}^{-w_s/ku_*} \qquad (21)$$

where P_0 is the concentration at the reference level given by the height of the viscous sublayer, z_0, and $K = ku_*z$.

By using Equation (20) the profiles of light transmission will provide values of $\frac{w_s}{K}$ without any assumptions concerning the shape of the profile of $\frac{w_s}{K}$. In fact, the purpose of this section is just to show that the values of $\frac{w_s}{K}$ obtained in this manner are similar to values obtained using more conventional instruments such as current meters and bottle samples.

Using the equations for P and P' outlined in Section A of this chapter and the coefficients as specified in Table I values of $\log \frac{w_s}{K}$ can be obtained. With reasonable estimates of the value of w_s, the value of K, the eddy diffusion coefficient can be obtained and compared to results from other techniques.

The settling velocity of a particle size distribution must, by definition, also be a distribution itself. However, by considering the particle size distribution as having a single-valued flux and a single valued mass concentration then a unique settling velocity is obtained

(Peterson, 1978). This settling velocity is termed the "concentration-weighted settling velocity" (CWSV) and this is what the value of "w_s" equals in Equation (20). The CWSV may be determined by considering the equivalence of the vertical continuity equation for a whole particle size distribution and the sum of the vertical continuity equations for each size component within that distribution. That is:

$$\sum_{m=1}^{n} \{\frac{\partial P_m}{\partial t} + \nabla \cdot w_m P_m\} = \frac{\partial P}{\partial t} + \nabla \cdot w_s P \qquad (22)$$

(J. D. Smith, personal communication)

where P_m = volume concentration of the m size component of the distribution

w_m = settling velocity of the m size component of the distribution.

$$\frac{\partial}{\partial t} \sum_{m=1}^{n} P_m + \nabla \cdot \sum_{m=1}^{n} w_m P_m = \frac{\partial P}{\partial t} + \nabla \cdot w_s P \qquad (23)$$

by definition $\sum_{m=1}^{n} P_m = P$

therefore Equation (23) becomes

$$\sum_{m=1}^{n} w_m P_m = w_s P \qquad (24)$$

and

$$w_s = \frac{\sum_{m=1}^{n} w_m P_m}{P} = \frac{\sum_{m=1}^{n} w_m P_m}{\sum_{m=1}^{n} P_m} \qquad (25)$$

Equation (25) indicates that the CWSV, given by w_s, is equal to the ratio of the sum of the individual fluxes to the total concentration. Thus with a measurement of the particle size distribution and assuming spherical particles with Stokesian settling it is possible to determine the CWSV. It is found that for the water samples in the HEBBLE region at the bottom of the water column a mean value of CWSV = $6.25 \times 10^{-3}\ \frac{cm}{sec}$ is found, with a standard deviation of $2.85 \times 10^{-3}\ \frac{cm}{sec}$ (largely due to one measurement of $11.5 \times 10^{-3}\ \frac{cm}{sec}$ at Station 36). A nearly identical value is found for all samples at depths within 100 meters of the bottom ($\overline{CWSV} = 6.52 \times 10^{-3}\ \frac{cm}{sec}$; S.D. = $2.51 \times 10^{-3}\ \frac{cm}{sec}$). For the samples within 500 meters of the bottom the mean value of the CWSV increases to $10.31 \times 10^{-3}\ \frac{cm}{sec}$. This increased $\overline{CWSV}$, however, is accompanied by an increase in the standard deviation to $7.25 \times 10^{-3}\ \frac{cm}{sec}$, leaving a significant overlap in the range of values of CWSV, and consequently the CWSV may still be considered as having only small variations. If viewed as the settling velocity of a single particle the mean value of the CWSV in the deeper samples would characterize a silt particle (density = $2.65\ \frac{g}{cm^3}$) of diameter 8.3 μm while the "shallower" mean corresponds to a 10.7 μm particle or a change in ϕ of only 0.36. Again, it is important to note that the variations of CWSV over a large temporal and spatial range are really very small. From one station to the next, for example, the total variation in the mean value of CWSV at the bottom is less than $3 \times 10^{-3} \frac{\text{cm}}{\text{sec}}$.

By assuming a reasonable value for the settling velocity, w_s, it now becomes possible to extract estimates of the value of the eddy diffusion coefficient from Equation (20). The solutions for $\log \frac{w_s}{K}$ may now be transformed into solutions for log K at the bottom of the water column since it has been determined that a rough estimate of w_s is given by

$$-2.5 \leq \log w_s \leq -2.0 \qquad (26)$$

from the Coulter Counter data.

The determination of the eddy diffusion coefficient, K, using the model outlined above can only be significant if it can be verified. Corroborative data were collected during this experiment making such a comparison reasonably straightforward. A string of rotor current meters, called the Chandelier, was deployed by Weatherly of Florida State University at a site very near Station 11 in approximately 4900 meters of water. This array of instruments was set up to detect currents at elevations of 0.7, 2.0, 3.9, 8.6, 18.4 and 28.9 meters above the bottom and they were allowed to operate for almost nine days, from 1700 Z 14 September to 1600 Z 23 September, 1979. Current speeds were averaged and recorded every hour.

Of the stations under consideration in this experiment two are of importance in terms of comparison with the current meter data: Stations 11 and 12. These two stations satisfy the requirement of being virtually coincident temporally and spatially with the current meter string. While Station 11 was actually taken just prior to the deployment of the current meter string, the time delay was really quite small (only five hours, compared to the time delay of the next nearest station, Station 36, which was taken 102 hours after the array was recovered). Station 12 was taken while the current meters were in operation and was located just to the southwest. The bottom depths at the current meter site, and Station 11, and Station 12 were all within 15 meters of each other. The similarities in space and time of these stations and the current meter string location should allow comparisons of the data obtained herein and the data derived from the currents.

Figure 42 shows the variation in u_* over time during the period of deployment of the current meter array (data obtained from Weatherly). Weatherly makes use of Equation (17), the basic equation for the eddy diffusion coefficient, to determine values of K. Specifically, the following equation is used to determine the friction velocity, u_*, and the roughness parameter, z_o, using two or more current meters:

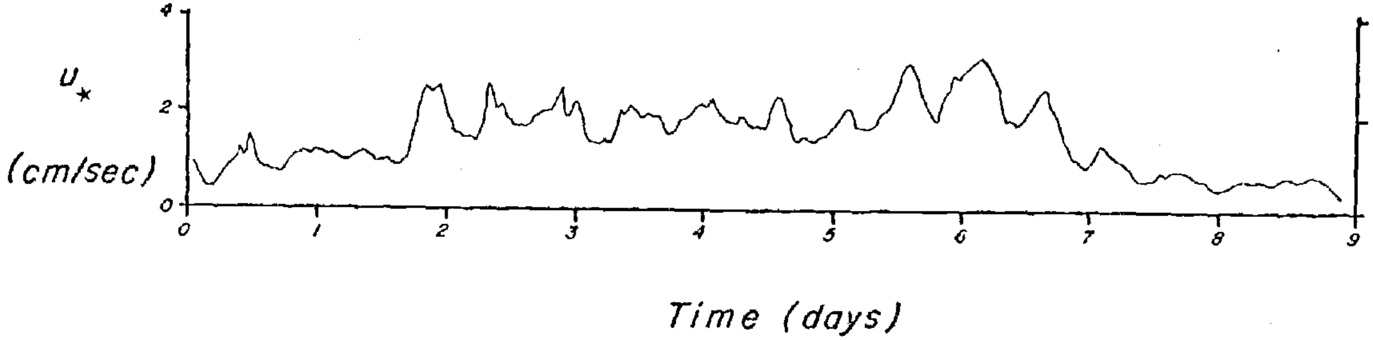

Figure 42. Variation of u_* with time as obtained from current meters.

(from Weatherly ; pers. comm.)

$$u = \frac{u_*}{k} \ln \frac{(z+z_o)}{z_o} \quad \text{(see, for example, Shepard, 1963)} \tag{27}$$

but

$$\rho\, u_*^2 = \tau \tag{28}$$

and also

$$\rho K \frac{\partial u}{\partial z} = \tau \tag{29}$$

so, in order for Equation (28) to be used, the value of K that one uses must be:

$$K = k u_* z \tag{17}$$

Station 12 was recorded at the bottom at 0300 hours, GMT, on 14 September 1979. This time corresponds very closely to a time of ten hours on the current meter data. Using the data available from one hour before to one hour after the "bottom time" for Station 12 (i.e., from 2200 to 2400 hours) it is found that u_* only varies from 0.95 $\frac{cm}{sec}$ to 1.43 $\frac{cm}{sec}$, with a mean value of 1.17 $\frac{cm}{sec}$. The Coulter Counter data described earlier in regard to settling velocities were obtained at an altitude of $z = 400$ cm above bottom. Consequently, at this height, using Equation (17), the eddy diffusion coefficient is given by the range:

$$2.2 \leq \log K \leq 2.4 \tag{30}$$

corresponding to the range of values of u_* given above.

For Station 12, at a height of 4 m ($\xi \cong 0.03$) it is found that the transmissometer model yields a value of $\log \frac{w_s}{K}$ of -4.9. As stated earlier the range of values of $\log w_s$ is from -2.0 to -2.5. As a result, with a value of $u_* = 1.43 \frac{cm}{sec}$ and a value of $w_s = 3.2 \times 10^{-3} \frac{cm}{sec}$ (both of which are in the range of applicability) it is found that the transmissometer model yields the same value for the eddy diffusion coefficient as obtained using the time series of currents at different altitudes.

Station 11 was taken immediately prior to the deployment of the current meter string. The "bottom time" for this station was 1200 Z, 14 September 1979, five hours before the current meters began data acquisition. From the current meter data shown in Figure 42 a periodic fluctuation in u_* is seen with a period of between 10 and 15 hours. This information is necessary to make a reasonable estimate of the value of u_* just prior to the time at which data acquisition began with the current meters. The extrapolation involved is shown in Figure 43, in which the best fit is found to have a period of 14.4 hours (standard error for this fit is 0.18 $\frac{cm}{sec}$). The exact fit is given by

$$u_* = 0.5 \sin \left[\left(\frac{t + 6.8}{7.2} \right) \pi \right] + 0.9 \qquad (31)$$

t = time from start (hours).

From this curve (Figure 43) and the equation given above, an extrapolated value of $u_* \cong 1.3 \frac{cm}{sec}$ is obtained

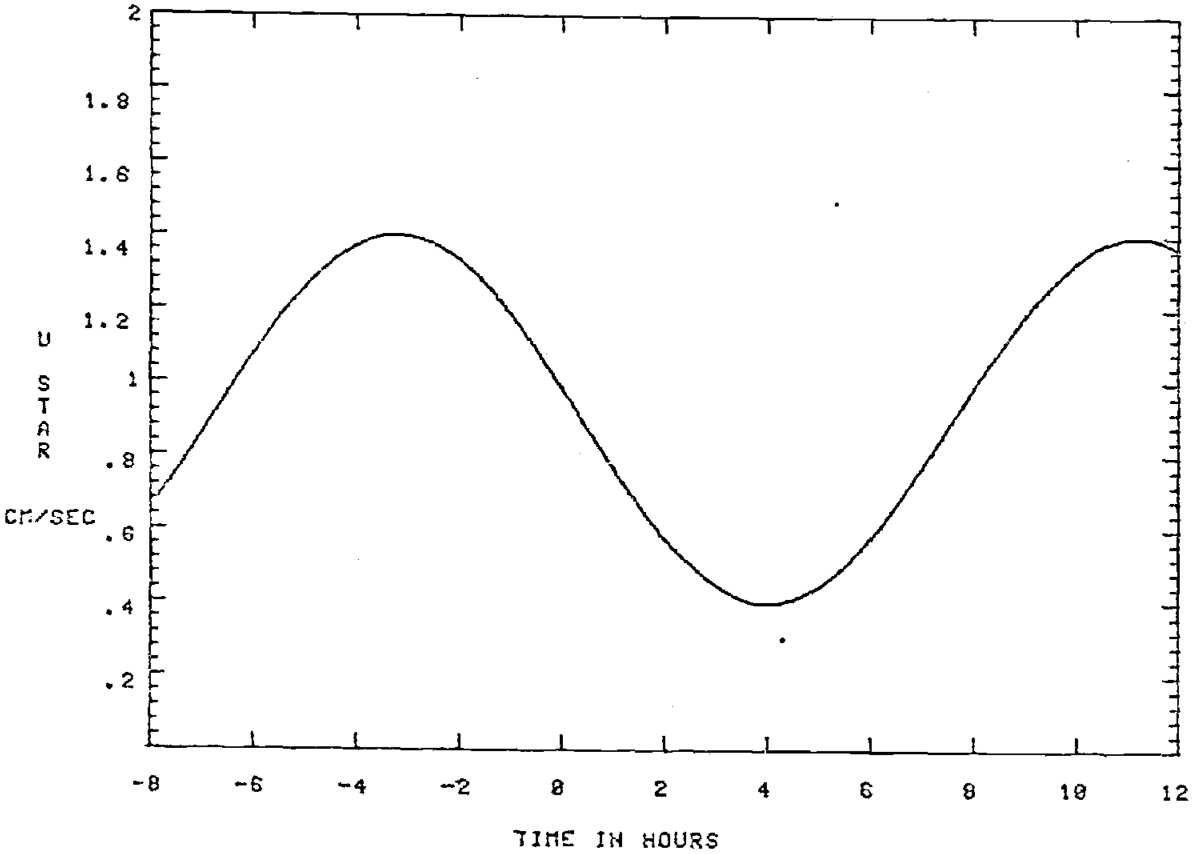

Figure 43. Extrapolated values of u_* for period prior to current meter deployment .

for t = -5 hours. Using Equation (17) again at an altitude of four meters above bottom, this value of u_* yields an eddy diffusion coefficient of 208 $\frac{cm^2}{sec}$; that is, log K = 2.3. At four meters above the bottom the transmissometer yields a value of log $\frac{w_s}{K}$ of -4.8. Using the range of values of log w_s as outlined in Equation (26) the transmissometer profile indicates a range of values of the eddy diffusion coefficient at this station as being $2.3 \leq \log K \leq 2.8$. Once again, identical solutions are obtained when a low value of the settling velocity, w_s, is used. In this case, the best agreement is obtained using $w_s = 3.2 \times 10^{-3} \frac{cm}{sec}$, just as it was in the case of Station 12 discussed previously. It is apparent that the transmissometer model developed herein will yield values of the vertical eddy diffusion coefficient which compare well with values obtained by observing the current shear. In the two examples presented previously it is convincing that complete agreement between the two methods occurred when the same settling velocity was used in both cases. That is to say, it is reassuring to see that in order for the present model to work in two examples which were relatively close spatially and temporally the settling velocity of the particles (and thus, the nature of the particles and their size distributions, themselves) remained constant.

Any discrepancies between transmissometer findings and current meter results may have arisen as a result of the lack of precise coincidence between the two transmissometer stations and the current meter string. Station 11 was taken prior to the start of data acquisition on the current meters and there may be a source of error in the extrapolation of the current meter data to determine the form of the current profile five hours beforehand. Similarly, Station 12 was offset spatially from the current meter string and that may have caused some discrepancies. While absolute fluctuations in u_* were small over the course of hours (on the order of 0.5 $\frac{\text{cm}}{\text{sec}}$ over six to ten hours) such fluctuations in the turbulence regime during the time it takes to travel the distance to Station 12 could account for the factor-of-three range seen in K. Such a threefold change is apparent if u_* goes from 0.5 $\frac{\text{cm}}{\text{sec}}$ to 1 $\frac{\text{cm}}{\text{sec}}$ and then to 1.5 $\frac{\text{cm}}{\text{sec}}$ in the course of hours. Consequently, the model developed herein gives results that agree within a half an order of magnitude with the results using a current meter, and may agree even better. However, to determine accurately the degree of agreement it is necessary to apply the present model to data taken concurrently and at the exact location as current meter data. Such data have recently become available with the advent of a multi-instrument package called the BASS (Benthic Acoustic Stress Sensor) developed at Woods Hole Oceanographic Institute and using some of the instrumentation developed at Oregon State University.

The BASS was deployed for a three-day period from 27 September 1980 to 30 September 1980 at a depth of 4,984 meters and a location of 39°46.1' N, 62°41.0' W. Three transmissometers were aligned at altitudes identical to three current rotors: 29 cm, 86 cm, and 189 cm above bottom. Current speed data were collected over half-hour intervals once every eight hours. Average speeds were computed for each interval and least square estimates were made of u_*. Transmission measurements were made continuously over the whole three-day period.

Since transmission measurements were made at three discrete altitudes, the value of $\frac{\partial P}{\partial z}$ in Equation (19) must be estimated as $\frac{\Delta P}{\Delta z}$. This results in three different estimates of $\frac{\Delta P}{\Delta z}$ for each time interval under consideration: one between the lowest and highest sensors, one between the lowest and middle sensors, and one between the two highest sensors. Similarly there are three values of $\frac{\partial u}{\partial z}$ for each time interval. It is necessary to obtain a value of $\frac{\partial u}{\partial z}$ since the evaluation of K in this case will be performed by using Equations (28) and (29) to yield:

$$K = \frac{u_*^2}{\frac{\partial u}{\partial z}} \tag{32}$$

Equation (32) implies that between sensors, K is constant. While this represents a simplification it is necessary for comparison purposes. The transmissometers only supply data on particle concentrations at specific locations and so, in determining $\frac{\Delta P}{\Delta z}$ one assumes this slope is constant between two sensors. That is, there is no way of knowing what the slope is at one sensor (i.e., one point). Consequently, if slopes of particle concentration are used in the calculation of K from transmission data then slopes of current speed should also be used in the calculation of K from current rotor data in order to be consistent. Simply, if Equation (17) were used to determine K from current data then it is ambiguous what value of z should be inserted for comparison with transmissometer data.

Equation (19) rather than Equation (20) was used to reduce the transmissometer data. This was done because the BASS data represent only a small segment of the flow and there was no way of knowing the thickness of the flow, h. Consequently, use of Equation (20), which is a function of h, was impossible. Equation (19) represents the same relationship and thus may be used without problems.

Figure 44 shows the time record of transmission from the BASS data at 1 m above bottom. Fluctuations in transmission were small during the half hour over which current speeds were averaged. As a result, approximate values of the beam transmission for each interval could be picked off the record with little fear of significant

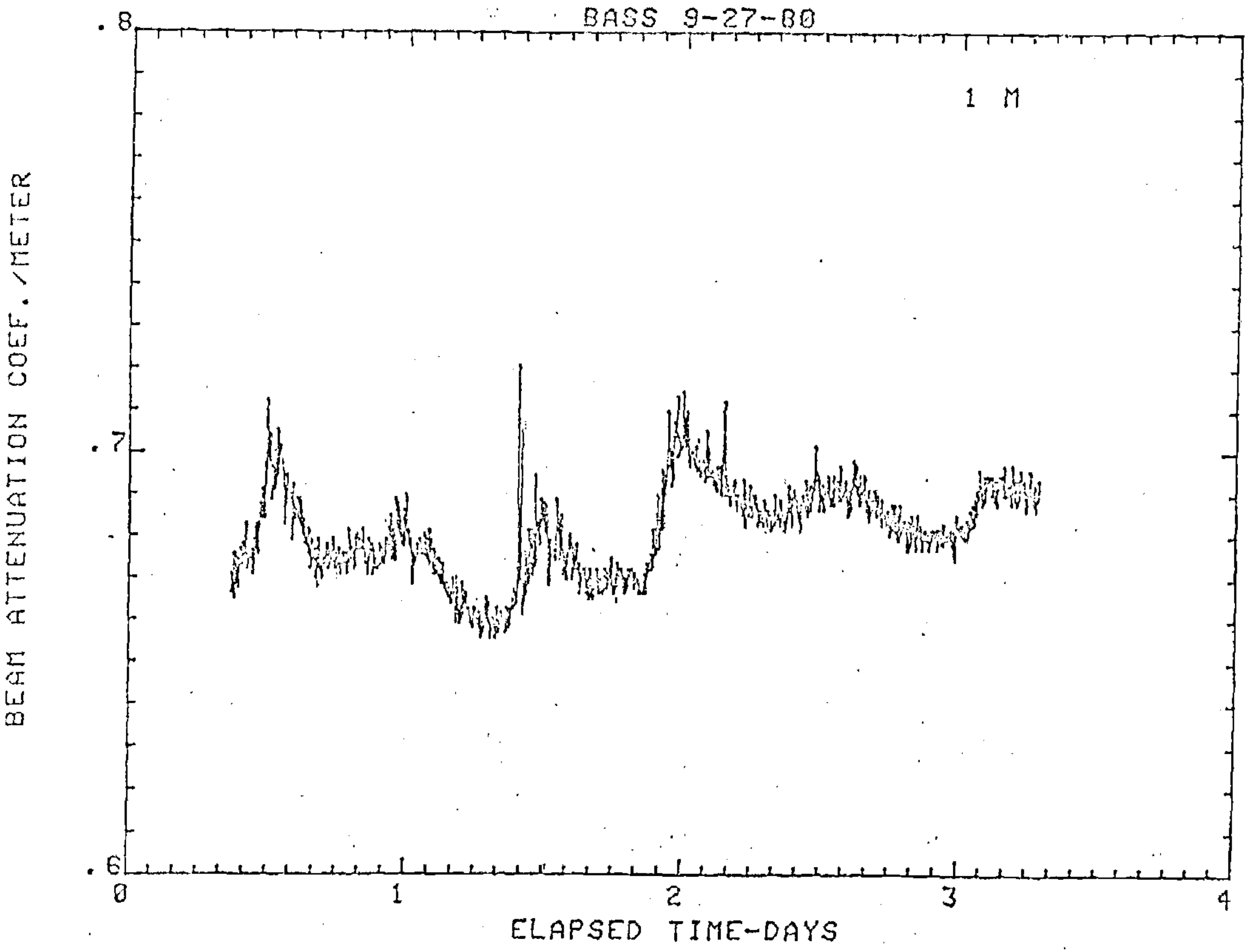

Figure 44. Time record of transmission from the BASS data at 1 m above bottom.

variation. Generally, over the half-hour intervals observed in this case c varied by less than 0.02 m^{-1}.

A comparison of calculations of log K using the transmissometers and current meters was quite convincing when a value of log $w_s = -2.0$ (recalling $-2.5 \leq \log w_s \leq -2.0$) was used. The results obtained (see Table III) were quite satisfactory. For each time interval the mean value of log K was also computed from the results of the three sensors. These mean values as well as the complete data set are plotted on Figure 45. For the sake of reference the approximate range of values of log K as previously discussed for Stations 11 and 12 is also shown in Figure 45. The line of perfect correlation has also been drawn on Figure 45 and clearly passes through both data sets. Extensive experimentation with current meters and transmissometers would be necessary to quantify the accuracy in determination of the vertical eddy diffusion coefficient optically.

Taken alone, the results of each of the two experiments described previously (one being Stations 11 and 12; the other being the BASS data) are reasonably convincing that the transmissometer component model is compatible with the simplified equation of vertical mass conservation. Together, the two data sets show that the model can work quite well over a range of values of log K. In addition, within the limits placed on the value of w_s the model works equally well within the bottom meter of

TABLE III

TRANSMISSOMETER LOG K	TIME		BASS LOG K
1.83	27 Sep 1980	1728Z	1.09
1.49		1728Z	1.16
1.38		1728Z	1.21
1.36	28 Sep 1980	0128Z	1.27
1.37		0128Z	1.43
1.38		0128Z	1.56
1.46		0928Z	1.39
1.20		0928Z	1.36
1.41		1728Z	1.30
1.21		1728Z	1.40
1.53	29 Sep 1980	0128Z	1.31
1.28		0128Z	1.36
1.28		1728Z	1.27
1.05		1728Z	1.29
1.23	30 Sep 1980	0128Z	1.40
1.00		0128Z	1.56

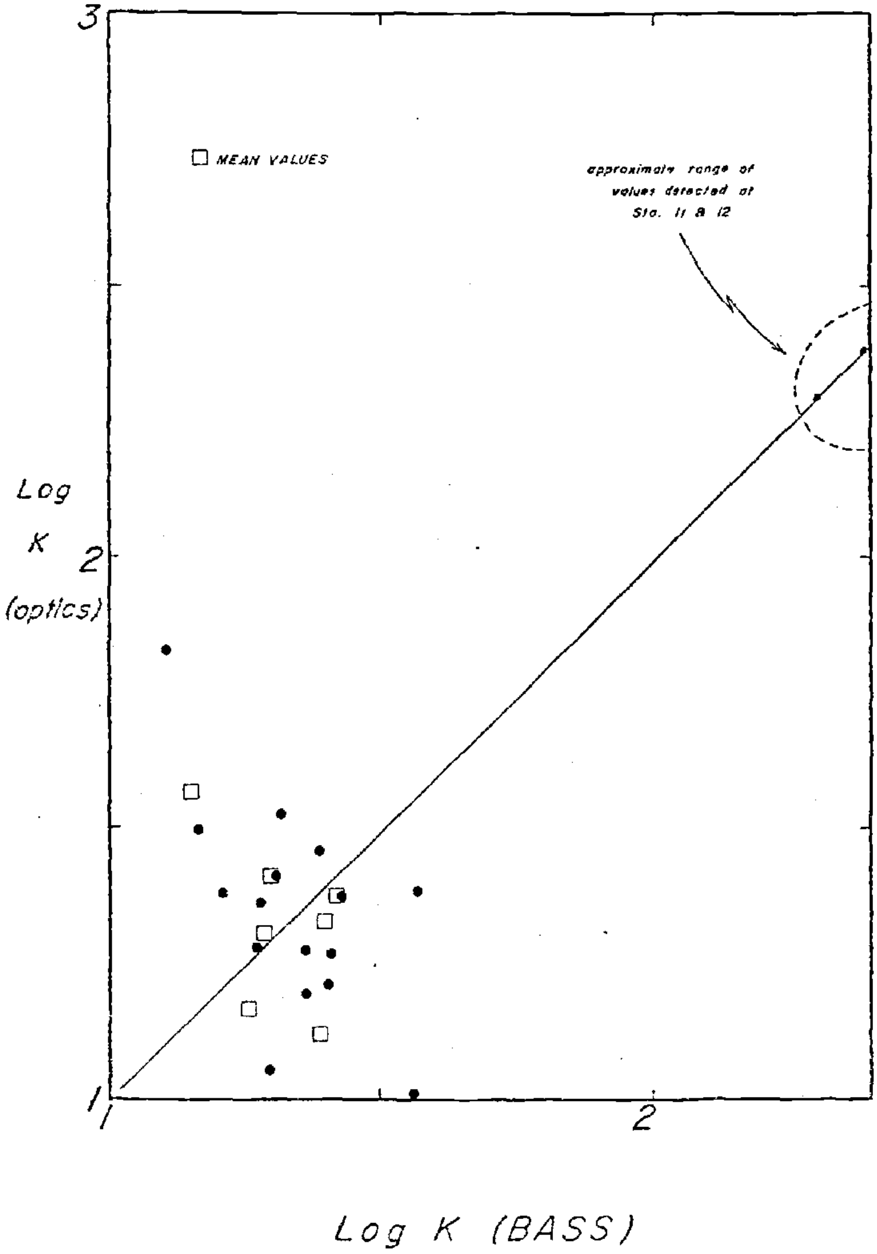

Figure 45. Comparison of values of eddy diffusion coefficient obtained from BASS data and from transmissometer model.

the benthic boundary layer as well as many meters above the bottom. The model even shows that best fit is obtained when a value of $w_s = 3 \times 10^{-3} \frac{cm}{sec}$ is used at four meters above bottom and a value of $w_s = 1 \times 10^{-2} \frac{cm}{sec}$ is used in the bottom meter of water. This result in itself is significant in that it indicates the existence of a small shift in the particle size distribution from larger particles very near the bottom to more smaller particles at an altitude of four meters. The range of values of u_* given by $0.4 < u_* < 0.8 \frac{cm}{sec}$ from the BASS data, when compared with well-established curves of the limits of "first motion" (such as the Sundborg curve), indicate that all particles smaller than roughly 30 μm will be transported. The largest particles would be transported as bed-load and smaller particles would presumably be carried in suspension. The appearance of more large particles nearer the bottom is, therefore, as it should be.

One cannot conclude from this discussion and presentation of data that a beam transmissometer is as viable a tool as a current meter in the determination of hydrodynamic parameters. The assumptions made in the initial part of this section serve to verify that the transmissometer results presented here are merely first order, very rough estimates of the characteristics of a flow. With the addition of temporal changes or vertical velocity structure to the system major complications would arise and large sources of error would develop in the model. The purpose of this section was to verify that the transmissometer model was merely compatible, to some degree, with the standard models of sediment transport. That is, that transmissometer results do integrate well with the other aspects of the whole physical system. This goal was attained; any further implementation of this model to define the flow more precisely would exceed the limitations of the model itself.

IV. OBSERVATIONS AND DISCUSSION

Observations made based on the vertical profiles and their components will now be discussed more fully. Some features of the profiles have already been explained and described but a more in-depth discussion of the significance of these features would be beneficial to an understanding of the processes involved in the HEBBLE area.

A. Detached Benthic Boundary Layers

The detached benthic boundary layers have been seen to exist in several profiles. The evolution and development of such a layer was detected at one station. The "driving force" behind separation of the benthic boundary layer seems unclear in this case. Pak et al. (1980) have shown similar intermediate nepheloid layers as a result of detachment of the benthic nepheloid layer at the break of the continental shelf. Such a process is intuitively feasible considering the topography involved between the shelf and the slope. Implicit in this description is the existence of a cross-shelf velocity component. A similar process could be involved in the development of the detached benthic nepheloid layer as seen in the HEBBLE area. Armi (1978) has detected a multiple-step structure in the nepheloid layer near the region known as the Corner Rise. The explanation for such a structure is given as the "...advected signature of bottom mixed layers formed at various depths..." (Armi, 1978). Material resuspended from the bottom is lifted and transported across the topographic contours to create an intermediate, or detached, nepheloid layer. So the detached benthic boundary layer really represents an advected benthic layer from a shallower depth. A requisite for such a process is a cross-slope component of velocity. The magnitude of such a component required to lift the benthic layer to an intermediate depth is given by Armi (1978) to be on the order of 10 to 30 $\frac{\text{cm}}{\text{sec}}$. Such a velocity is not atypical of HEBBLE current meter data yet the data are not available to determine exactly when a cross-slope component of such magnitude occurred. Shor and Tucholke (1980) have used studies of morphology and sediment structure in the HEBBLE area to verify that there are occasional cross-slope currents. It is these very currents which would provide the driving force needed to produce the detached benthic nepheloid layers such as described by Armi (1978) and as seen in the HEBBLE transmissometer data.

B. Trailing Fronts

The profiles of transmission provide valuable information regarding the magnitude of sediment transport that exists within the benthic boundary layer. The gradual clearing of the water column has been discussed in association with the passing of a trailing edge of a benthic cloud. This passage was seen to take place over a period of less than two hours (Figure 37). That is, from the time of detection of dirtiest water to the time of detection of clearest water was an interval of roughly 5×10^3 seconds (approximately 1 1/2 hours). Weatherly et al. (1980) have indicated that a reasonable steady velocity in this region is 20 to 60 $\frac{cm}{sec}$. Consequently, this indicates that the trailing edge of a benthic boundary layer has a length of between 1 and 3 km. Such a length indicates that the bottom nepheloid layers found in the HEBBLE experiment are very large scale features with the dominant dimensions being horizontal on the order of many kilometers (Weatherly et al. 1980, estimate horizontal length scales of 10^2 km). In fact *in situ* time series measurements of transmission made with the Bottom Ocean Monitor indicate that some benthic "storm clouds" exist for several days and are quite enormous. These data will be discussed further in a following section.

C. Volume and Mass Flux

The magnitude of sediment transport can also be perceived by considering the total mass concentration in the column of water sampled by the transmissometer. A vertical integration of the particle concentration derived from the transmissometer and using Equations (12a) through (12e) yields the total mass concentration within that column of water above an area of the bottom. If this concentration is multiplied by the velocity of the flow and by the width of the flow then the volume flux of material within that water column may be estimated. To achieve this result the components as shown in Table II were integrated over the thickness of the nepheloid layer and the appropriate coefficients were substituted to obtain the volume concentration above a unit area (i.e., standing crop) for each station (see Table IV). The units shown in Table IV are micrograms per square centimeter (a density of 2 $\frac{g}{cm^3}$ was used). Table IV indicates a range in values of the standing crop from 357 to 33,735 $\frac{\mu g}{cm^2}$ with a mean value of approximately 8000 $\frac{\mu g}{cm^2}$. Also shown in Table IV is the value of the beam attenuation coefficient at the bottom of the water column for each station. Figure 46 shows the general agreement between standing crop and C at the bottom. Obviously water that is more turbid near the sea floor is apt to have a higher total volume concentration integrated over the thickness of the benthic nepheloid layer. The magnitude of standing crop indicated in Table IV and Figure 46 becomes more significant when it is used to estimate the volume flux or mass flux at a specific site. To make such an estimate it is necessary to apply reasonable values of the water velocity and the width of the flow. An order-of-magnitude estimate of the width of the flow has been given by Weatherly et al. (1980) as being roughly 10^2 km (i.e., 10^5 m). The width estimate used by Weatherly et al. (1980) turns out to be consistent

TABLE IV

STATION	STANDING CROP ($\frac{\mu g}{cm^2}$)	C (m^{-1}) AT BOTTOM
8	1656	0.62
10	6526	1.20
11	1505	0.58
12	5250	0.89
19	3144	1.11
23	13448	1.31
24	6862	0.92
27	33735	$<\infty$
36	357	0.53
37	5358	0.89
40	6678	0.97
41	8400	1.08
44	6760	0.89

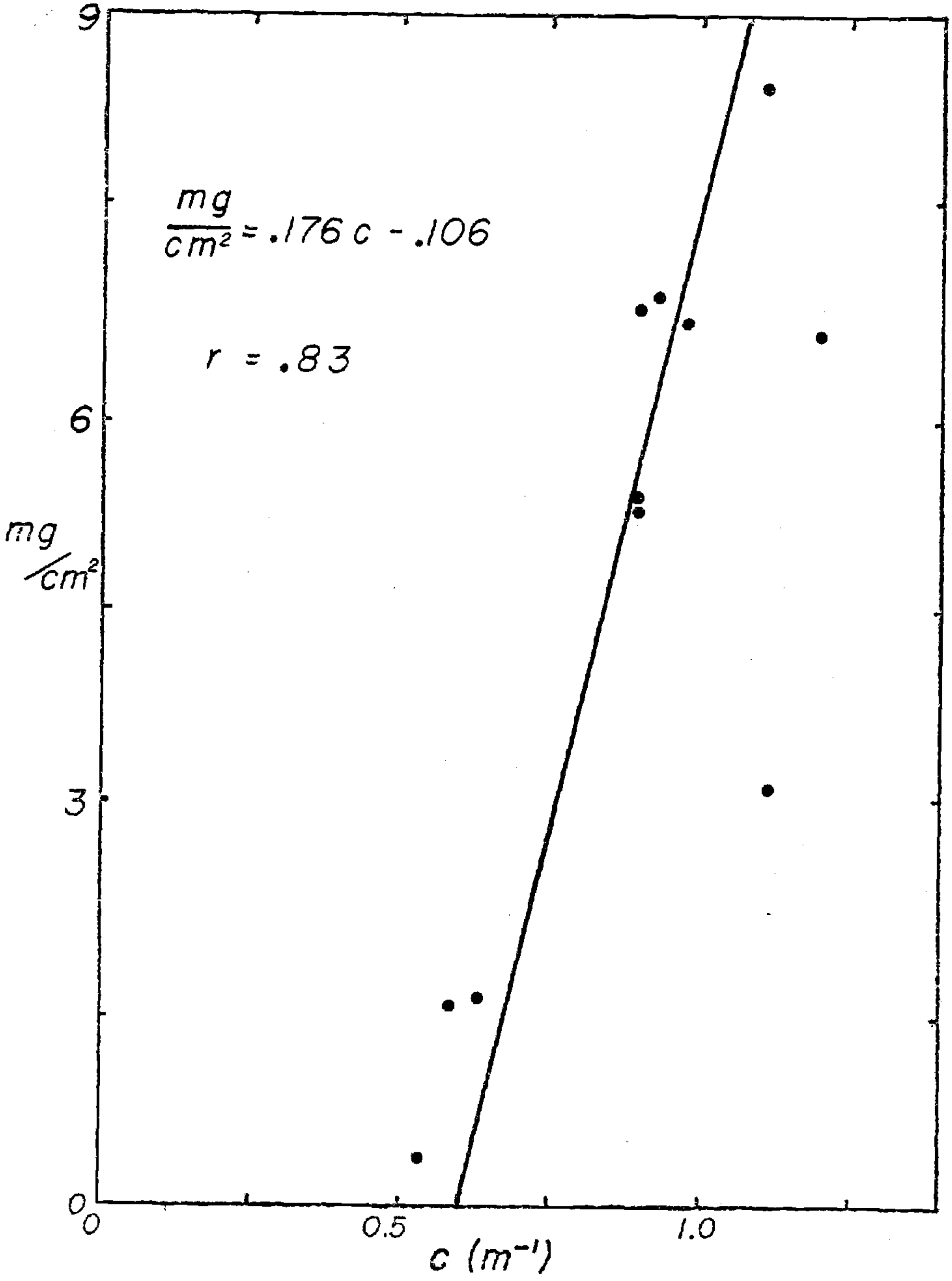

Figure 46. Comparison of particle standing crop and the beam attenuation coefficient at the bottom.

with the estimate these authors have made of the water volume transport within the HEBBLE area. In addition, several researchers (e.g., Richardson and Wimbush, 1980; Weatherly et al., 1980) have measured steady velocities of 10 $\frac{cm}{sec}$ to 70 $\frac{cm}{sec}$ within the nepheloid layer; for the order-of-magnitude estimate a velocity of 40 $\frac{cm}{sec}$ (i.e., $10^{1.6}$ $\frac{cm}{sec}$) will be used. Consequently, with an average value of standing crop being of order 10^4, then the resultant mass transport is given by

$$10^4 \frac{\mu g}{cm^2} \times 10^{1.6} \frac{cm}{sec} \times 10^7 \text{ cm} = 10^{12.6} \frac{\mu g}{sec}$$

or roughly 10^3 $\frac{kg}{sec}$ within a given benthic cloud in the HEBBLE area. This is roughly equivalent to the transport of the Congo River (between 980 $\frac{kg}{sec}$ and 2220 $\frac{kg}{sec}$; Eisma and Van Bennekom, 1978). However, it must be made clear that the transport estimate for the HEBBLE area is valid only during the passage of a nepheloid layer...a period which lasts for several days; the mass transport for the Congo River is continuous throughout the year. Still, in a given four-day storm a benthic nepheloid layer could transport some 3.5 x 10^5 metric tons of suspended sediment past a plane. This analysis points out dramatically that optical measurements have shown the HEBBLE area to be one of extremely active mass transport. It must be reiterated that the preceding discussion is an order-of-magnitude estimate, however the conclusion is most likely valid to within less than a factor of ten since the maximum variation of any of the three variables (standing crop, velocity and area) from the values used is $10^{0.7}$, $10^{0.6}$ and $10^{0.6}$, respectively. The maximum estimated possible mass flux is $10^{4.2}\ \frac{\text{kg}}{\text{sec}}$.

D. Large Scale Observations

In order to make sensible large scale observations of the optical data in HEBBLE some type of normalization must be used to bring the information into a cohesive form. One means of doing this is to use available velocity data to transform the time or location of each station in order to simulate a data set that is purely temporally or spatially variant. The data set as it presently stands contains the effects of both extensive temporal and spatial variations. It is most instructive to separate these two effects and study the large-scale system as it appears at a fixed point in space (Eulerian transformation) and as it appears over an area at a fixed time (Lagrangian transformation). Such a temporal or spatial transformation would serve to indicate to what extent the processes that are observed in HEBBLE are long-term, large-scale phenomena. Several questions may be answered by observing results obtained from these transformations:

i) Over what kind of time scale do processes occur in the HEBBLE area?

ii) Over what kind of spatial scale do processes occur in the HEBBLE area?

iii) What can be said about when or where the HEBBLE nepheloid layers develop?

The first transformation performed was the Eulerian plot of the stations relative to Station 11. Station 11 was chosen as the reference site since the Bottom Ocean Monitor was located very nearby. Thus, by using Station 11 as the reference, the time series obtained can be compared to the time series from the BOM. A current meter was deployed near Station 11 at a depth of 4935 m (50 meters above bottom) by Mary Jo Richardson of Woods Hole. The data obtained from the current meter for the period from 13 September 1979 to 24 September 1979 indicate a slow increase in current velocity followed by a period of steady flow followed by a sudden decrease (Figure 47). The flow was to the southwest and roughly parallel to the contours. Using the assumption that the flow extends over a wide swath ($\sim 10^2$ km) as claimed by Weatherly et al. (1980) and using the velocity data outlined above coupled with the location of each station, the "bottom time" (i.e., time at which the first downcast was complete) for each station was transformed to the time at which the water at that station would have been detected at or alongside Station 11. This represents a very simplified transformation but, nevertheless, it does provide a good first-order estimate of the coarse temporal

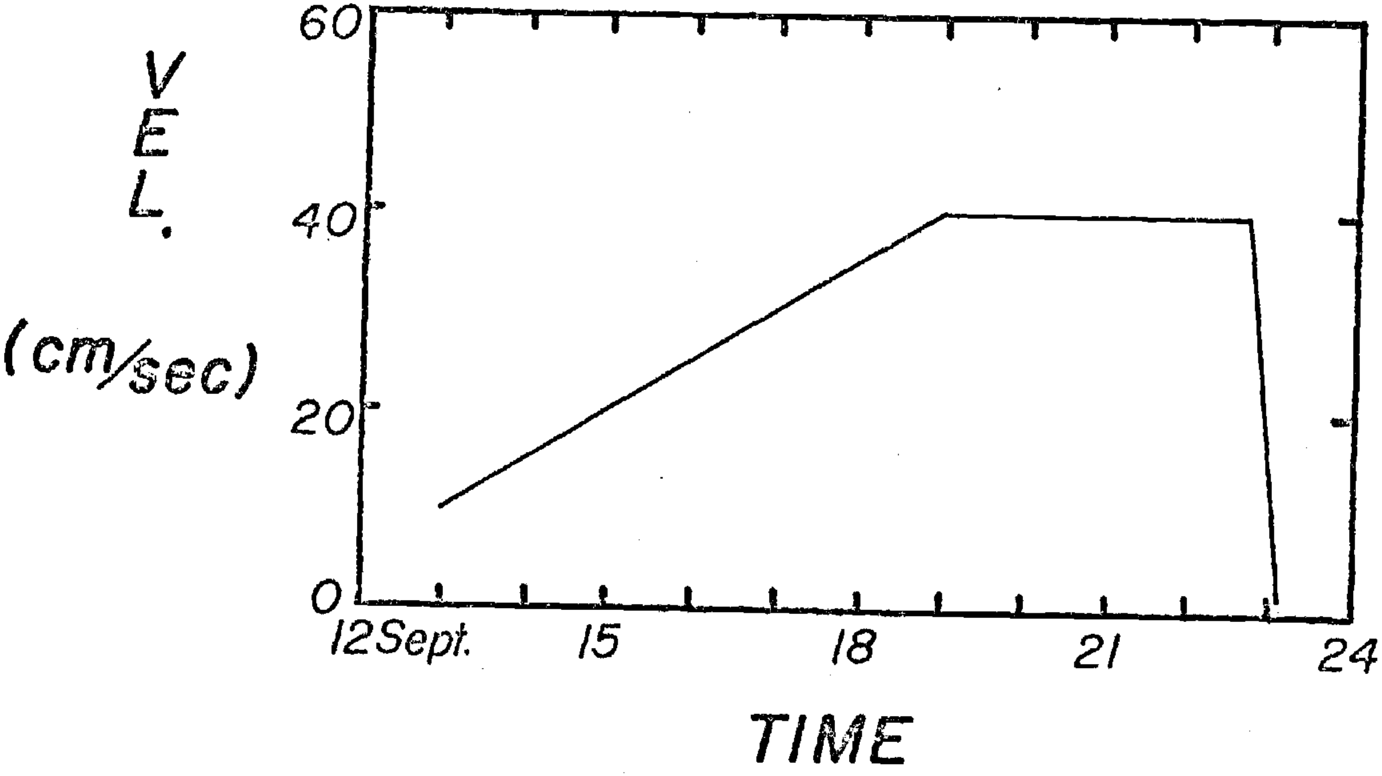

Figure 47. Simplified current profile for use in spatial and temporal transformations.

variations detected at Station 11. Figure 48a shows the resultant time-based plot of transmission obtained from the Eulerian transform for depths of 0 m, 100 m above bottom and 200 m above bottom. Also shown is the plot of transmission from the moored Bottom Ocean Monitor. The mean error in transmission between the BOM and the 0 m transmissometer plot is 10% transmission. This error may be ascribed to small local turbidity fluctuations. Figure 48b shows the time series of the depth profiles of transmission. The most obvious feature of Figures 48 a and b is the excellent qualitative agreement between the time series as obtained from the transformation and the actual <u>in situ</u> time series. Both the BOM and the transformed profiles indicate a strong benthic storm between 18 September and 20 September. Similarly, a weaker (i.e., less turbid) storm was detected by both techniques between 22 September and 23 September. The general "clean water" trends were detected at the start and finish of the time interval. It is important to note that the BOM plot is continuous over time while the transmissometer transformations are instantaneous. Thus, the actual fit of the two data sets may in fact be even better at the times in between those indicated for each transmissometer profile station.

The observation that is implicit from a study of Figures 48 a and b is that benthic "storms" in the HEBBLE area are large scale (temporally) and stable. The fact

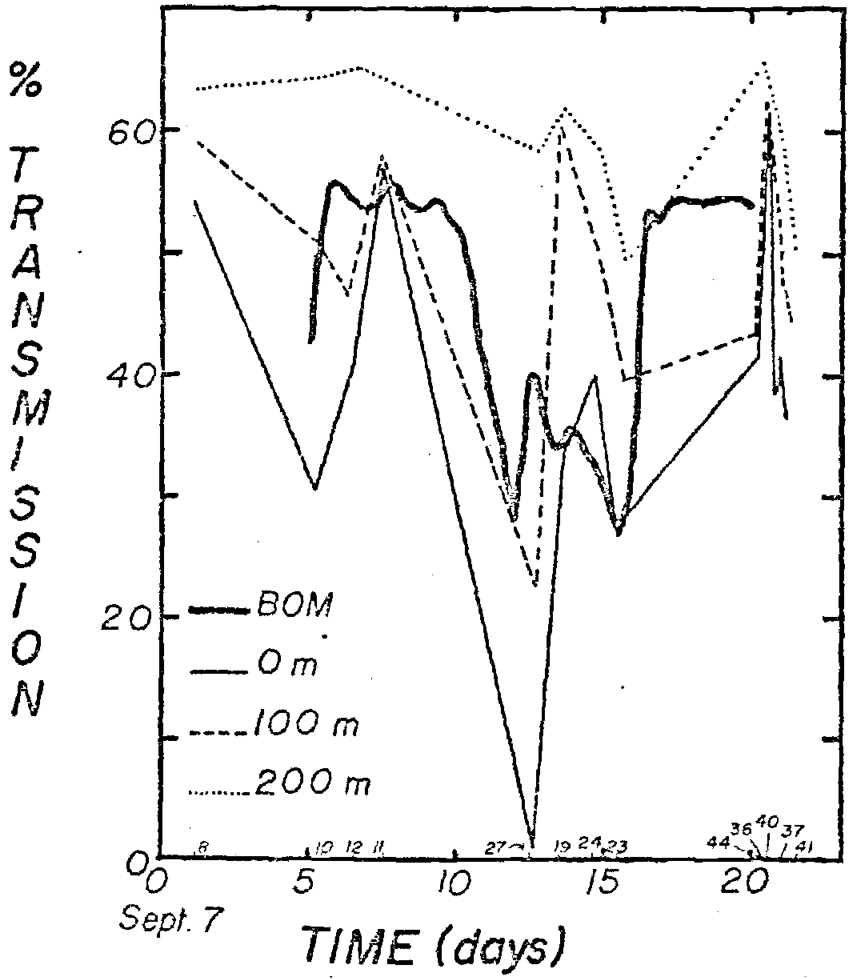

Figure 48a. Time series of transmission at 3 depths and for the BOM (small numbers are CTD Station numbers).

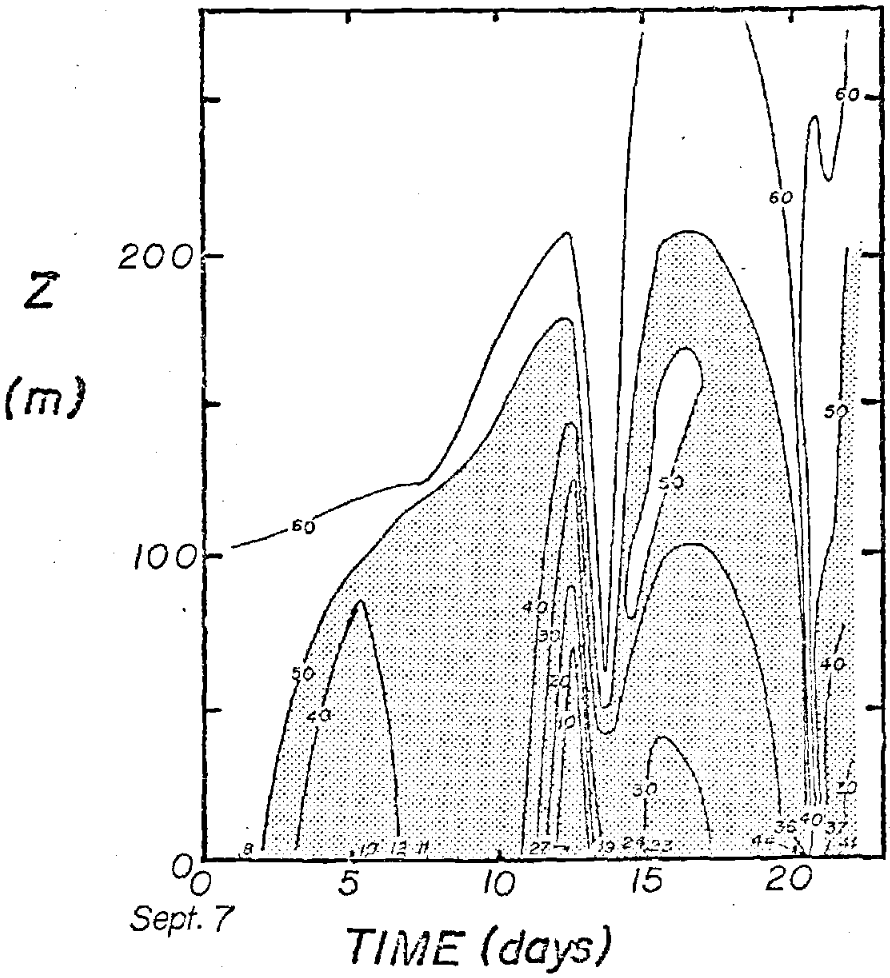

Figure 48b. Time series contours of transmission

that the transformation corresponds well with the BOM data indicates that the storm that was detected near 19 September at the BOM was the same storm that was detected at Station 27 on 23 September. In addition, the temporal transformation was performed for data collected over a period of some 19 days. Since this transformation agrees with the fixed-point data one must conclude that the processes detected at HEBBLE occur as well-defined, stable phenomena over time periods of two to three weeks. That is, the situation may be compared to a meterological one where a well-formed storm may be seen to pass over a given region during a period of weeks. The general form of the storm remains unchanged and the time record of meteorological activity at one station is consistent with the record at a distant station when the appropriate temporal transformation is made based on velocity information. The major optical features detected at HEBBLE remain relatively unchanged as they are transported downstream over periods of at least two weeks.

The logical extension of this observation is an analysis of spatial transformations. At a given time are there any obvious features of the suspended sediment profiles in the HEBBLE area? To answer this question a spatial (i.e., Lagrangian) transformation must be performed upon the data set. This was done in a manner nearly identical to that described previously with respect to the Eulerian transformation. However, in this case the unknown variable for which a solution is sought is the change in distance from Station 11, not the change in time. The same velocity profile as shown in Figure 47 was used. The actual time at which each station was taken was compared to the time for Station 11. The time difference between the two stations was applied to the velocity data to determine where the water sample from a given station would have been located at the time of measurement of Station 11. Again, flow was assumed to be parallel to the contours toward the southwest.

Figure 49a presents a section view of the transmissometer data. The most obvious feature of the figure is the length scale along the section. The result of applying the Lagrangian transformation to the data has been to effectively stretch the length of the section from roughly 150 miles (see Figure 1) to almost 400 miles. Thus, the effects that were described previously as being large-scale temporally can now also be considered to be large-scale spatially. The fact that the Eulerian transformation yielded good results, coupled with the consequent large size scale induced by the Lagrangian transformation indicates that the phenomena detected in HEBBLE travel over distances of hundreds of kilometers while keeping their basic optical structure. Also seen in Figure 49a is the appearance of the two storms which were detected in the time plot. These storms appear as an increase in altitude of the lines of equal transmission

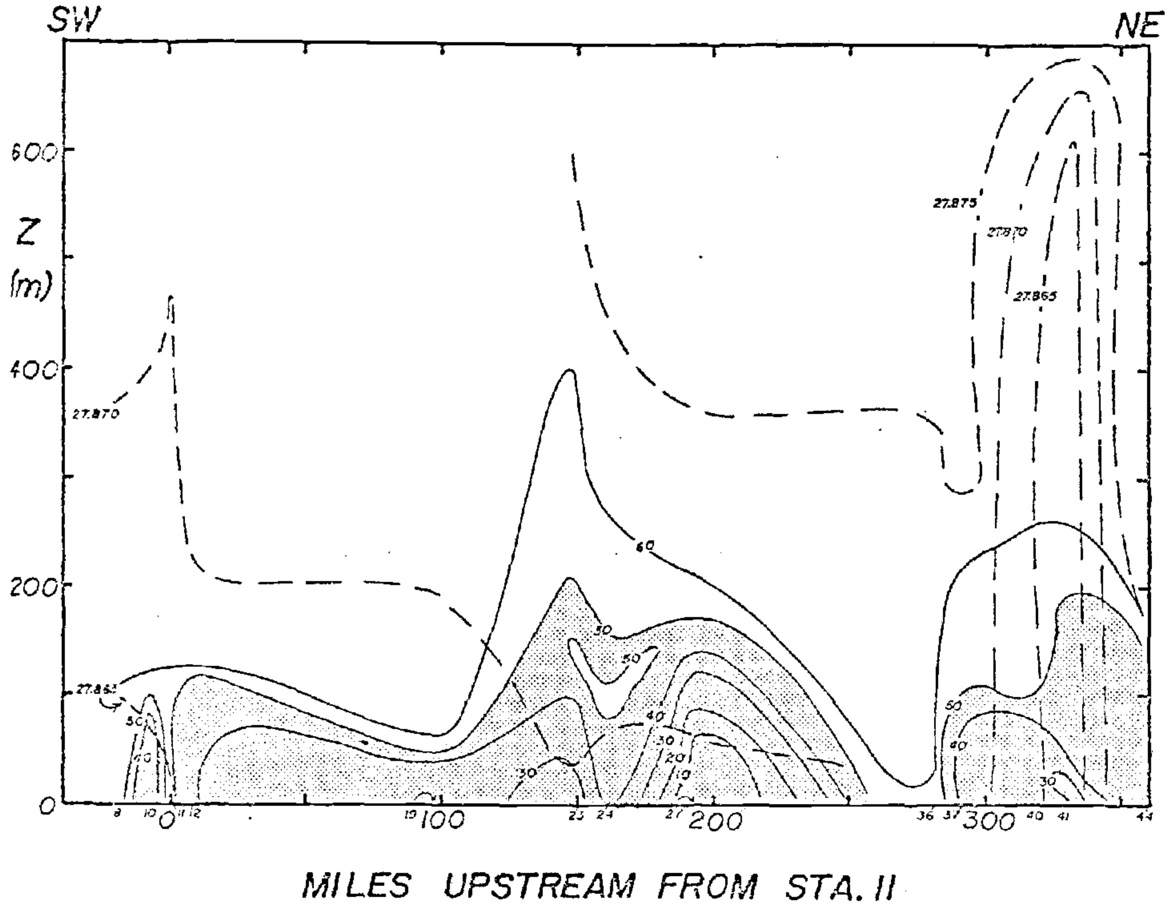

Figure 49a. Section of transmission and σ_t data (small numbers are CTD Station numbers).

(isonephs). The large storm which was most apparent at Station 27 and which was seen to occur between 18 September and 20 September on Figures 48 a and b can be seen as the ascension of the isonephs between 120 miles and 240 miles upstream. Similarly the isoneph plot shows the second storm between 280 miles and 360 miles upstream. The small disturbance in the isonephs seen at seven miles downstream corresponds to the small feature seen in Figures 48 a and b between 12 September and 13 September.

Also plotted on Figure 49a is the density data obtained from the CTD profiles. Density variations with altitude are very small ($< 2 \times 10^{-5} \frac{gm}{cm^3}$ over 700 meters) although there is a system of higher density at higher altitude within this region (a consequence of slight salinity increase with altitude; Weatherly et al., 1980). More importantly, the transmission profile and density profile are found to have very little significant correlation. Intersection of transmission and density features indicates that turbidity variations do exist in an isopycnal environment and density variations occur in an isonepheloid environment. The transmission profiles cannot be explained by changes in the density profiles. In fact the changes in density are minute while transmission changes are quite large. The apparent density instability seen in Figure 49a is well documented in additional σ_t data taken within the same area (Weatherly, personal communication) and is a consequence of decreased salinity within the bottom water. In the geostrophic analyses performed by other researchers in the HEBBLE area (e.g., Weatherly) the 5000 db isobar is used as a level of no motion and consequently a value of σ_5 rather than σ_t is sought. The purpose of the present work, however, is to determine the relationship of turbidity sections to actual density sections which are best represented by σ_t profiles.

Figure 49b shows the spatial plot of transmission at the bottom for the Lagrangian section. Also shown are the plots of bottom temperature and salinity. The correlations between transmission and each of the other parameters are very poor. Qualitatively it appears, however, that the extremely turbid water mass associated with Station 27 can be related to a water mass that is both saltier and warmer than the adjacent water masses (yet of nearly the same density). Nonetheless, this observation cannot be applied as a rule. It has been shown that the behavior of the density plot indicates that turbidity is not constrained by the density structure within the water column.

The results of the temporal and spatial transformations indicate that the HEBBLE area is one in which large benthic clouds are formed hundreds of kilometers upstream and transported to the southwest remaining relatively unchanged. The measurements show that a profile of transmission at a given station accurately represents

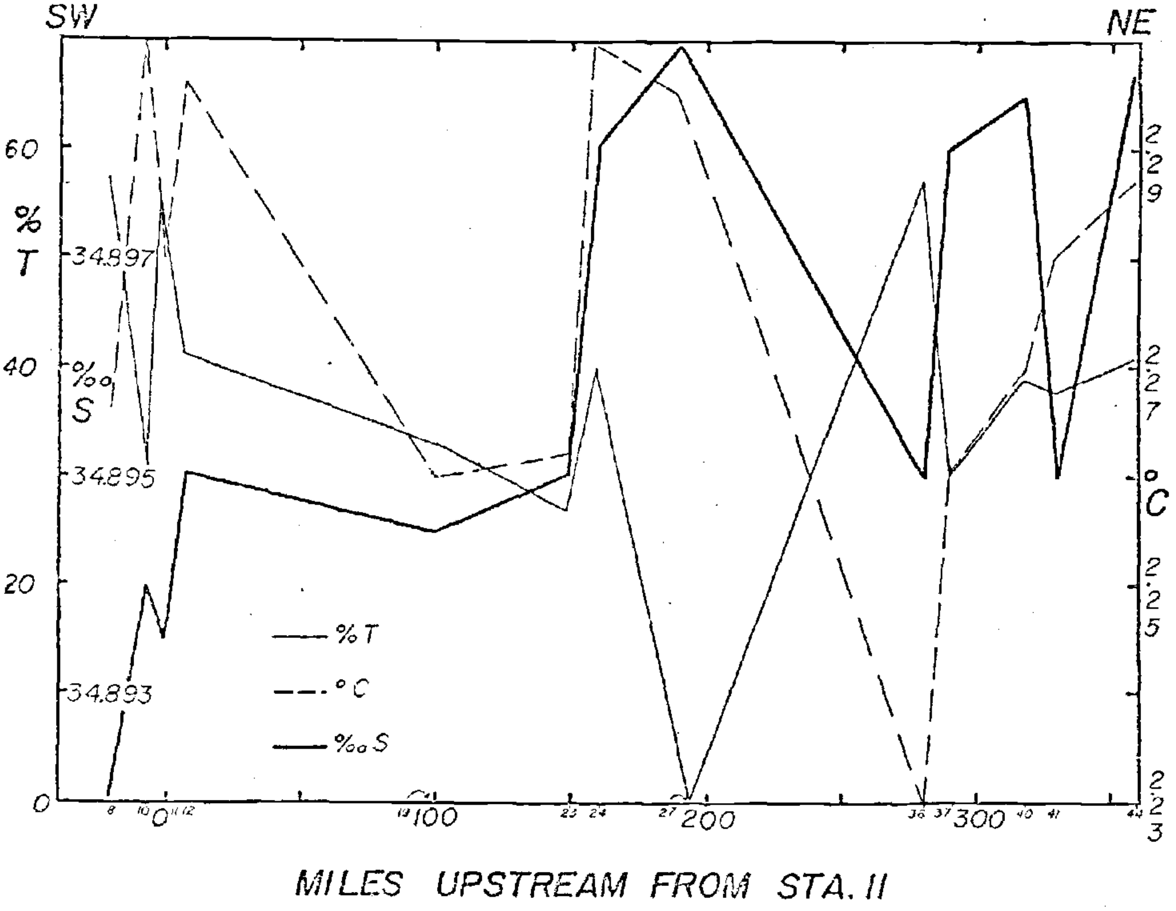

Figure 49b. Spatial plot of near bottom transmission, temperature and salinity.

what one should expect the profile to look like at a future time downstream. More importantly it suggests that the major features (i.e., large benthic storms) detected optically are formed in a remote region and are transported along the topographic contours cohesively. Earlier it was shown that the formation of smaller-scale features (e.g., detached benthic nepheloid layers) may be stimulated by small-scale (i.e., $\sim 10^2$ m) cross-slope effects. The large-scale features presently under discussion, however, appear to be formed well upstream and they resist significant changes as they move through the HEBBLE area.

The relationship of the large scale features to gross topography can be further understood by considering the maps of various bottom water parameters.

Figure 50 is a map of the bottom transmission values. Figure 51 is a similar map showing the thickness of the bottom nepheloid layer in meters. Both figures demonstrate a southwest-northeast axis of alignment. In the transmission map (Figure 50) this is seen as the core of more turbid water and in the thickness map (Figure 51) this is seen as the zone of the thickest bottom nepheloid layers. Clearer, thinner nepheloid layers are seen on either side of this core which lies roughly parallel to the bathymetric contours. Also, Station 27 in the far southwest corner is characterized by very low bottom transmission ($\sim$ 0%) and a very thick bottom nepheloid

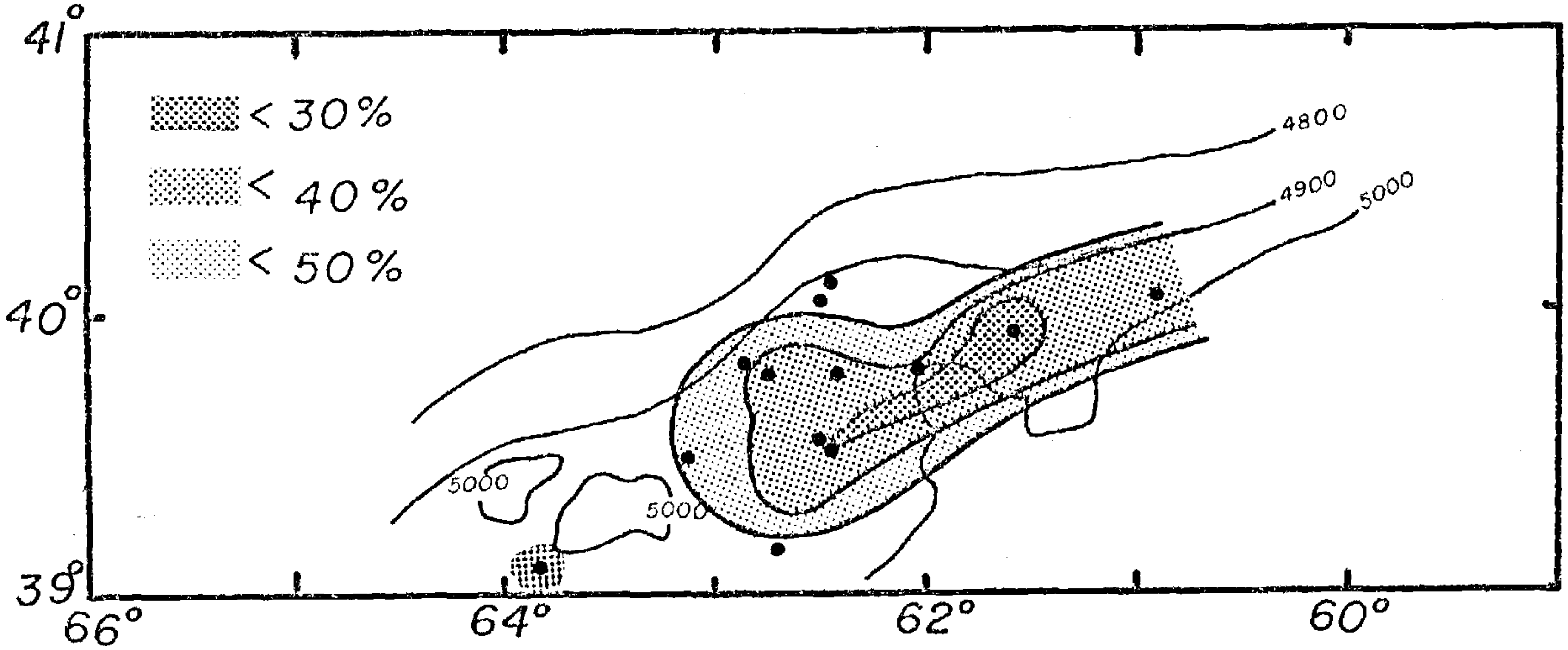

Figure 50. Map of bottom contours and bottom transmission values.

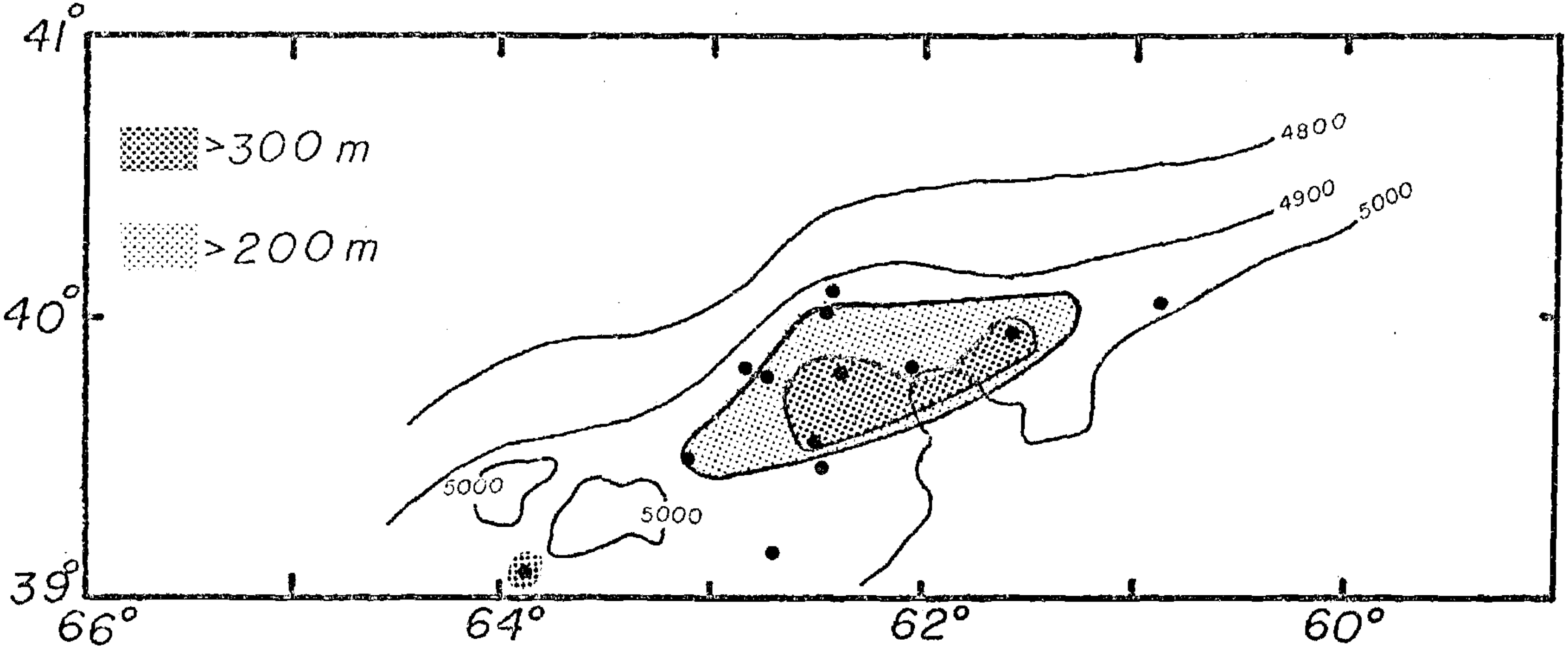

Figure 51. Map of bottom contours and thickness of bottom turbid layer

layer (325 m). In addition it is seen to lie just downstream of a large depression. Flow over the depression could be inducing a higher degree of turbidity and a much thicker nepheloid layer. Station 19 at the northeast corner has a high level of turbidity which would classify it as being in the core, however it is also defined by a very thin (60 m) benthic nepheloid layer and consequently is not considered part of the core as defined above. The explanation for this discrepancy is unclear. This may be a consequence of the small scale local topography (e.g., depression or elevation affecting the flow) but the data do not exist to test this hypothesis. One cannot make a definitive statement relating the thickness of the bottom nepheloid layer to the magnitude of bottom turbidity, however it is clear that there does exist a thick core of generally more turbid water flowing along the contours from the northeast to the southwest.

V. CONCLUSIONS

Vertical profiles of turbidity have been shown to be a useful parameter for the study of particle dynamics in the deep benthic ocean. Quantitatively, the transmission values (actually the beam attenuation coefficients) were found to have a very high correlation with suspended volume determinations. This excellent correlation indicates that in the HEBBLE region the nature of the particles remains nearly unchanged in the lower kilometer of the water column over a period of several weeks. This was further verified by independent measurements taken more than a year later and yielding a very similar correlation. The conversion of beam attenuation coefficient, c, to volume concentration, P (parts per billion), for this work was given by

$$P = -265.1 + 569.5\, c.$$

The constancy of the nature of the particles was further verified by the analysis of the particulate index of refraction. The result of this analysis was a calculated index of roughly 1.55 to 1.60. This result agrees with estimates of the index of refraction of most aluminosilicate clays found in deep oceanic sediments. The material responsible for fluctuations in turbidity in the benthic region has the same range of refractive indices as inorganic resuspended material as described by Jerlov (1976).

Using the well-defined correlation of particle concentration and beam attenuation coefficient a model was developed to quantitatively describe the transmissometer profiles. All the profiles were described by a variety of combinations of five components. Each component was of a simple mathematical form and the components were shown to be representative of different physical systems. The model was developed in order to analyze the processes involved in sediment transport in HEBBLE. However, before such an analysis was performed it was necessary to verify that the model was, in fact a good representation of the system. A test of the model showed that in a steady, uniform, two-dimensional flow, the component model as applied to the simplified mass conservation equation yielded results which were compatible with the results obtained from two independent data sets. Specifically, current meter measurements, both near the bottom ($\leq$ 2 m a b) and at altitudes of tens of meters above the bottom yielded values of $\frac{w_s}{K}$ (w_s = settling velocity, K = eddy diffusion coefficient) which matched the values obtainable from the component model for the range of applicable settling velocities. Therefore the component model was deemed viable to the extent of providing insight into what processes were involved in the creation of the transmissometer profiles.

Both large-scale and small-scale processes were discovered to prevail in the temporal and spatial analysis of the optical data. The general scheme of transport was seen to be one combining advection and settling. It was shown that these two processes could explain the appearance of the most dominant components of the transmissometer profiles: the linear, logarithmic and exponential. By varying the magnitudes of either settling or advection, the shape of the profile was found to also vary accordingly. The other phenomena observed directly from the vertical transmissometer profiles were the detachment of the benthic nepheloid layer and the appearance of the trailing edge of a benthic "cloud". The detached benthic nepheloid layer was shown to be due most likely to cross-slope-current-induced benthic layer detachment followed by transport along the contours by the dominant regional flow to the southwest. Due to the infrequency of cross-slope currents such a process cannot be considered common and in fact was detected in only several stations. The observation of the trailing edge of a benthic cloud was demonstrated by the periodic fluctuations in transmission within 100 meters of the bottom followed by the drastic decrease in the turbidity of the water column. The occurrence of this phenomenon agreed in appearance with the form of benthic clouds that was later described by the Eulerian and Lagrangian maps and sections. The Eulerian transformation of the data produced a fixed-point time series representation of the profiles obtained over a wide area. The result was in good agreement with the time series obtained from the fixed-point in situ transmissometer used on the Bottom Ocean Monitor. Similar "storms" and clearing periods were detected with both techniques. The Lagrangian transformation of the data yielded a section map of transmission at a given time. The widely varying bottom transmission values yielded little or no correlation between transmission and density (density was shown to be nearly constant at the bottom). Together, the temporal and spatial transformations of the data indicated that the major optical features detected in the HEBBLE area (i.e., large benthic clouds) were stable and nearly constant in form over periods of greater than two weeks and over distances travelled of several hundred kilometers. In addition, first order calculations of mass flux indicated that a typical benthic cloud may transport one metric ton of suspended sediment per second. This mass flux is comparable to that of the Congo River. It is not, however, a continuous transport and thus differs from that of the river.

Consideration of the transmissometer results obtained herein with deep-ocean optical data from elsewhere in the world yields some interesting comparisons. In general, bottom nepheloid layers of a similar nature to those in the HEBBLE area are found in regions characterized by detectable bottom currents. Highly turbid bottom nepheloid layers have been detected with nephelometers on the ridges and rises of the Canada Basin (Hunkins et al., 1969), on the continental margin of the North American Basin (Eittreim et al., 1969), in the Indian-Pacific Antarctic Sea (Eittreim et al., 1972), and in the Cape Basin of the South Atlantic (Connary and Ewing, 1972). Similarly, all of these regions are characterized by relatively high average bottom currents (on the order of $10^1 \frac{\text{cm}}{\text{sec}}$). Other benthic areas having lower or near-zero bottom velocities are not, generally, characterized by the intensely turbid benthic boundary layers. Examples are the Angola and Guinea Basins (Connary and Ewing, 1972; Zaneveld et al., 1979), the abyssal plains of the North Pacific (Ewing and Connary, 1970) and South Pacific (Pak et al., 1979), and the Canada abyssal plain (Hunkins et al., 1969).

It is the form of the turbidity profiles that seems to be unique to the HEBBLE area. The component defined in this work by the sloping (i.e., logarithmic or exponential) increase in turbidity near the bottom was also found in the continental rise of the North American Basin by Eittreim et al. (1969) as well as in the Indian-Pacific Antarctic (Eittreim et al., 1972) and the Southeast Atlantic (Connary and Ewing, 1972). The well mixed linear component was seen in some nephelometer profiles made on the ridges within the Canada Basin (Hunkins et al., 1969) and also in some of the deep basins of the Western North Atlantic (Eittreim et al., 1972). Near-bottom intermediate nepheloid layers (similar to the detached nepheloid layers discussed previously) are rarely seen and usually are only recorded hundreds of meters above the bottom in regions near topographic highs (Pak et al., 1980; Eittreim et al., 1969).

Concluding, it appears that the optical profiles seen in the HEBBLE area are similar to turbidity profiles obtained in other deep-ocean areas of the world which are characterized by relatively strong benthic currents. The uniqueness of the HEBBLE area seems to lie in the diversity of profiles obtained. All of the other areas discussed are presented as having somewhat non-varying turbidity profiles. At least it is safe to say that the variations in turbidity within the same time frame and spatial separation are much larger within the HEBBLE area than in any of the other areas cited. The weak link in this argument lies in comparing the very precise data obtained from the transmissometer with the somewhat coarser data obtained from the nephelometer. In any event, upon first comparison it appears that the HEBBLE profiles of turbidity represent a conglomeration of the turbidity profiles one would obtain from a variety of deep-ocean benthic zones around the world.

The data described and analyzed in this thesis are for a specific oceanic region, yet the techniques used and the results obtained are applicable for other data sets as well. Several processes have been detected and suggested. These are processes whose geographical extent is not limited to the HEBBLE area. Indeed, optical determination of benthic layer detachment or benthic "storm" transport is universally applicable. Results may differ but the important point is that the use of transmission measurements can provide more information than just whether or not a water column is turbid. Together with other instruments, such as the CTD and current meter, many important transport processes can be detected and traced. It is my hope that future work in the analysis of transport processes will include increased emphasis on the use of optical methods for qualitative determinations.

BIBLIOGRAPHY

ARMI, L., Some evidence for boundary mixing in the deep ocean, J. Geophys. Res., 83:1971, 1978.

ARMI, L. and E. D'Asaro, Flow structures of the benthic ocean, J. Geophys. Res., 85:469, 1980.

BADER, H., The hyperbolic distribution of particle sizes, J. Geophys. Res., 75:2823, 1970.

BARTZ, R., J. R. V. Zaneveld, H. Pak, A transmissometer for profiling and moored observations in water, Soc. Photo-Opt. Instr. Eng., v. 160, Ocean Optics V, SPIE, 1978.

BASSIN, N. J., Suspended matter and the stability of the water column: Central Caribbean Sea, in Suspended Solids in Water, R. J. Gibbs, ed., Plenum Press, 1974.

BASSIN, N. J., J. E. Harris, A. H. Bouma, Suspended matter in the Caribbean Sea: a gravimetric analysis, Mar. Geol. 12:M1, 1972.

BEARDSLEY, G. F., Jr., H. Pak, K. Carder, Light scattering and suspended particles in the Eastern Equatorial Pacific Ocean, J. Geophys. Res., 75:2837, 1970.

BISCAYE, P. E. and S. L. Eittreim, Variations in the benthic boundary layer phenomena: nepheloid layers in the North American Basin, in Suspended Solids in Water, R. J. Gibbs, ed., Plenum Press, 1974.

BURT, W. V., A light-scattering diagram, J. Mar. Res. 15:76, 1956.

CARDER, K. L., P. R. Betzer, D. W. Eggiman, Physical, Chemical and Optical measures of suspended particle concentrations: their intercomparisons and applications to the West African Shelf, in Suspended Solids in Water, R. J. Gibbs, ed., Plenum Press, 1974.

CONNARY, S. D. and M. Ewing, The nepheloid layer and bottom circulation in the Guinea and Angola Basins, in Studies in Physical Oceanography, v. 2, A. L. Gordon, ed., Gordon and Breach Sci. Pub., 1972.

DRAKE, D. E., Suspended sediment and thermal stratification in Santa Barbara Channel, California, Deep-Sea Res. 18:763, 1971.

EITTREIM, S. and M. Ewing, Suspended particulate matter in the deep waters of the North American Basin, in *Studies in Physical Oceanography*, v. 2, A. L. Gordon, ed., Gordon and Breach Sci. Pub., 1972.

EITTREIM, S., M. Ewing and E. M. Thorndike, Suspended matter along the continental margin of the North American Basin, Deep-Sea Res., 16:613, 1969.

EITTREIM, S., A. L. Gordon, M. Ewing, E. M. Thorndike, P. Bruchhausen, The nepheloid layer and observed bottom currents in the Indian-Pacific Antarctic Sea, in *Studies in Physical Oceanography*, v. 2, A. L. Gordon, ed., Gordon and Breach Sci. Pub., 1972.

EWING, M. and S. D. Connary, Nepheloid layer in the North Pacific, Memoir Geol. Soc. Amer., v. 126, J. Hays, ed., Geol. Soc. Amer., 1970.

GIBBS, R. J., ed., *Suspended Solids in Water*, Plenum Press, N. Y., 1974a.

GIBBS, R. J., The suspended material of the Amazon Shelf and tropical Atlantic Ocean, in *Suspended Solids in Water*, R. J. Gibbs, ed., Plenum Press, N. Y., 1974b.

GIBBS, R. J., Principles of studying suspended materials in water, in *Suspended Solids in Water*, R. J. Gibbs, ed., Plenum Press, N. Y., 1974c.

GOLDBERG, E. D., I. N. McCave, J. J. O'Brien, J. H. Steele, *The Sea*, v. 6, John Wiley and Sons, N. Y., 1977.

GRAF, W. H., *Hydraulics of Sediment Transport*, McGraw-Hill, N. Y., 1971.

HARLETT, J. C. and L. D. Kulm, Suspended sediment transport on the Northern Oregon Continental Shelf, Bull. Geol. Soc. Amer. 84:3815, 1973.

HOLLISTER, C. D., A. R. M. Nowell, J. D. Smith, The third annual report of the High Energy Benthic Boundary Layer Experiment, Woods Hole Oceanographic Institution, Rep. 80-32, 1980.

HUNKINS, K., E. M. Thorndike and G. Mathieu, Nepheloid layers and bottom currents in the Arctic Ocean, J. Geophys. Res., 74:6995, 1969.

ICHIYE, T., N. J. Bassin, J. E. Harris, Diffusivity of suspended matter in the Caribbean Sea, J. Geophys. Res., 77:6576, 1972.

JERLOV, N. G., Particle distribution in the ocean, Rep. Swedish Deep-Sea Exped., 3:73, 1953.

JERLOV, N. G., A transparency-meter for ocean water, Tellus 9:229, 1957.

JERLOV, N. G., Maxima in the vertical distribution of particles in the sea, Deep-Sea Res., 5:173, 1959.

JERLOV, N. G., Marine Optics, Elsevier, Amsterdam, 1976.

JERLOV, N. G., and E. Steemann-Nielsen, eds., Optical Aspects of Oceanography, Academic Press, London, 1974.

KALLE, K., Bericht 2: Teilfahrt der deutsche nordatlantischen Expedition 'Meteor 5', 5, Die chemischen Arbeiten auf der 'Meteor' - Fahrt, Januar bis Mai, 1938, Ann. Hydrog. Mar. Meteorol., Suppl. Paper, Jan. 23-30, 1939.

KALLE, K., The problem of the Gelbstoff in the sea, Oceanogr. Mar. Biol. Ann. Rev., 4:91, 1966.

KITCHEN, J. C., J. R. V. Zaneveld, H. Pak, The vertical structure and size distributions of suspended particles off Oregon during the upwelling season, Deep-Sea Res., 25:H53, 1978.

KULLENBERG, G., The distribution of particulate matter in a Northwest African coastal upwelling area, in Suspended Solids in Water, R. J. Gibbs, ed., Plenum Press, N. Y., 1974.

MIE, G., Beiträge zur Optik trüber Medien, speziell kolloidalen Metalllösungen, Ann. Phys. 25:377, 1908.

PAK, H., TColumbia River as a source of marine light scattering particles, Ph.D. Thesis, Oregon State University, Corvallis, 1970.

PAK, H., Distribution of suspended particles in the Equatorial Pacific Ocean, in Suspended Solids in Water, R. J. Gibbs, ed., Plenum Press, N. Y., 1974.

PAK, H., L. A. Codispoti and J. R. Zaneveld, On the intermediate particle maxima associated with oxygen-poor water off Western South America, Deep-Sea Res., 27: 783, 1980.

PAK, H. D. Menzies and J. R. Zaneveld, Optical and Hydrographical Observations off the coast of Peru during May-June 1977, Oregon State Univ. Sch. Ocean., Reference 79-14, 1979.

PAK, H. and J. R. V. Zaneveld, Bottom nepheloid and bottom mixed layers observed on the continental shelf off Oregon, J. Geophys. Res., 82:3921, 1977.

PAK, H., J. R. V. Zaneveld and J. Kitchen, Intermediate nepheloid layers observed off Oregon and Washington, J. Geophys. Res., 85:6697, 1980.

PETERSON, R. L., A study of suspended particulate matter: Arctic Ocean and Northern Oregon Continental Shelf, Ph.D. Thesis, Oregon State University, Corvallis, 1978.

RAUDKIVI, J., Loose Boundary Hydraulics, Pergamon, Oxford, 1967.

ROACH, D. M., The determination of refractive index distributions for oceanic particles, Ph.D. Thesis, Oregon State University, 1975.

SHEPARD, F. P., Submarine Geology, 2nd ed., Harper and Row, New York, 1963.

SHOR, A. N. and B. E. Tucholke, Geologic effects of turbidity currents and contour currents on the Nova Scotian Rise, EOS, 61:1015, 1980.

SMITH, J. D. and S. R. McLean, Spatially averaged flow over a wavy surface, J. Geophys. Res., 82:1735, 1977.

SMITH, R. C., R. W. Austin, T. J. Petzold, Volume scattering functions in ocean waters, in Suspended Solids in Water, R. J. Gibbs, ed., Plenum Press, N. Y., 1974.

SPINRAD, R. W. and J. R. V. Zaneveld, Irradiance and beam transmittance measurements off the West Coast of the Americas, J. Geophys. Res., 84:355, 1979.

THORNDIKE, E. M. and M. Ewing, Photographic nephelometers for the deep sea, in Deep-Sea Photography: Johns Hopkins University Oceanographic Studies, v. 3, Johns Hopkins University Press, Baltimore, 1967.

TYLER, J. E., R. W. Austin, T. J. Petzold, Beam transmissometers for oceanographic measurements, in Suspended Solids in Water, R. J. Gibbs, ed., Plenum Press, N. Y., 1974.

VAN DE HULST, H. C., Light scattering by small particles, John Wiley and Sons, N. Y., 1957.

WEATHERLY, G. L., E. A. Kelley, J. R. V. Zaneveld, H. Pak, M. J. Richardson, M. Wimbush, A deep, narrow, thin filament of the Western Boundary Undercurrent (WBUC), EOS, 61:1016, 1980.

YALIN, M. S., Mechanics of Sediment Transport, Pergamon, Oxford, 1972.

ZANEVELD, J. R. V., J. C. Kitchen, R. Bartz, D. Menzies, S. Moore, R. Spinrad, H. Pak, Optical, hydrographic, and chemical observations in the Monterey Bay area during May and September, 1977, Oregon State Univ. Sch. Ocean. Reference 78-13, 1978.

ZANEVELD, J. R. V., D. M. Roach, H. Pak, The determination of the index of refraction distribution of oceanic particulates, J. Geophys. Res., 79:4091, 1974.

ZANEVELD, J. R. V., R. W. Spinrad, D. W. Menzies, Optical and hydrographic observations in the Congo River and Angola Basin during May, 1978, Oregon State Univ. Sch. Ocean. Reference 79-3, 1979.